Nonlinear Optical Signal Processing Using Time- and Wavelength-Interleaved Laser Pulse Source

LEI, Kin Pang

A Thesis Submitted in Partial Fulfillment
of the Requirements for the Degree of
Doctor of Philosophy
in
Electronic Engineering

The Chinese University of Hong Kong
September 2011

Abstract of Thesis Entitled:
Nonlinear Optical Signal Processing Using Time- and Wavelength-Interleaved Laser Pulse Source
Submitted by: LEI, Kin Pang
for the degree of Doctor of Philosophy in Electronic Engineering
at the Chinese University of Hong Kong in September 2011

In recent years, the Internet traffic has been increasing dramatically. The data rates of communications are expected to increase rapidly to meet the growing demand in the near future. At the same time, the requirement for processing high-speed data signals will become more stringent. More advanced electronic and optical components will be needed for processing at higher speeds, thus significantly increasing the operation cost.

In this thesis, we introduce a new scheme to process high-speed optical communication signals using relatively low-speed, low-cost optical components. Our scheme uses time- and wavelength-interleaved laser pulses that allow processing of signals at a fraction of the line rate. By making use of external modulators, we demonstrated the generation of 40 GHz time- and wavelength-interleaved pulses with electro-absorption modulator and phase modulator. We will describe the generation methods and characteristics in details. We will also compare their advantages and disadvantages. By using high-speed modulators, we also achieved 80 GHz time- and wavelength-interleaved pulses. We will also demonstrate how the pulsed source can be used to reduce the bandwidth requirement on signal processing.

Optical nonlinearities in fibers and semiconductor devices are of great importance in the field of nonlinear optical signal processing. By applying the time- and wavelength-interleaved pulses in nonlinear processing, we have achieved different applications for use in optical networks, including wavelength multicasting, OTDM-to-WDM conversion, and optical add/drop multiplexing. For OTDM-to-

WDM conversion, we demonstrated two schemes to achieve the process: cross-absorption modulation in an electro-absorption modulator and four-wave mixing in a nonlinear photonic crystal fiber. Error-free operations of 40 Gb/s OTDM to 4 x 10 Gb/s WDM signal conversion have been achieved using both schemes. To further improve the performance, optical parametric amplifier (OPA) is used to enhance the signal-to-noise ratio of the demultiplexed channels. The use of OPA can also provide the system with add/drop multiplexing function based on pump depletion. Details of the experimental setup and results will be described.

Wavelength multicasting is an important process in optical networks when information from a single location is required to be delivered to multiple locations. Using the time- and wavelength-interleaved pulses, we demonstrated wavelength multicasting of both NRZ-OOK and NRZ-DPSK signals. Among the multicast channels, a delay time is introduced to suit the need for different optical networks. We will also discuss the possibility of achieving multicast with regeneration function.

To further investigate the capability of the time- and wavelength-interleaved pulses, we demonstrate other applications including high-speed wavelength conversion using low-speed devices and all-optical sampling. Finally, the thesis will be concluded by a description on possible future applications of the pulsed source and the challenges to operate at higher processing speeds.

摘 要

近年，互聯網的發展一日千里，互聯網的頻寬需求日益增長。爲了應付這個急速的增長，在可見將來，數據的傳輸率將會以幾何級數上升。與此同時，數據的處理速度要求將會越趨嚴苛。用於處理高速訊號的電子和光電子零件將會令成本嚴重增加。

在這篇論文，我們會引入一種基於低速、低成本光學零件的新方法來處理高速的光訊號。這種方法利用一種名爲時域－波域區隔激光器，以低於訊號速度的零件來實現高速訊號處理。利用外置的致電－吸收調制器或相位調制器，我們實現了４０ＧＨｚ的時域－波域區隔脈衝激光源。我們將會詳細描述其生成方法和所產生脈衝的表徵，並且比較利用不同調制器所產生的脈衝。而在使用高速的調制器時，我們能夠生成８０甚至１００ＧＨｚ的激光源。我們將會討論如何利用這種特別的激光源來減低處理高速訊號時所需要的頻寬。

光纖和半導體光學零件的非線性對於非線性光學訊號處理是十分重要的。結合時域－波域區隔脈衝激光源和這兩種媒介的光學非線性，我們能夠達成在光學網絡的不同功能。這些功能包括波長多播、時分復用－波分復用的訊號轉換和塞取多工器。我們利用了兩個不同的方法進行時分復用－波分復用的訊號轉換，包括在致電－吸收調制器的交叉吸收調變效應和在光子晶體光纖的四波混頻效應。我們實現了４０Ｇｂ／ｓ的時分復用訊號到四通道１０Ｇｂ／ｓ波分復用訊號的轉換。使用這兩種方法達成的訊號轉換都能達到無誤的操作。爲了進一步改善經過轉換後訊號的訊噪比，我們另外使用了光參數放大器來進行全光解復用。除了進行全光解復用外，利用光參數放大器的泵抽空現

象，我們還實現了全光的塞取多工器。我們將會討論詳細的實驗設計和實驗結果。

當一個地方的資訊需要同時被傳送到多個目的地時，在全光網絡內需要進行波長多播。利用時域－波域區隔脈衝激光源，我們示範了不歸零－振幅偏移調變訊號和不歸零－差分相位偏移調變訊號的波長多播。在不同的多播頻道之間，我們引入了一個固定的延遲，令到不同的多播頻道能夠適合不同的網絡。我們亦會探討在進行波長多播的過程中加入訊號再生功能的可能性。

爲了進一步了解時域－波域區隔激光器的實用性，我們亦示範了其他的應用實例，如全光的模擬訊號取樣和利用低速的零件進行高速的波長轉換。最後我們對這篇論文作總結，並且探討利用這個光源進行高速訊器處理時將會遇到的問題。

Acknowledgement

I would like to express my deepest gratitude to my supervisor, Prof. Chester Shu, for his continuous support during my study. His novel ideas and helpful guidance led me to a successful life in my Ph.D. study. Also his patience and knowledge provided me with an excellent environment for research and for growth-up. Prof. Shu has been teaching me since my first year of Bachelor degree, and I have really learnt a lot from him.

I would also like to thank Prof. H. K. Tsang, Prof. K. T. Chan, Prof. L. K. Chen, Prof. C. W. Chow, and Prof. C. L. Pan for their support during my study. I have gained a lot of knowledge on theories and practical skills of fiber-optic communications from them.

Thanks also go to Dr. Mable P. Fok and Mr. Alan L. K. Cheng. They introduced me a lot of useful knowledge in the optoeletronics laboratory. If they didn't teach me how to use the equipment, I cannot finish my experiments smoothly. Also they taught me a lot of techniques on manuscript writing and also the attitude of research.

I would also like to thank Miss Barbara Ho, for her continuous support on equipment and components, and thank Mr. Y. Dai, Mr. J. Du, Mr. L. Wang, Ms. X. Fu, Dr. K. L. Lee, Dr. K. S. Lee, Dr. D. Chen, Ms. Y. Gao for their fruitful discussions on my research projects. They have given me numerous suggestions and comments on experimental setups and results and also my future career.

Also I would like to appreciate discussions with Dr. X. Chen, Dr. C. Li, Dr. K. Chen, Mr. S. M. G. Lo, Mr. Z. Cheng, Mr. Y. Chen, Mr. K. Xu, Mr. C. Y. Wong, Mr. Z. Zhang, Ms. J. Liu and Ms. M. Chen on both research matters and daily life. They have enriched my research life with laughs, foods and new experience with mainland and Hong Kong students.

Moreover, I really thank my friends and family in Macau. When I was experiencing a low tide in my research life, they gave me invaluable encouragement. We chatted a lot and finally I could overcome the difficulties in these years. Although I did not have much time gathering and accompanying with them, they supported me whenever I have troubles. Last but not least, I would like to thank my dearest and unique one for her daily support and continuous love. I have been busy with my research and did not pay enough attention on her, but she still provides me with encouragement. I feel lucky to know her and receive her love during these hard days.

I will miss the days in CUHK where I have spent 8 years here and it is a place filled with memories, hard but successful days, love and consideration.

Table of Content

Nonlinear Optical Signal Processing Using Time- and Wavelength-Interleaved Laser Pulse Source

1 Introduction

Since the first proposal to use silica fiber for optical communications by Hockham and Kao in 1966 [1], the deployment of fiber-optic communication systems has been increasing dramatically. Compared with conventional copper-wire-based or microwave-based communication systems, optical systems provide advantages including low transmission loss, large bandwidth and small size. Nowadays, most of the backbone architectures of communication networks are using optical systems. The system capacity has also evolved from Mb/s at the beginning to over 10 Tb/s [2, 3] in recently reported results. To process the data in these systems, optical-electrical-optical conversion is the main stream in today's technology. However, for future communication systems with baseband rate of 100 Gb/s or beyond, the bandwidth limit of electronics will result in a bottleneck of the processing speed. Therefore, signal processing in the optical domain is a desirable candidate for future communication systems.

To realize an optical signal processer, many different devices and approaches have been proposed to achieve a variety of functions. Commonly used device candidates include nonlinear optical fibers [4, 5] and semiconductor/glass based devices that are sometimes fabricated using a waveguide structure [6-9], in which high-speed optical signal processing has been achieved with satisfactory performances. We can foresee that these devices will have a promising potential in future development of high-speed optical networks.

However, the popularity of lower speed devices cannot be ignored in current operating systems. To adopt the current technology to high-data-rate operations, it is not practical to abolish the old equipment all at once. A solution to this dilemma is to transform a high-speed data channel into multiple lower speed channels. This process is named serial-to-parallel conversion. Serial-to-parallel conversion has been adopted for many different applications, including label recognition in packet-switched networks [10], analog-to-digital conversion [11], and all-optical demultiplexing in optical networks [12]. In this thesis, we focus on this serial-to-parallel conversion process achieved by nonlinear interaction of the signal with a time- and wavelength-interleaved laser source. Different generation schemes of time- and wavelength-interleaved pulsed sources will be discussed. A number of applications achieved with serial-to-parallel conversion will also be demonstrated and analyzed in detail.

Apart from serial-to-parallel conversion, the time- and wavelength-interleaved laser source can also be used to achieve many other functions in nonlinear optical signal processing for fiber networks. The performances of these demonstrations will be described and analyzed in this thesis.

1.1 Outline of the Thesis

The thesis focuses on the generation and application of time- and wavelength-interleaved laser pulses. In Chapter 1, the motivation and outline of the thesis are given. In Chapter 2, different components and nonlinear phenomena are introduced. These components and effects will be utilized in following sections of the thesis.

In Chapter 3, three different schemes are demonstrated for the generation of time and wavelength-interleaved laser source. The temporal and spectral profiles of the generated pulses will be discussed. Results are presented on successful demonstration of 40 GHz and 80 GHz time- and wavelength-interleaved pulses. Also, a comparison among the three different schemes will be reported.

After generating the pulses, we investigate their application in processing different types of signals. In Chapter 4, we demonstrate all-optical sampling of an optical analog signal. A sampling rate of 40 GSample/s has been achieved while only using electronic processors of 10 GHz bandwidth. Characterization of the all-optical sampler has also been performed.

In Chapter 5, wavelength multicasting of digital signals will be discussed. Multicasting is of great importance when the data from a single location is to be transmitted to different destinations. We will demonstrate 1-to-4 wavelength multicasting using the pulsed source. Both amplitude-shift keying (ASK) and phase-shift keying (PSK) signals can be processed using a similar approach. Also, we

demonstrate wavelength conversion of high-speed data signals using lower speed devices by applying the time- and wavelength-interleaved laser source.

In Chapter 6, optical time-division multiplexing (OTDM)-to-wavelength-division multiplexing (WDM) conversion is achieved. By the OTDM-to-WDM process, high-speed OTDM channels can be separated into multiple channels at different wavelengths, making it possible to bridge different optical networks. By using cross-absorption modulation in an electro-absorption modulator, or four-wave mixing in a photonic crystal fiber, the operation can be achieved with error-free operations. We will introduce the principles and results of these two approaches.

Optical parametric amplifier (OPA) has been a topic of much interest in recent years. It offers advantages including low noise figure, arbitrary pump wavelength and ability for high-speed optical signal processing [13]. Key properties of OPA will be described in Chapter 7. Using the pump depletion effect in an OPA, reconfigurable OTDM demultiplexing has been achieved with time- and wavelength-interleaved pulses. Also, some preliminary results on all-optical signal regeneration with an OPA will be discussed in this chapter.

In Chapter 8, we will discuss other potential applications of the pulsed source, including the processing of high-speed signals and advanced modulation format signals. Finally, a summary will be presented by concluding the works achieved in the thesis.

1.2 References

[1] K. C. Kao and G. A. Hockham, "Dielectric-fibre surface waveguides for optical frequencies," *Proc. IEE*, vol. 113, pp. 1151 – 1158, July 1966.

[2] T. Richter, E. Palushani, C. Schmidt-Langhorst, M. Nölle, R. Ludwig, and C. Schubert, "Single wavelength channel 10.2 Tb/s TDM-data capacity using 16-QAM and coherent detection," *in National Fiber Optic Engineers Conference, OSA Technical Digest (CD)* (Optical Society of America, 2011), Los Angeles, CA, March 2011, paper PDPA9.

[3] J. Sakaguchi, Y. Awaji, N. Wada, A. Kanno, T. Kawanishi, T. Hayashi, T. Taru, T. Kobayashi, and M. Watanabe, "109-Tb/s (7x97x172-Gb/s SDM/WDM/PDM) QPSK transmission through 16.8-km homogeneous multi-core fiber," *in Optical Fiber Communication Conference, OSA Technical Digest* (CD) (Optical Society of America, 2011), Los Angeles, CA, March 2011,paper PDPB6.

[4] H. Hu, H. C. H. Mulvad, M. Galili, E. Palushani, J. Xu, A. T. Clausen, L. K. Oxenløwe, and P. Jeppesen, "Polarization-insensitive 640 Gb/s demultiplexing based on four wave mixing in a polarization-maintaining fibre loop," *J. Lightw. Technol.*, vol. 28, pp. 1789 – 1795, June 2010.

[5] C.-S. Brès, A. O. J. Wiberg, B. P.-P. Kuo, J. M. Chavez-Boggio, C. F. Marki, N. Alic, and S. Radic, "Optical demultiplexing of 320 Gb/s to 8 × 40 Gb/s in single parametric gate," *IEEE J. Lightw. Technol.*, vol. 28, pp. 434 – 442, February 2010.

[6] T. Hirooka, Member, M. Okazaki, T. Hirano, P. Guan, M. Nakazawa, and S. Nakamura, "All-optical demultiplexing of 640-Gb/s OTDM-DPSK signal

using a semiconductor SMZ switch," *IEEE Photon. Technol. Lett.*, vol. 21, pp. 1574 – 1576, October 2009.

[7] E. Tangdiongga, Y. Liu, H. de Waardt, G. D. Khoe, A. M. J. Koonen, H. J. S. Dorren, X. Shu, and I. Bennion, "All-optical demultiplexing of 640 to 40 Gbits/s using filtered chirp of a semiconductor optical amplifier," *Opt. Lett.*, vol. 32, pp. 835 – 837, April 2007.

[8] H. Ji, M. Pu, H. Hu, M. Galili, L. K. Oxenløwe, K. Yvind, J. M. Hvam, and P. Jeppesen, "Optical waveform sampling and error-free demultiplexing of 1.28 Tb/s serial data in a nanoengineered silicon waveguide," *J. Lightw. Technol.*, vol. 29, pp. 426 – 431, February 2011.

[9] J. V. Erps, F. Luan, M. D. Pelusi, T. Iredale, S. Madden, D.-Y. Choi, D. A. Bulla, B. Luther-Davies, H. Thienpont, and B. J. Eggleton, "High-resolution optical sampling of 640-Gb/s data using four-wave mixing in dispersion-engineered highly nonlinear As_2S_3 planar waveguides," *J. Lightw. Technol.*, vol. 28, pp. 209 – 215, January 2010.

[10] R. Takahashi, T. Nakahara, H. Takenouchi, and H. Suzuki, "40-Gbit/s label recognition and 1 × 4 self-routing using self-serial-to-parallel conversion," *IEEE Photon. Technol. Lett.*, vol. 16, pp. 692 – 694, February 2004.

[11] M. P. Fok, K. L. Lee, and C. Shu, "4 × 2.5 GHz repetitive photonic sampler for high-speed analog-to-digital signal conversion," *IEEE Photon. Technol. Lett.*, vol. 16, pp.876-878, March 2004.

[12] A. H. Gnauck, R. M. Jopson, R. W. Tkach, C. J. McKinstrie, and S. Radic, "Serial-to-parallel demultiplexing using WDM sampling pulses," *IEEE Photon. Technol. Lett.*, vol. 21, pp. 97 – 99, January 2009.

[13] M. E. Marhic, "Fiber optical parametric amplifiers, oscillators and related devices," *Cambridge Univ. Press*, 2008.

2 Background

In this chapter, the principles of the components used in this thesis research are introduced, including different optical modulators and nonlinear optical fibers. Also, different types of nonlinear phenomena in the above components are described. The principle of wavelength division processing is also discussed, which is an important processing technique used throughout the thesis.

2.1 Optical Modulators

Optical modulator is a device for converting electrical signals into optical signals. Usually, a laser is used for the optical carrier. A laser beam can carry information by either changing its amplitude or phase, depending on the modulator utilized. Different modulators are optimized for different modulation schemes.

For amplitude modulation, Mach-Zehnder electro-optic modulator and electro-absorption modulator are two most popular candidates. The principles of these two modulators are described in Section 2.1.1.

For phase modulation, either a straight-line electro-optic modulator or Mach-Zehnder modulator can be used. The details are discussed in Section 2.1.2.

2.1.1 Amplitude Modulators

Electro-Optic Mach-Zehnder Modulator

Eletro-optic Mach-Zehnder modulator, or simply MZM, is based on the Pockels effect. According to the Pockels effect, the refractive index of a medium depends on the amount of applied electric field. The refractive index change depends linearly on the electric field change. Materials exhibiting the Pockels effect are called electro-optic materials. Only non-centrosymmetric materials (mostly crystals) exhibit the Pockels effect that is sometimes referred as the linear electro-optic effect. An example of non-centrosymmetric material is $LiNbO_3$.

In a MZM, a Mach-Zehnder interferometer is fabricated with $LiNbO_3$ waveguides. A sample structure is shown in Fig. 2.1.1.1 [1]. Electrodes are added on both arms of the interferometer, which is called a dual-drive MZM. Either single-electrode or dual-electrode MZM can achieve amplitude modulation. By applying electrical signal on the electrode, the phase of the respective path can be changed. Combining the two paths of different phases, an amplitude modulation can be produced.

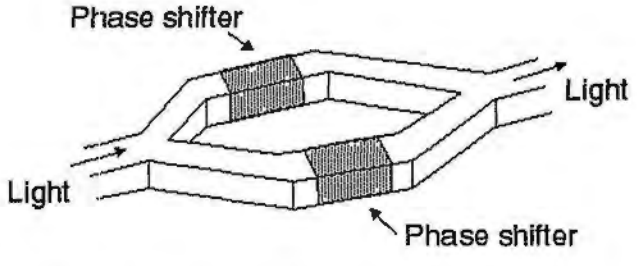

***Fig. 2.1.1.1** A picture of a MZM with two electrodes.*

Apart from applying electrical signals on the electrodes, a MZM usually has a DC bias port to alter the transfer characteristic of the modulator. Shown in Fig. 2.1.1.2 is the transfer characteristic of a typical MZM [2]. The transfer curve of the

MZM is a cosine-squared function. For different applications, the DC bias voltage is chosen to adopt different values.

MZM can be used for amplitude modulation, phase modulation and pulse carving application with different biasing voltage and modulation signal. For example, the MZM is biased at the linear region for the generation of on-off keying signal [3]. For pulse generation, the MZM is biased near the null region. Another important parameter for the MZM is the half-wave voltage ($V\pi$) of the modulator. It is the required voltage for the MZM to generate a π phase shift of the input light. Usually a lower $V\pi$ is preferable for pulse generation as the requirement for electrical amplifier is lower.

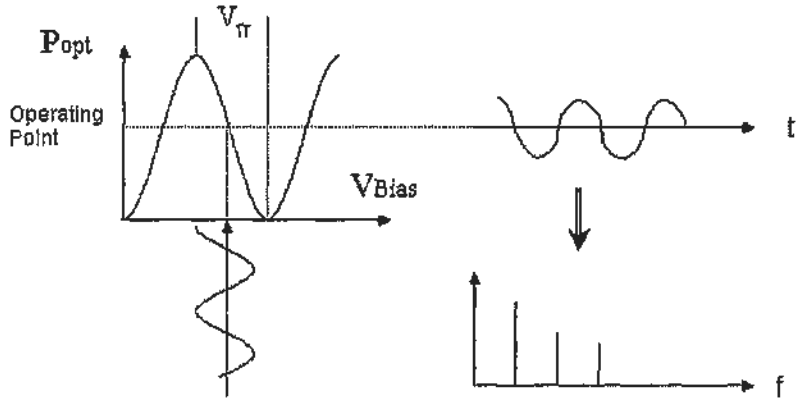

***Fig. 2.1.1.2** Transfer characteristic of a MZM.*

Electro-absorption Modulator

Electro-absorption modulator (EAM) is an important device in optical communication networks. Usually, EAM is used with its electro-absorption effect. EAM is usually used for on-off keying signal generation or pulse carving application. During electro-absorption, by either Franz–Keldysh effect [4] or quantum-confined Stark effect [5], the absorption spectrum of the modulator depends on the amplitude of the applied electric field, thus affecting the intensity of the optical carrier. The

advantages of EAM include low driving voltage (usually several volts), small polarization dependency, and integrability with other devices.

Fig. 2.1.1.3 shows the relationship between the output optical power P_{out} from an EAM and the applied reverse voltage V_R. When the reverse voltage increases, the output power drops significantly. As a result, when a stream of electrical data with a swinging voltage V_{SW} is applied to the EAM, the data can be transferred to the input light beam by the voltage-dependent absorption spectrum. The extinction ratio (ER) is linearly increased with the applied swing voltage V_{SW} as shown in Fig. 2.1.1. V_{SW} is usually in the range of 1.5 to 4 V for most EAMs, and the induced dynamic ER is in the range of 11 to 13 dB.

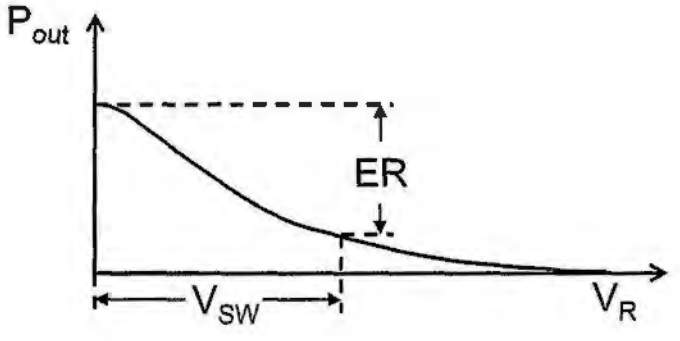

Fig. 2.1.1.3 *Relationship between applied reverse voltage and output optical power in an EAM*

Because the electric field in the active region modulates not only the absorption characteristics but also the refractive index, the EAM produces some chirp. However, this chirp usually is much less than that of a directly modulated laser. A small on-state (bias) voltage around 0 to 1 V is often applied to minimize the modulator chirp.

2.1.2 Phase Modulators

For phase modulators (PM), usually the voltage dependent refractive index by Pockels effects is utilized. PM can be fabricated in a straight-line $LiNbO_3$ waveguide or in the Mach-Zehnder interferometer (MZI) configuration [3]. By applying an electrical signal on the electrode, the phase of the input light can be changed. Fig. 2.1.2.1 shows an illustration of phase modulation with a straight-line $LiNbO_3$ PM. At the optical output, it should be noted that the phase change can also be regarded as a frequency change. As a result, the frequency components on the optical carrier are increased, resulting in a spectral broadening effect. The larger the phase modulation is introduced, the broader is the output spectrum.

A phase modulator can be used for the generation of phase-shift keying signal. For data modulation, the amplitude of the modulation signal should be of $V\pi$ to achieve a π phase shift.

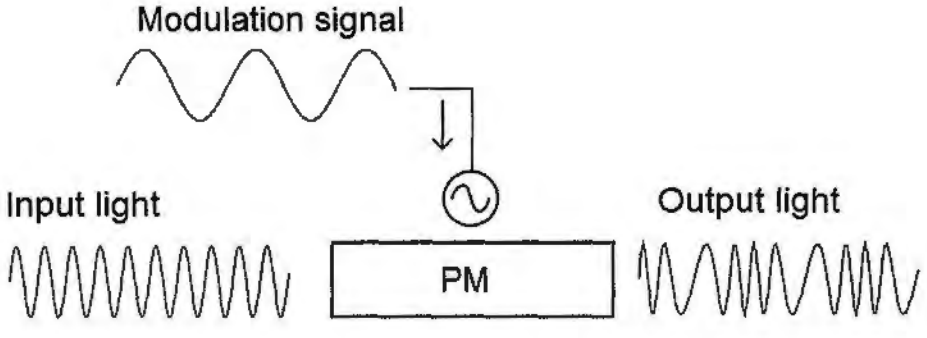

Fig. 2.1.2.1 *Phase modulation with a single waveguide phase modulator.*

A phase modulator can also be used for pulse generation. As mentioned above, spectral broadening occurs when phase modulation is added on the input light. By passing thorough a dispersive medium, different frequency components propagate at different speeds and an optical pulse can be generated. It is an important feature that will be utilized in a later chapter of this thesis.

2.2 Dispersion

Fiber dispersion plays a critical role in optical fiber communications because different spectral components travel at different speeds given by c/n(ω). The effect is especially pronounced for short pulse as it occupies a wide spectrum. Fig. 2.2.1 shows the variation of refractive index n and group index n_g.[6]

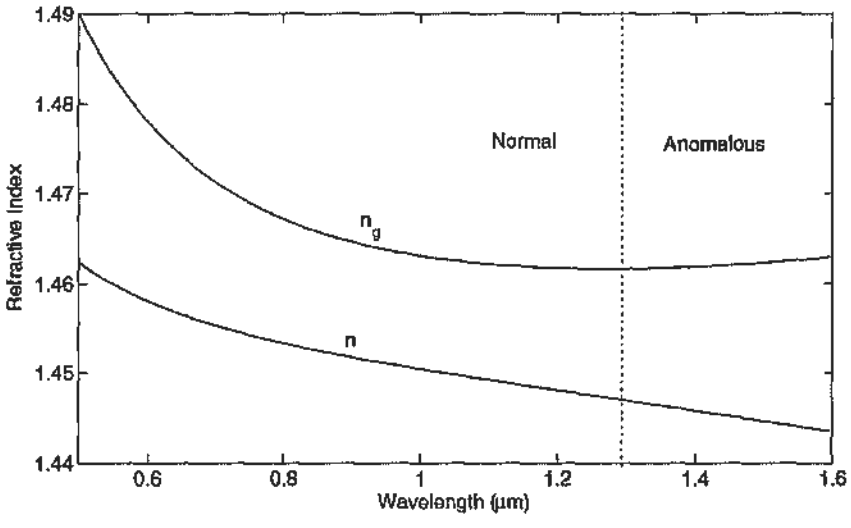

Fig. 2.2.1. *Variation of refractive index and group index with wavelength for fused silica [6].*

Mathematically, the effects of fiber dispersion are accounted for by expanding the mode-propagation constant β in a Taylor series about the frequency ω_0 at which the pulse spectrum is centered:

$$\beta(\omega) = n(\omega)\frac{\omega}{c} = \beta_0 + \beta_1(\omega - w_0) + \frac{1}{2}\beta_2(\omega - \omega_0)^2 + \ldots \qquad [2.1]$$

$$\text{where } \beta_m = \left(\frac{d^m \beta}{d\omega^m}\right)\omega = \omega_0 \ (\text{m} = 0, 1, 2\ldots) \qquad [2.2]$$

The parameters β_1 and β_2 are related to the refractive index n(ω) and its derivatives through the relations:

$$\beta_1 = \frac{1}{\upsilon_g} = \frac{n_g}{c} = \frac{1}{c}(n + \omega\frac{dn}{d\omega}) \qquad [2.3]$$

$$\beta_2 = \frac{1}{c}(2\frac{dn}{d\omega} + \omega\frac{d^2n}{d\omega^2}) \qquad [2.4]$$

where n_g is the group index and v_g is the group velocity. Figure 2.2.1 also shows the group index n_g changes with wavelength for fused silica. The group velocity can be found using $v_g = c/n_g$. Physically speaking, the envelope of an optical pulse moves at the group velocity, while the parameter β_2 represents dispersion of the group velocity and is responsible for pulse broadening. This phenomenon is known as the group-velocity dispersion (GVD), and β_2 is the GVD parameter. The dispersion parameter D, defined as $\frac{d\beta_1}{d\lambda}$, is also used in practice. It is related to β_2 and n as

$$D = \frac{d\beta_1}{d\lambda} = \frac{-2\pi c}{\lambda^2}\beta_2 = -\frac{\lambda}{c}\frac{d^2n}{d\lambda^2} \qquad [2.5]$$

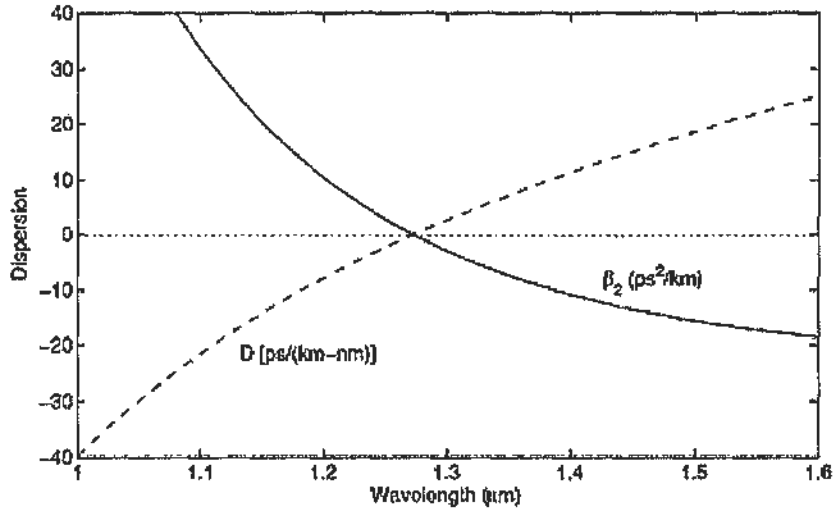

Fig. 2.2.2. *Variation of β_2 and D with wavelength for fused silica. Both β2 and D vanish at the zero-dispersion wavelength occurring near 1.27 μm. [6]*

Figure 2.2.2 shows how β_2 and D vary with wavelength λ for fused silica. It is worth mentioning that at around 1.27 μm, both β_2 and D vanish and change sign for longer wavelengths. This wavelength is referred to as the zero-dispersion wavelength

and is denoted as λ_0. For standard-single mode fiber, the λ_0 is at around 1.31 μm after some doping on the fiber. The dispersion can also be tailored by changing the core size and core-cladding refractive index difference.

For nonlinear optical signal processing, the zero-dispersion wavelength is important as it is a requirement for some nonlinear phenomena such as optical parametric amplification. Another important factor affecting efficiency of nonlinear optical signal processing is the dispersion slope of the optical fiber. Dispersion slope D_λ is defined as $D_\lambda = dD/d\lambda$. It is generally useful to know its value at λ_0. For standard single-mode fiber the value is of the order of 0.07 $ps \cdot nm^{-2}km^{-1}$, and for highly nonlinear fiber (HNLF) the value is around 0.02 – 0.03 $ps \cdot nm^{-2}km^{-1}$. To further enhance the nonlinear effect efficiency, higher-order dispersion should also be considered. In [7], tailor-making the 4-th order dispersion has been reported with enhanced nonlinear effect. HNLFs with different dispersion values are discussed in the following.

For pulse generation, GVD can be a useful tool to generate short pulses. As discussed in last section, by phase modulation we can increase the spectrum of a continuous wave (CW) light. In optical fiber, different frequency components travel at different speeds due to the GVD in optical fiber. If the CW light is located in the normal dispersion region (red light travel faster), at a certain GVD the low frequency components catch up high frequency components in the time domain. This is a phase-to-intensity conversion. The details on the required GVD and the pulse generation process will be further described in Chapter 3.

2.3 Nonlinear Effects

Nonlinear effects, or nonlinearities, refer to some special phenomena when an intense light is directed to a nonlinear medium. For example, in the case of weak light, the refractive index in an optical fiber is usually regarded as a constant. However, in the case of intense light, the refractive index becomes a function of the light intensity. Apart from refractive index, optical absorption, phase and intensity also depend on the input light intensity in different devices and materials. In this section, we focus on several common nonlinearities in optical fibers and semiconductor devices.

Four-Wave Mixing

Four-wave mixing (FWM) is related to the third order susceptibility (χ^3) in optical fibers. As per its name, the process involves four optical waves. When three intense waves are directed into a nonlinear medium, a fourth wave is generated. Usually two of them are pumps, donated by ω_1 and ω_2, and the other one is a signal, donated by ω_s. The frequency of the generated wave, or idler $\omega_i = \omega_1 + \omega_2 - \omega_s$. This is called non-degenerate FWM, involving three input light waves.

If the input waves are reduced to two, for example only ω_1 and ω_2 exist, two new waves are be generated at ω_3 and ω_4 where $\omega_3 = 2\omega_1 - \omega_2$ and $\omega_4 = 2\omega_2 - \omega_1$. This is named degenerate FWM. A typical spectrum of degenerate FWM is shown in Fig. 2.3.1.

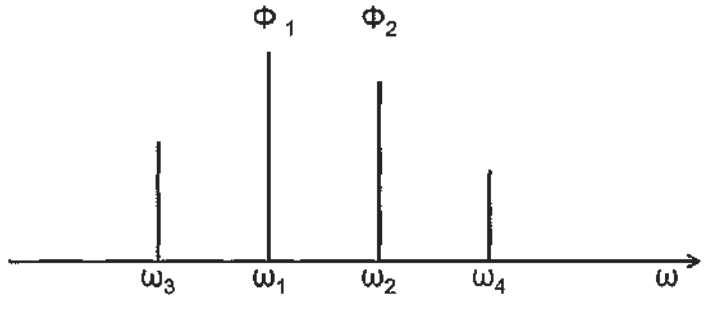

Fig. 2.3.1. *A typical optical spectrum of degenerate FWM.*

During four-wave mixing, the phase and amplitude are transferred from the pump and signal light to the generated waves. The amplitude and phase of ω_3 and ω_4 are governed by the following equations:

$$E_3 = (E_1 \bullet E_2^*)E_1\gamma(\omega_1 - \omega_2)\exp[i(\omega_3 t + \Delta\Phi_3)] \quad [2.6]$$

$$E_4 = (E_2 \bullet E_1^*)E_2\gamma(\omega_2 - \omega_1)\exp[i(\omega_4 t + \Delta\Phi_4)] \quad [2.7]$$

where $\Delta\Phi_3=2\Phi_1-\Phi_2$ and $\Delta\Phi_4=2\Phi_2-\Phi_1$, E_m is the respective fields of the waves, ω_m is the respective frequencies of the waves (m = 1, 2, 3, 4), and γ is the complex coupling coefficient.

Due to the fast response of FWM (~ several fs), it is suitable for high-speed signal processing. As a result, FWM is one of the most important phenomena in nonlinear optical signal processing. The applications of four-wave mixing are broad, including all-optical wavelength conversion, multicasting, demultiplexing and 3R regeneration. The use of optical signal processing can avoid the optical-electrical-optical conversion, which is the bottle-neck of today's signal processing technique. Also the power consumption and cost are lower when signals > 100 Gb/s are needed to be processed. FWM is utilized in some of the applications demonstrated in this thesis.

Cross-Absorption Modulation

As mentioned before, the modulation scheme in an EAM is achieved by changing the applied electric field. Instead of using an electrical approach to change the field amplitude, another method to manipulate the electrical field is by directing an intense light into the EAM. When an intense light is input to the EAM, the electric field is screened out and thus the transmission spectrum changes. An example is that when an intense data pattern is input to the EAM, several continuous wave (CW)

lasers from another input experience the change in the data-dependent transmission window. As a result, the CW lights are modulated by the data. So the data information is transferred to the CW lights. This phenomenon is named cross-absorption modulation (XAM). Details on the XAM effect have been previously explored. The XAM effect has been applied to different applications, including 3R regeneration [8] and optical demultiplexing [9].

Fig. 2.3.2 is a measured plot showing the characteristic of XAM. Two CW lights counter-propagate in an EAM with the one of larger power named as pump and the other named as probe. Without the pump light, the probe light is totally absorbed by the EAM. With the pump light, the electric field applied to the EAM is screened out and the power of the probe light is increased as shown in the figure. Also at different bias voltage, the responses of the XAM effect are different.

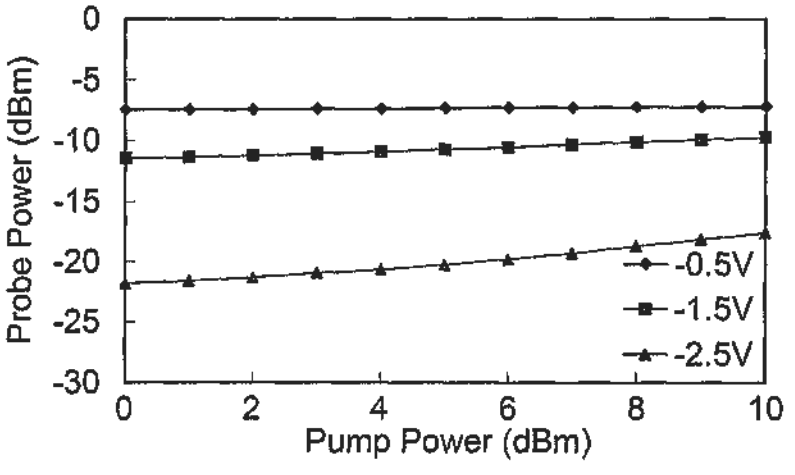

Fig. 2.3.2. *Characteristic of XAM effect in EAM.*

Optical Parametric Amplifier

The research on optical parametric amplifier (OPA) has been a hot topic in recent years. It exploits nonlinear optical properties of optical fibers. The main nonlinear effect utilized is the third order susceptibility χ^3 in silica fibers. Compared with the common optical amplifiers, OPA can provide some interesting properties as listed below [10]:

- Gain bandwidth increasing with pump power
- Arbitrary pump wavelength
- Large gain
- Wavelength conversion
- Low noise figure
- Unidirectional gain and spontaneous emission

Much research has been focused on the gain, bandwidth and the noise figure in the OPA. Besides acting as an optical amplifier, OPA has attracted much interest for applications in nonlinear optical signal processing due to its wavelength conversion properties and also fast response of the optical gain.

Usually OPA is pumped by an intense optical wave. Fig. 2.3.3 (a) shows a typical wavelength assignment in the case of one-pump OPA. The pump ω_p is located at the anomalous dispersion region (frequency lower than zero-dispersion frequency ω_0). A point to notice is that the pump wavelength must be close to the zero-dispersion wavelength to achieve the parametric amplification. The signal at ω_s is also located at the anomalous dispersion region to maintain phase-matching condition throughout the HNLF. Fig. 2.3.3 (a) also represents the situation before the pump and the signal are directed to a highly nonlinear fiber (HNLF). After HNLF,

OPA occurs and the situation is shown in Fig. 2.3.3 (b). An idler is generated at $\omega_i = 2\omega_p - \omega_s$. The pump energy is redistributed and transferred to signal and idler during the OPA process. As a result, the signal at ω_s experiences gain while the pump energy is depleted. Further details on OPA will be discussed in Chapter 7.

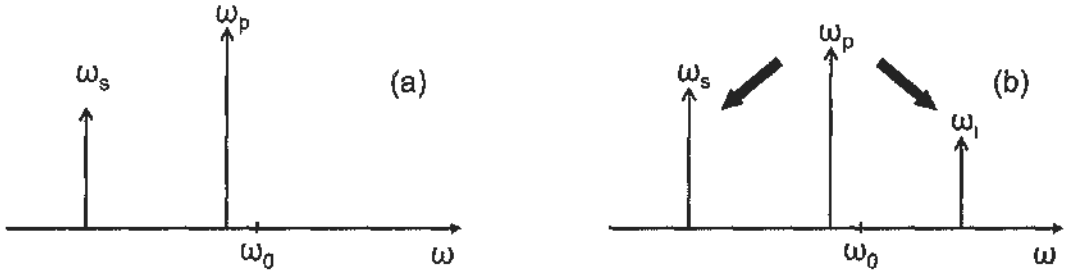

Fig. 2.3.3. *(a) Frequency assignment for pump and signal in the case of one-pump OPA, pump wavelength at anomalous dispersion region. (b) Frequency assignment after parametric process in HNLF.*

Pump Depletion Effect in Optical Parametric Amplifier

During amplification in an OPA, as mentioned before the pump energy is redistributed to the signal and the idler. As a result, the pump energy is decreased. This phenomenon is named pump depletion. For pump depletion operation, usually the pump should be of high peak power to achieve reasonable gain on the probe wavelength. As a result, it is easier to achieve pump depletion with pulsed pump rather than CW pump.

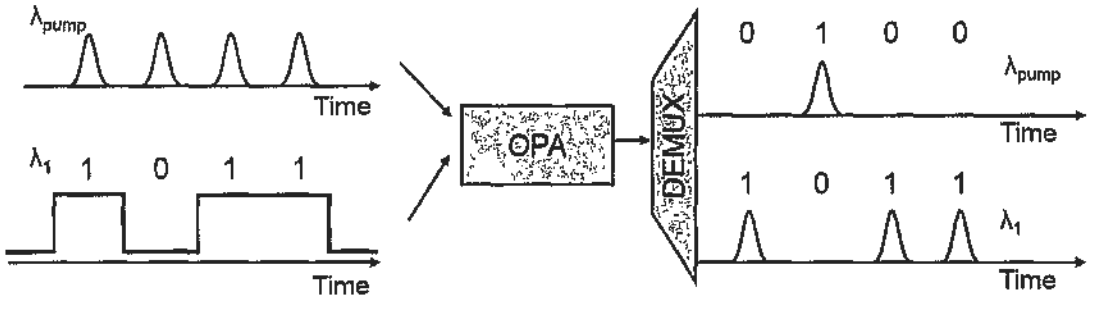

Fig. 2.3.4. *Operation principle of depletion in a pulsed-pump OPA*

Fig. 2.3.4 shows the principle of pump depletion effect. A pulse train at λ_{pump} acts as the pump in the OPA, while a fixed-pattern data "1011" at λ_1 acts as the probe. When there is a bit "1", the data experiences the gain provided by the pulse train. So the respective bit is amplified and its pulse format is converted from non-return-to-zero (NRZ) to return-to-zero (RZ). Also the pulses are depleted (or representing a bit "0"). When there is a bit "0", the correspondent pulse is not depleted (or representing a bit "1"). As a result, the waveform of the pulse train is always an inverse version of the data pattern, which is a NOT gate operation. By using the pump depletion effect, we can achieve different functions which will be demonstrated in Chapter 7.

2.4 Nonlinear Fibers

For nonlinear optical processing, the most important part is to select a suitable nonlinear medium. Nonlinear media include optical fibers, semiconductor devices, nonlinear crystal and waveguide devices. In this section, we focus the discussion on nonlinear fibers. The two types of nonlinear fibers are photonic crystal fiber and highly nonlinear step-index fiber. Both types of fibers are used in this thesis for different applications.

Photonic Crystal Fiber

The invention of photonics crystal fiber (PCF) happened only in last decade of the 20th century. It is also known as micro-structured fiber as its structure is different from the traditional core-cladding structure. It can be categorized into bandgap fiber, holey fiber and Bragg fiber. In this thesis, the PCF utilized is a triangular-core fiber [11]. The image of the PCF cross-section is shown in Fig. 2.4.1.

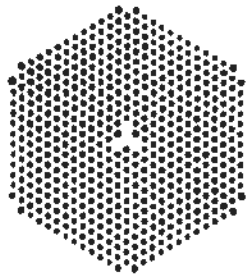

Fig. 2.4.1. *Cross section of a triangular-core PCF.*

The dispersion slope around 1550 nm is flat, with a value of 10^{-3} ps· km^{-1}nm^{-2}. The dispersion coefficient is ~ 1.3 ps·km^{-1}nm^{-1} in C-band. The nonlinearity is 11 W^{-1}km^{-1}. The loss of the PCF is 9.9 dB/km. However, only a short length of 64 m is used throughout the thesis as the light confinement is tight in the PCF. The required length can be relatively short for the occurrence of nonlinear effects.

As mentioned in Section 2.2, the dispersion in an optical fiber affects the efficiency for nonlinear optical signal processing. By the low dispersion and small dispersion slope of the PCF, the achieved 3-dB FWM bandwidth is 16 nm as shown in Fig. 2.4.2. Such a wide conversion bandwidth is beneficial to multi-channel signal processing. However, the PCF does not have a zero-dispersion wavelength. For applications in optical parametric amplifier, PCF is not a suitable candidate.

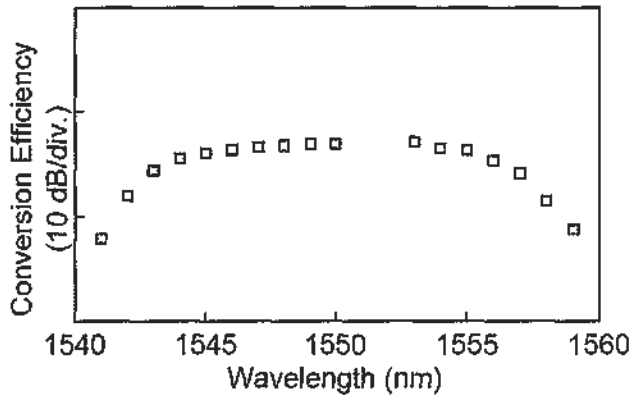

Fig. 2.4.2. *Conversion efficiency against wavelength in PCF. The conversion efficiency is defined as the intensity ratio between output idler and input signal.*

Highly Nonlinear Step-Index Fiber

Instead of using specially designed fiber for nonlinear effect generation, traditional optical fiber can also be used for nonlinear signal processing purposes with modifications. Usually, the core size of the optical fiber is reduced to increase light confinement and to shift the zero-dispersion wavelength to ~1550 nm. Also, different dopants are used to increase the refractive index contrast. In this thesis, the highly nonlinear fiber (HNLF) is doped with germanium. The length of the HNLF is 1 km. The nonlinear coefficient is 11.7 $W^{-1}km^{-1}$ around 1550 nm. The zero dispersion wavelength of the HNLF is 1549 nm, while the dispersion slope is less than 0.02 $ps \cdot km^{-1}nm^{-2}$ at 1550 nm. This HNLF will be utilized in OPA applications.

2.5 Wavelength Division Processing

Current technologies can process optical signals of 10 or 40 Gb/s using optical-electrical-optical conversion. However, for future development over 100 Gb/s, electronic processors can hardly handle the information at high speed. To continue utilizing the electronic equipment, one of the methods is to reduce the speed of optical signals using wavelength division processing. The concept is similar to multi-core central processing units (CPU) in computers. A high-speed signal is divided into multiple low-speed channels using multiple optical waves at different wavelengths. The repetition rate of individual channel depends on the number of wavelength utilized. Fig. 2.5.1 shows a schematic diagram of wavelength division processing.

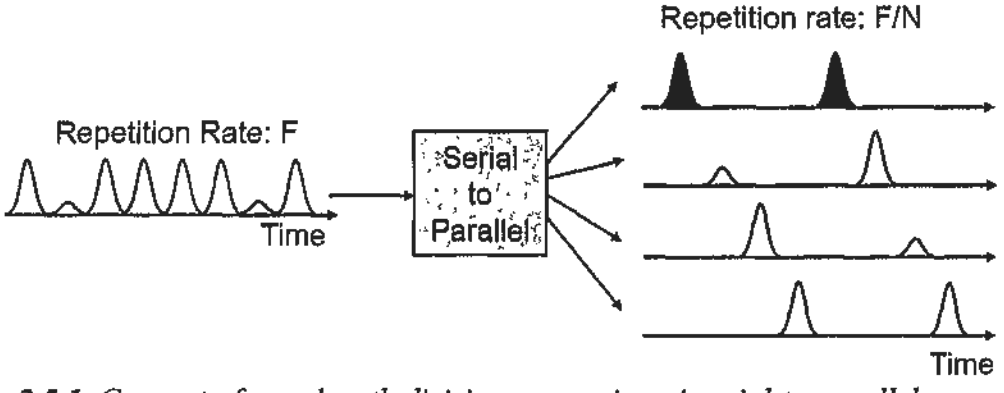

Fig. 2.5.1. *Concept of wavelength division processing. A serial-to-parallel processor is utilized as a gateway between high-speed signal and low-speed channels.*

For example, if the input data rate is at F and the number of channel is N, the repetition rate of individual channel is F/N, which is possible to be processed by electronic devices or low-speed optoelectronic devices. A serial-to-parallel processor is used to convert the high-speed signal into low-speed channels. It is worth mentioning that without the serial-to-parallel operation, the low-speed devices cannot handle the high-speed signals. The design and the applications of the serial-to-parallel processor is the main focus in this thesis.

2.6 Summary

In this chapter, we discussed the components and nonlinear effects that will be utilized in this thesis. For different applications, different nonlinear media should be adopted to maximize the performance. Detailed implementations of these effects and components will be discussed in later chapters.

2.7 References

[1] Adopted from the web, http://radio-weblogs.com/0105910/2004/07/18.html

[2] Adopted from the web, http://www.shf.de/en/communication/downloads/tutorial_notes/getfile/72/288/ mach-zehnder modulator

[3] P.J Winzer. and R.-J. Essiambre, "Advanced optical modulation formats," *Proceedings of the IEEE*, vol. 94, pp. 952 – 985, May 2006.

[4] J. D. Dow and D. Redfield, "Electroabsorption in semiconductors: the excitonic absorption edge," *Phys. Rev. B*, vol. 1, no. 8, pp. 3358 – 3371, April 1970.

[5] D. A. B. Miller, D. S. Chemla, T. C. Damen, A. C. Gossard, W. Wiegmann, T. H. Wood, and C. A. Burrus, "Band-edge electroabsorption in quantum well structures: the quantum-confined Stark effect," *Phys. Rev. Lett.*, vol. 53, no. 22, pp. 2173 – 2176, November 1984.

[6] G. P. Agrawal, "Nonlinear fiber optics," 4th edition, *Academic Press*, 2006.

[7] M. Hirano, T. Nakanishi, T. Okuno, and M. Onishi, "Silica-based highly nonlinear fibers and their application," *IEEE J. Sel. Topics. Quantum Electron.*, vol. 15, pp. 103 – 113, January/February 2009.

[8] K. K. Chow and C. Shu, "All-optical signal regeneration with wavelength multicasting at 6×10 Gb/s using a single electroabsorption modulator," *Opt. Express*, vol. 12, pp. 3050 – 3054, June 2004.

[9] E. J. M. Verdurmen, Y. Liu, G. D. Khoe and H. de Waardt, "Study on the limits of all-optical time-domain demultiplexing using cross-absorption modulation in an electroabsorption modulator," *IEE Proc. Optoelectron.* , vol. 153, pp. 75 – 83, April 2006.

[10] M. E. Marhic, "Fiber optical parametric amplifiers, oscillators and related devices," *Cambridge Univ. Press*, 2008.

[11] K. P. Hansen, J. R. Folkenberg, C. Peucheret, and A. Bjarklev, "Fully dispersion controlled triangular-core nonlinear photonic crystal fiber," *in Optical Fiber Communication Conference, Technical Digest (Optical Society of America, 2003)*, Atlanta, GA, March 2003, paper PD2-1.

3 Generation of Time- and Wavelength-Interleaved Laser Source

Optical pulses can be generated by many approaches including gain modulation of laser diodes [1], external modulation of laser beams with optical modulators and mode-locked fiber lasers/laser diodes [2 – 4]. Usually, an optical pulsed source is generated at a single central wavelength. For wavelength-division multiplexing optical system, multi-wavelength pulses are preferred as a single pulsed source can support multiple user channels. Different approaches have been proposed to generate multi-wavelength pulses with spectral slicing of a supercontinuum pulsed source [5] or multi-wavelength mode-locked semiconductor optical amplifier (SOA) or erbium-doped fiber amplifier (EDFA) lasers [6, 7].

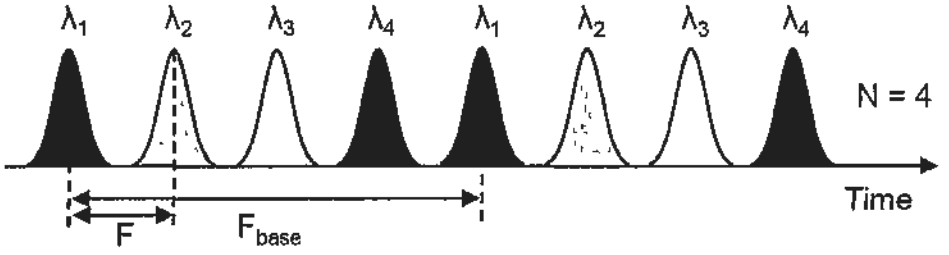

Fig. 3.1. *Profile of a time- and wavelength-interleaved laser source*

Instead of having all the pulses from a multi-wavelength pulsed source appearing at the same time, researches were carried out to generate pulses allocated in different time slots. One special case is that the wavelengths of the pulses are switching sequentially in time. It is named time- and wavelength-interleaved laser source. Fig. 3.1 shows a general time/wavelength profile of a time- and wavelength-interleaved pulsed source. It is shown that the wavelengths of pulses are switching from λ_1 to λ_4. As a result, time-to-wavelength mapping is achieved by the pulsed source – that means it has the capability to transfer different time information into

different wavelengths. This characteristic is very important when the pulsed source is applied to different applications.

Another important characteristic of time- and wavelength-interleaved pulsed source is that the bandwidth requirement on electronics is reduced. Also shown in Fig. 3.1 is that for individual wavelength channel, say for λ_1, the frequency is assumed to be F_{base}. As the frequency of the overall pulsed source is determined by the time spacing between adjacent channels, if the number of channel is N, the overall repetition rate of the pulsed source F becomes $F_{base} \times N$. For example, if the repetition rate of the individual channel is 10 GHz and there are four channels in the pulsed source, the overall repetition rate is 40 GHz. If more channels can be inserted in the pulsed source, higher repetition rate can be achieved, but the components used in the generation is only of 10 GHz bandwidth. However, to avoid inter-channel crosstalk between adjacent channels, the pulse width of an individual channel should be small enough. As a result, short pulse generation is a requirement for the time- and wavelength-interleaved pulses. To generate short pulses, different schemes can be adopted including the use of mode-locked lasers [2 – 4], pulse compression techniques [8 – 11] and soliton [12 – 14]. But to generate multi-wavelength short pulses, some other techniques should be utilized. Also to generate a time-interleaved laser pulse source, it is necessary to separate pulses of different wavelengths in the time domain.

To summarize, there are three requirements for the generation of time- and wavelength-interleaved pulses

1. Multi-wavelength pulse generation
2. Short pulse generation
3. Time spacing generation

To evaluate the quality of the generated pulsed source, the time-bandwidth product is an important parameter. Theoretically, we want to have an impulse response for each pulse which is represented by infinitely small pulse width. However, by Fourier transform, the bandwidth of the pulse is infinitely large. As a result, there is a tradeoff between bandwidth and pulse width. The product of these two parameters is named as time-bandwidth product. For different pulse profiles, the time-bandwidth products are different. Table 3.1 shows different time-bandwidth products:

***Table 3.1**: Time-bandwidth products of different pulse profiles*

Lorentzian	0.22
$Sech^2$	0.315
Gaussian	0.44

If the time-bandwidth product of the generated pulse is similar to that of a specific pulse profile, it is called a transform-limited pulse. If the difference between the theoretical value and the measured value is large, the pulse quality is not favorable as the bandwidth is not fully utilized. Also it is easily affected by dispersion as the pulsed source is chirped when the time-bandwidth product is large.

Previously, different approaches for the generation of time- and wavelength-interleaved pulses have been proposed, including sub-harmonic pulse gating in a self-seeded laser diode [15], harmonic mode-locking in a semiconductor optical amplifier (SOA) [16] or EDFA ring laser, multi-wavelength pulse carving with cascaded electro-optic modulators [17], and chirped pulse generation by supercontinuum process and chirped fiber Bragg grating [18]. In this chapter, we report three different schemes for the generation of time- and wavelength-interleaved laser source.

3.1 Cross-Absorption Modulation in Electro-Absorption Modulation and Group Velocity Dispersion by Chirped Fiber Bragg Grating

As mentioned before, the modulation scheme in an electro-absorption modulator (EAM) is achieved by changing the applied electric field. Instead of using an electrical approach to change the field amplitude, the optical approach to change the absorption spectrum is by cross-absorption modulation (XAM). Details on the XAM effect have been previously explored. The XAM effect has been applied to different applications, including 3R regeneration [19] and optical demultiplexing [20].

For pulse generation application, both electro-absorption effect and XAM effect can be adopted. However, a 10 GHz commercial available EAM can only generate pulses with pulse width of ~ 20 ps [21] which is too broad for the generation of time- and wavelength-interleaved pulses. On the other hand, XAM has a response time of less than 10 ps [22] which has a potential to generate short pulses with proper configuration. In the following, the generation of time- and wavelength-interleaved pulses will be described in details.

For the generation of time- and wavelength-interleaved pulses, we adopt the XAM effect in EAM to achieve multi-wavelength pulse generation. The schematic diagram of the pulse generation is shown in Fig. 3.1.1. The EAM is reversely biased at -3 V and all the CW lights from a WDM source are absorbed by the EAM in the absence of the mode-locked fiber laser (MLFL). The MLFL generates intense short pulses with a full-width half maximum (FWHM) pulse width of ~ 2 ps and average power of 13 dBm. The pulse shape is squared hyperbolic secant. When the output from MLFL is directed to the EAM, the intensity of the short pulse screens out the

electric field applied to the EAM. XAM occurs and the four CW lights are modulated by the pulses. A multi-wavelength pulsed source is thus generated.

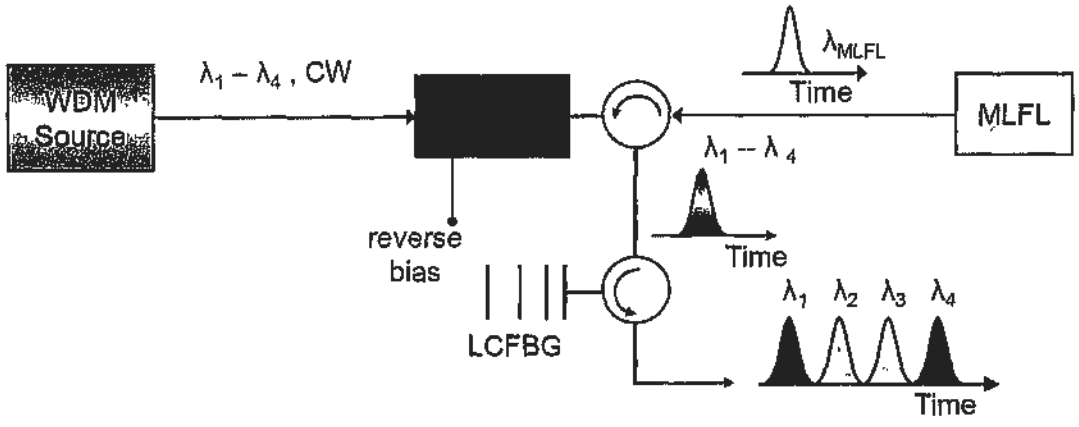

Fig. 3.1.1. *Schematic diagram for generation of time- and wavelength-interleaved pulses. LCFBG: linearly chirped fiber Bragg grating MLFL: mode-locked fiber laser.*

To achieve the time-interleaved property, a linearly chirped fiber Bragg grating is utilized. The reflection spectrum of the LCFBG is shown in Fig. 3.1.2. The bandwidth of the grating is ~ 30 nm with group velocity dispersion (GVD) of ~20 ps/nm. The relationship between wavelength and the introduced delay is shown in Fig. 3.1.3. It can be observed that the relative delay has a linear relationship with the wavelength.

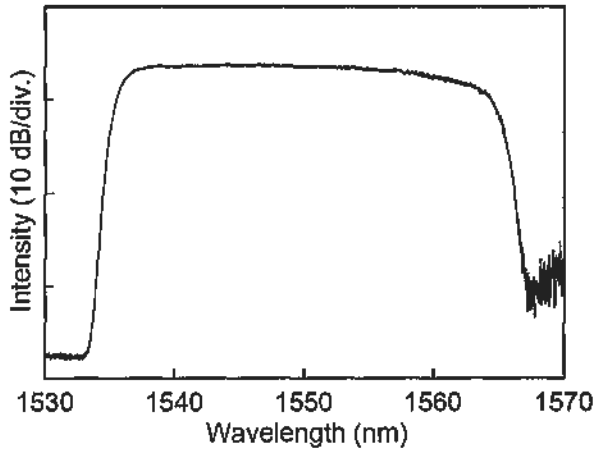

Fig. 3.1.2. *Reflection spectrum of the LCFBG.*

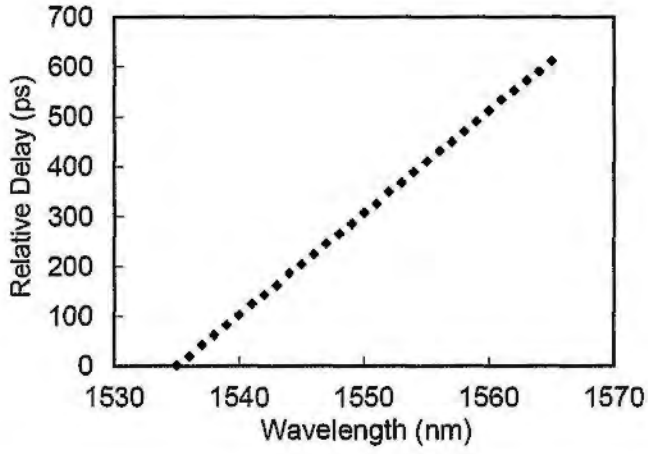

Fig. 3.1.3. *Relationship between relative delay and wavelength of the LCFBG.*

Inside the LCFBG, different wavelength components are reflected at different locations inside the grating. As a result, a time delay is introduced between adjacent channels in the multi-wavelength pulsed source. A time- and wavelength interleaved laser source is thus achieved. In the experimental setup, only 10 GHz components are needed: 10 GHz EAM and MLFL, but the repetition rate of the output pulses is of 40 GHz.

Waveforms of the time- and wavelength–interleaved pulses are shown in Fig. 3.1.4 (a) – (d). The time spacing between adjacent channels is 25 ps, making an overall repetition rate of 40 GHz. The pulse width of the individual channel is ~ 16 ps, as confirmed by measuring with a 500-GHz optical sampling oscilloscope. The extinction ratio of individual pulse channel is 25 dB. The optical spectrum of the pulsed source is shown in Fig. 3.1.5. The wavelength spacing is 1.25 nm, matching the dispersion value of the LCFBG (20 ps/nm). The time-bandwidth product (TBP) of the pulses is 0.472. Comparing with a transform-limited Gaussian pulse with TBP of 0.44, the pulsed source is slightly chirped. It is caused by the chirp introduced inside the EAM and also pulse broadening by the LCFBG.

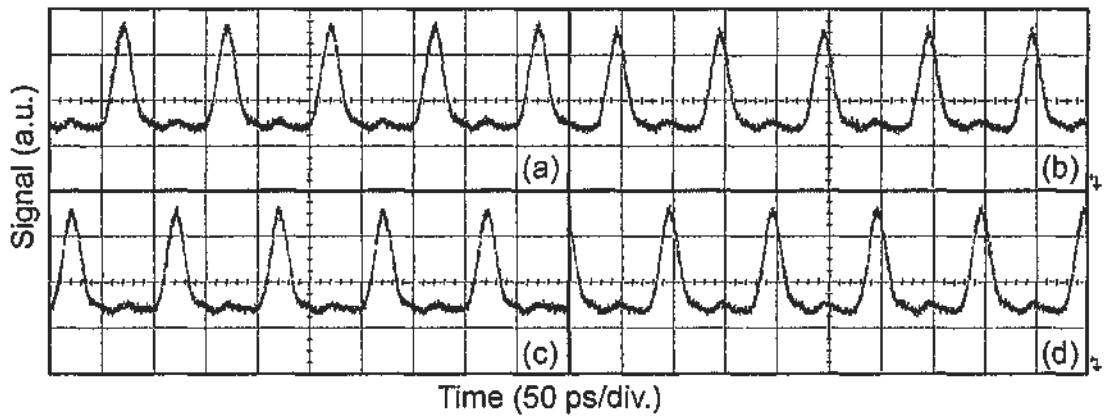

Fig. 3.1.4. *(a) – (d) Waveforms of the time- and wavelength-interleaved pulses. The time spacing between adjacent channels is 25 ps. (a) 1548.41 nm (b) 1549.66 nm (c) 1550.92 nm (d) 1552.17 nm.*

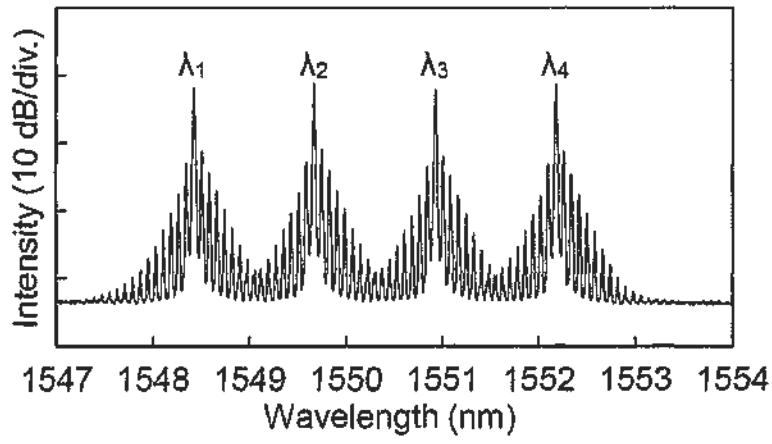

Fig. 3.1.5. *Optical spectrum of the time- and wavelength-interleaved pulse.*

Although we can obtain shorts pulses using XAM in EAM, several issues should be addressed:

1. The use of a MLFL is expensive. Although mode-locked laser diode (MLLD) can be used instead, additional optical amplifier is needed as usually MLLD has a low output optical power.
2. The bandwidth of EAM is around 20 – 30 nm. If additional pulsed channels are needed, the performances across different channels may vary.
3. EAM has a relatively high insertion loss of around 9 dB and is poorer than that of an electro-optic modulator. As a result, an optical amplifier is needed for

compensating the loss. As a result, the signal-to-noise ratio of the pulsed source degrades.

4. The LCFBG can be used to separate pulses in the time domain but it also broadens the pulse in each pulsed channel.

In conclusion, a time- and wavelength-interleaved laser source is generated by XAM in EAM with GVD provided by LCFBG. The pulse width obtained is ~ 16 ps. Although the pulse quality is satisfactory, further improvements are needed for generating the pulsed source.

3.2 Phase Modulation with Chirp Compensation

Instead of using EAM, phase modulator is used to generate time- and wavelength-interleaved pulses in this section. In general sense, phase modulator can generate instantaneous phase change on the input light beams and no intensity change is made. The phase change can also be viewed as a frequency change on the light beam, which means new frequency components are generated during phase modulation. As different frequency components travel at different speeds in a dispersive medium, pulses are generated at the output of the medium. The principle is illustrated in Fig. 3.2.1.

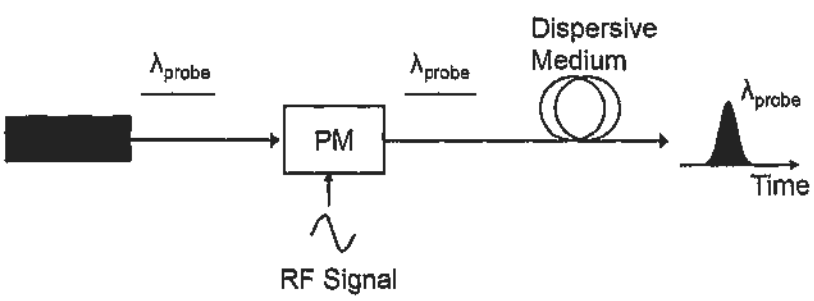

Fig. 3.2.1. *Principle of pulse generation with phase modulation and dispersive medium.*

A CW light from a laser diode is directed to the input of a phase modulator. The phase modulator is driven with a sinusoidal signal at a frequency F. After the phase modulation, new frequency components are generated at different time. By travelling in a dispersive medium, the CW light is compressed into pulses. The frequency of the pulses depends on that of the applied sinusoidal signal.

To optimize the output pulse width, the amplitude of the applied sinusoidal signal and the amount of dispersion must be well chosen at a specific repetition rate. The following equations present the relationship.

Assume that a CW light with angular frequency ω_0 is phase-modulated by a sinusoidal signal with frequency f_m, the field of the modulated light can be expressed as a summation of frequency components with Bessel amplitudes:

$$E(t) = E_0 \exp\left[j\omega_0 t - j\Delta\theta \sin 2\pi f_m t\right]$$
$$= E_0 \sum_{q=-\infty}^{+\infty} J_q(\Delta\theta) \exp\left[j(\omega_0 - 2\pi q f_m)t\right] \qquad [3.1]$$

where q is an integer, $\Delta\theta$ is the modulation index, and J_q is the Bessel function of first kind. In this case, the instantaneous frequency of the modulated light is given by

$$\nu(t) = \omega_0 / 2\pi - \Delta\theta f_m \cos(2\pi f_m t) \qquad [3.2]$$

and the maximum chirp rate is found to be

$$(\partial\upsilon / \partial t)_{\max} = \pm 2\pi f_m{}^2 \Delta\theta . \qquad [3.3]$$

Fig. 3.2.2 shows the frequency of the modulated light at different temporal positions [23]. The frequency components from ¼ fm to ¾ fm have higher frequencies than the CW light angular frequency, while those from 3/4 fm to 5/4 fm have lower frequencies. In normal dispersion, higher frequencies travel faster. So at the end of the fiber, the components from 1/4 to 3/4 f_m move to the right and catch up with the components from 3/4 to 5/4 f_m. As a result, pulse train can be generated with the peak at the frequency of $\omega_0/2\pi$.

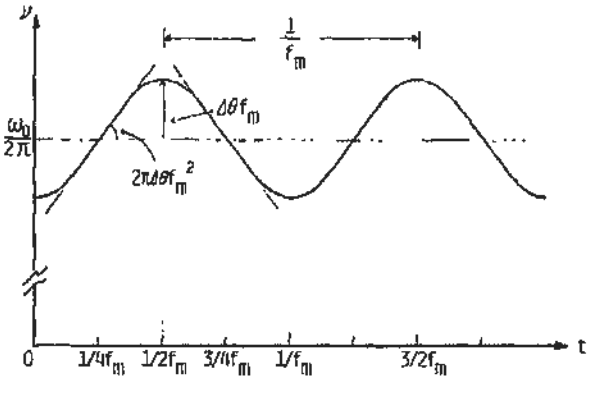

Fig. 3.2.2. *Instantaneous optical frequency of sinusoidally phase-modulated light [23].*

After passing through a dispersive medium, an additional phase delay is added to the light field. The field equation can be further expressed as

$$E(t) = E_0 \exp\left[j(\omega_0 - \theta_0)\right] \sum_{q=-\infty}^{+\infty} J_q(\Delta\theta) \bullet \exp\left[-j2\pi q f_m (t - \tau(\omega_0)) - j\pi q^2 f_m{}^2 (\partial\tau / \partial\upsilon)\right] \quad [3.4]$$

where $$\tau(\varpi) = \partial\theta / \partial\varpi \quad [3.5]$$

corresponds to the group delay the light experiences inside the dispersive medium and $\partial\tau / \partial\upsilon$ corresponds to the frequency dispersion of the group delay.

To obtain the shortest pulse, we define a bunching parameter B where

B = (frequency chirping rate) × (group delay dispersion)

$$= (\partial\nu / \partial t)_{extreme} \times (\partial\tau / \partial\upsilon) \approx \mp 2\pi f_m{}^2 \Delta\theta (\partial\tau / \partial\upsilon) \quad [3.6]$$

When B =1, the falling edge just catches up with the leading edge in the chirped optical field, and the pulses become highest and steepest [23]. Accordingly, at B =1,

$$(\partial\tau / \partial\upsilon) \approx -1/(2\pi f_m{}^2 \Delta\theta) \quad [3.7]$$

which is approximately the required dispersion for generating pulses with shortest pulse width at a specific modulation depth and modulation frequency.

As discussed in [23, 24], the shortest pulse width τ at a specific applied modulation index that can be achieved is defined as

$$\tau \approx 0.7 / 2\Delta\theta f_m \quad [3.4]$$

For generating a 10 GHz pulsed train, a 10 GHz sinusoidal signal is used for the modulation. The pi-voltage of the phase modulator is 5V, while the applied signal

voltage is 5V.The modulation index, defined as $\frac{Vsig}{V\pi} \bullet \pi$ (signal voltage divided by the modulator pi-voltage), is π. As a result, the shortest pulse achievable is 11.14 ps.

To generate time- and wavelength-interleaved pulses with the proposed scheme, the wavelength spacing needs to be determined. For a 40 GHz time- and wavelength-interleaved pulsed source, the time spacing between adjacent pulses is 25 ps. An 8.4-km standard single-mode fiber is used for the dispersive medium. The total group velocity dispersion (GVD) D is 142.8 ps•nm^{-1}. Assuming that the pulse separation between adjacent pulses is Δt, the period of the individual pulsed channel is T, the wavelength separation is Δλ, the total GVD is D, we can conclude an equation:

$$\Delta\lambda \bullet D = n \bullet T \pm \Delta t$$

By substituting the above parameters with n = 2, T = 100ps, Δt =25 ps, D = 142.8 ps•nm^{-1}, the required wavelength spacing is either 1.23 nm or 1.57 nm.

The experimental setup is shown in Fig. 3.2.3. Four CW lights from a WDM source are modulated by a phase modulator. The wavelength spacing between adjacent channels is ~1.25 nm. After passing through an 8.4-km SMF, time- and wavelength-interleaved pulses can be generated.

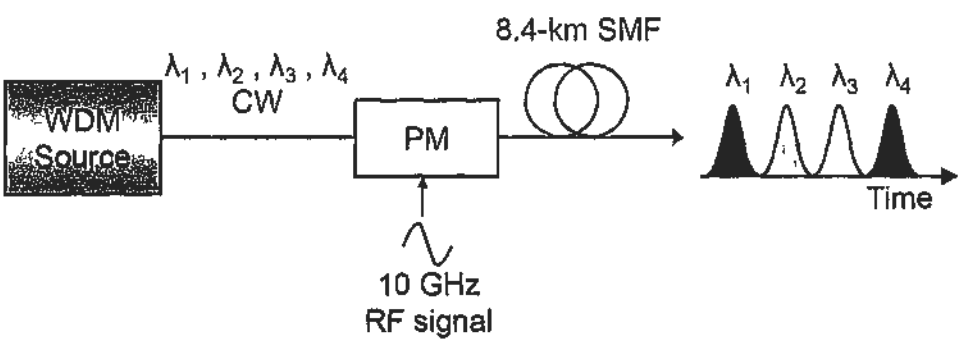

Fig. 3.2.3. *Experimental setup for generating 40 GHz time- and wavelength-interleaved pulses.*

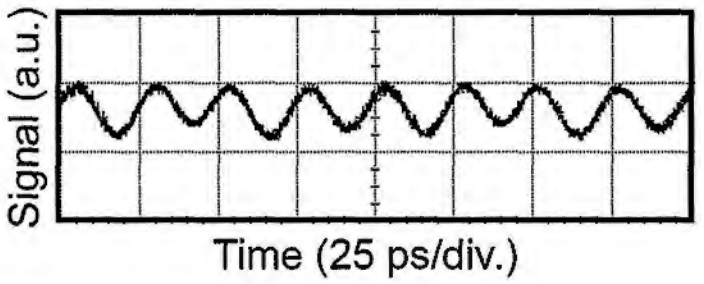

Fig. 3.2.4. *Waveform of the 40 GHz time- and wavelength-interleaved pulses.*

The waveform of the pulsed source is shown in Fig. 3.2.4. The overall frequency of the pulsed source is 40 GHz, while the fundamental frequency is 10 GHz for each of the four pulsed channels. The spectrum of the pulsed source is shown in Fig. 3.2.5. The pulses are generated at 1548.35, 1549.60, 1550.85, and 1552.10 nm, respectively.

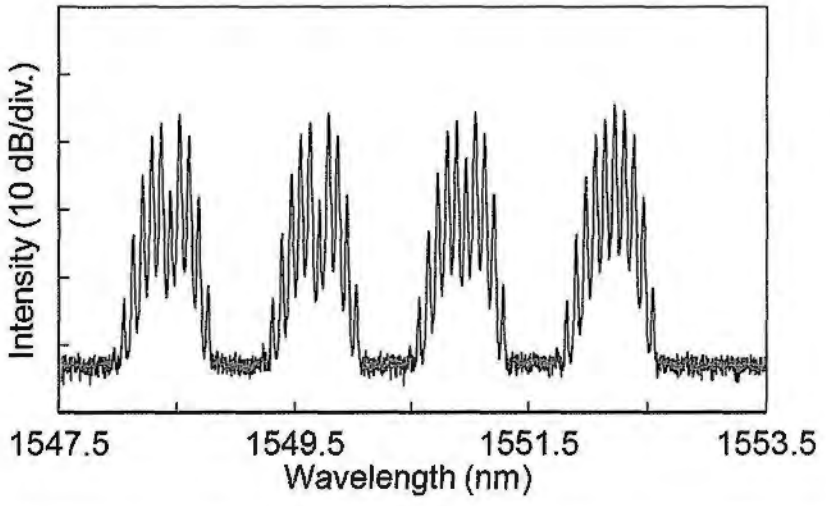

Fig. 3.2.5. *Optical spectrum of the 40 GHz time- and wavelength-interleaved pulsed source.*

The pulse width of the pulses is ~ 14 ps for each channel. The pulse width is larger than that of the shortest pulse width achievable with the π modulation index. It is because the chirp is not fully compensated using the 8.4-km optical fiber. The 3-dB bandwidth of an individual pulsed channel is 0.326 nm, measuring using the optical spectrum analyzer. Compared with the Gaussian transform-limited TBP of 0.44, the TBP of the generated pulses is 0.558, again showing that the chirp exists.

As mentioned before, by changing the applied modulation index, the pulse width can be adjusted. Table 3.2.1 shows the relationship between the applied RF power and the output pulse width.

***Table 3.2.1**: Relationship between input RF power and output pulse width*

RF Power (dBm)	Pulse width (ps)
19	19
20	18.2
21	16.8
22	15.2
23	13.7
24	12.7
25	12.1
26	11.6

The adjustment of the RF power is achieved by using a tunable RF attenuator. A 500-GHz optical sampling oscilloscope (OSO) is used to measure the pulse width. The tuning range of the pulse width is from 11.6 ps to 19 ps, limited by the tuning range of the attenuator. The tunability of pulse width can help to adopt the pulsed source in optical systems with different pulse width requirement.

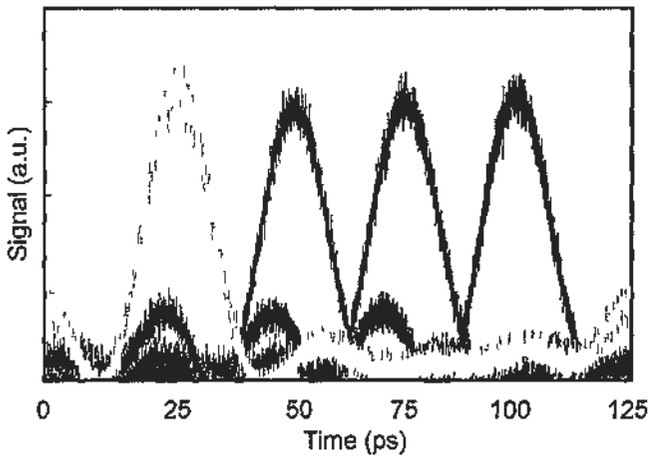

***Fig. 3.2.6.** Waveform of 40 GHz time- and wavelength-interleaved pulses captured with a 500-GHz optical sampling oscilloscope.*

As the response of the oscilloscope used to capture the waveform in Fig. 3.2.3 is only 17 ps, the pulse profile is further characterized using the OSO. As the OSO can only detect a single-wavelength signal, the overall pulse profile is superimposed after individual detection. The reconstructed waveform is shown in Fig. 3.2.6. With the high-speed detection, the overlapping part between adjacent pulses can now be resolved. Pedestal is observed at the leading and trailing edges and it occupies the time slot of adjacent channel. The phenomenon is also observed as reported in [11], showing that it is an inherent property of the proposed generation scheme. It is not a favorable characteristic because during nonlinear optical signal processing, cross-talk may occur between the adjacent channels because of this overlapping. To solve this problem, we make use of another generation approach and it will be discussed in Section 3.3.

3.3 Phase and Amplitude Modulation with Chirp Compensation

As discussed in the last section, the width of the pulses generated using phase modulator with chirp compensation by GVD is ~ 14 ps. However, the pedestals appearing at leading edge may distort the performance during nonlinear optical signal processing with the generated time- and wavelength-interleaved laser source. In this section, we replace the phase modulator with a dual-drive Mach-Zehnder modulator (DDMZM) and both amplitude and phase modulation are performed on the CW light. In previous reports [25 – 27], short pulses were generated by driving the DDMZM with large RF powers applied on both arms. However, due to the equipment limit, we can only drive the DDMZM at one of the arms. In this section, we will discuss the generation of time- and wavelength-interleaved pulses with DDMZM with chirp compensation by GVD.

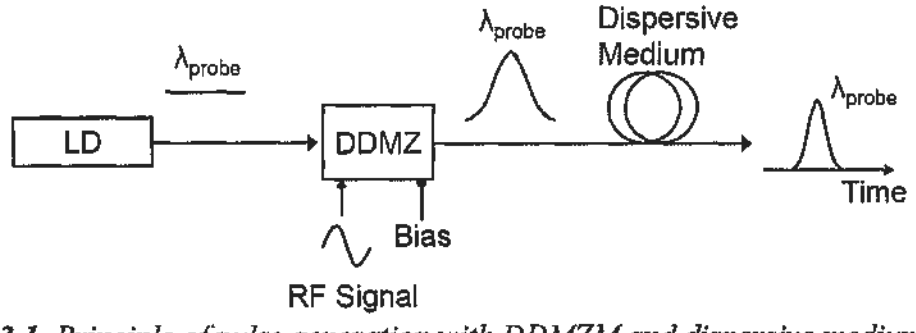

Fig. 3.3.1. *Principle of pulse generation with DDMZM and dispersive medium.*

Fig. 3.3.1 shows the experimental setup for generating pulses with a DDMZM. The setup is identical to the one using a PM. A CW light is directed to the input of the DDMZM. The DDMZM is driven with a sinusoidal signal with a RF power of 23 dBm. The V_π of the DDMZM is 5.5V. The bias of the DDMZM is optimized to generate the largest number of sidebands. After the DDMZM, both amplitude and phase modulation are applied to the CW light. An 8.4-km SSMF is

used to compensate for the chirp induced on the CW light. After the SSMF, short pulses are generated.

Fig. 3.3.2 shows the profile of a 10-GHz pulse train generated with DDMZM and chirp compensation. The waveform was captured with a 500-GHz OSO. The pulse width is 18.1 ps. Although the pulse width is not as short as that generated with a phase modulator, the pedestals are clearly removed. We anticipate that a higher RF power can decrease the pulse width as the V_π of the DDMZM is higher than that of phase modulator.

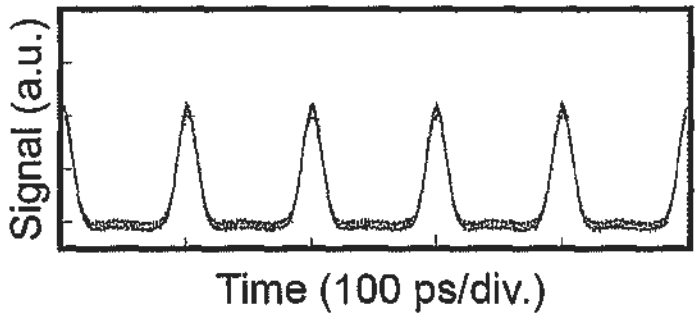

Fig. 3.3.2. *Waveform of a 10 GHz pulse train generated with DDMZM and chirp compensation. The pulse width is 18.1 ps, measured with a 500-GHz OSO*

Table 3.3.1*: Relationship between input RF power and output pulse width*

RF Power (dBm)	Pulse width (ps)
19	23.7
20	23.2
21	21.3
22	19.5
23	18.1
24	16.9
25	15.9
26	15.7

Again, to demonstrate the tunability of the pulse width, the relationship between the pulse width and the applied RF power is studied and is shown in Table 3.3.1. The pulse width can be tuned from 15.7 ps to 23.7 ps. However, pedestals are observed when the RF power is larger than 25 dBm due to the nonlinear phase

applied on the DDMZM. It is shown that the pulse profile is favorable for the generation of time- and wavelength-interleaved pulsed source as the crosstalk between adjacent channels is reduced.

As a demonstration, we generate 40 GHz time- and wavelength-interleaved pulses with four pulsed channels. The experimental setup is shown in Fig. 3.3.3. Four CW lights from a WDM source are modulated by a DDMZM. The wavelength spacing between adjacent channels is ~1.25 nm. The spacing is governed by the GVD of 8.4-km SSMF, which is 142.8 ps•nm^{-1}. The applied RF power is 25 dBm. The DC bias is optimized for generating the shortest pulse. After passing through the optical fiber, time- and wavelength-interleaved pulses can be generated.

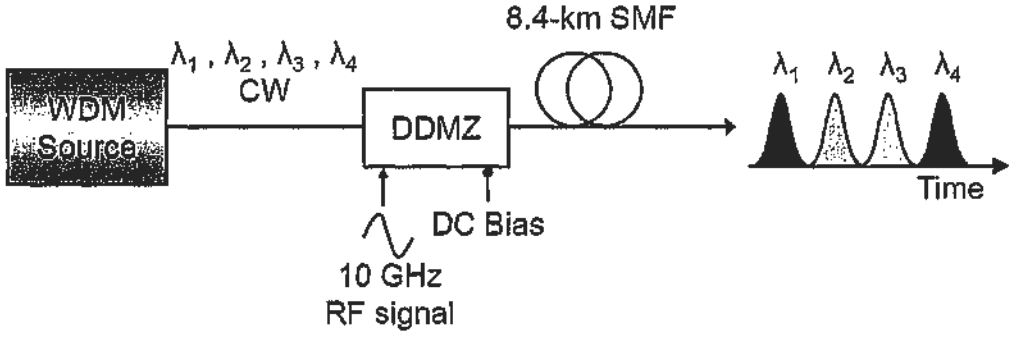

Fig. 3.3.3. *Experimental setup for generating 40 GHz time- and wavelength-interleaved pulse train generated with DDMZM and chirp compensation.*

The overall time profile is shown in Fig. 3.3.4. The measured pulse width is 15.9 ps. The optical spectrum of the pulsed source is shown in Fig. 3.3.5. The pulses are generated at 1547.80, 1549.04, 1550.35, 1551.61 nm respectively.

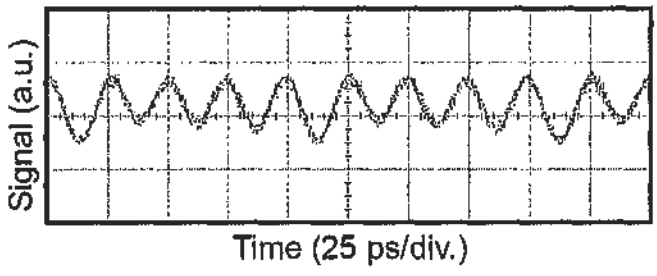

Fig. 3.3.4. *Waveform of a 40 GHz pulse train generated with DDMZM and chirp compensation. The pulse width is 15.9 ps.*

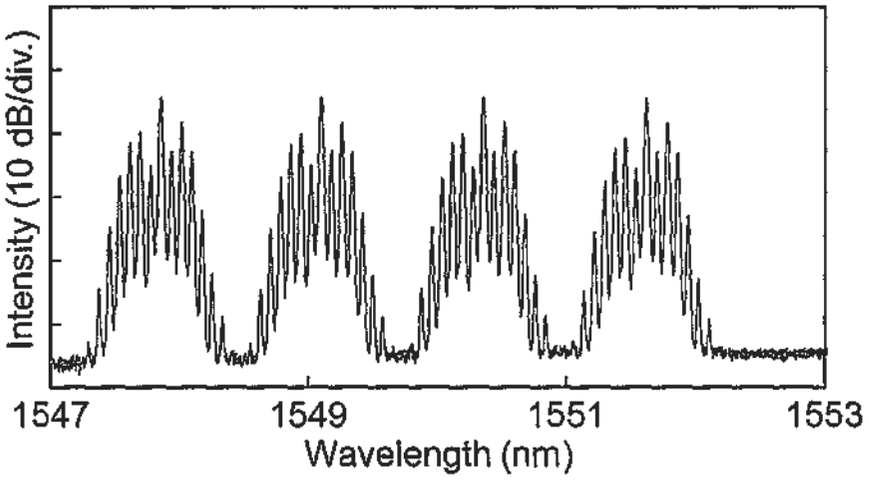

Fig. 3.3.5. *Optical spectrum of the 40 GHz time- and wavelength-interleaved pulses. Channel spacing: 1.25 nm.*

Again we calculate the TBP of the generated pulse source. The 3-dB bandwidth is estimated to be ~ 0.3 nm and the pulse width is 15.9 ps. So the calculated TBP is 0.596, larger than the Gaussian transform-limited value of 0.44. The dispersive medium used during the experiment should be further optimized to obtain the shortest pulse width achievable.

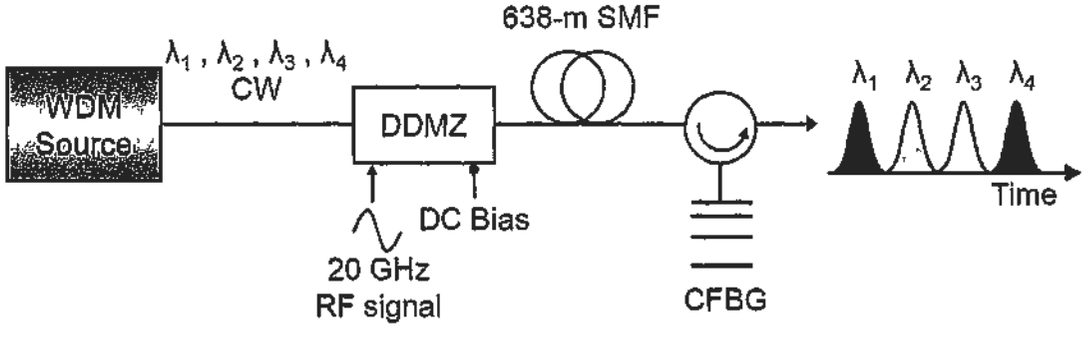

Fig. 3.3.6. *Experimental setup for generating 80 GHz time- and wavelength-interleaved pulse train generated with DDMZM and chirp compensation. CFBG: chirped fiber Bragg grating.*

Using similar approach, we can generate 80 GHz time- and wavelength-interleaved pulses by using a high-speed modulator. The experimental setup is shown in Fig. 3.3.6. A 40 GHz DDMZ is used for both amplitude and phase modulation.

Four CW lights are modulated by the DDMZ. The sinusoidal signal is of 20 GHz and the RF power is 25 dBm. The V_π of the DDMZ is 3.5 V, so the modulation depth $\Delta\theta$ is ~1.14π. The channel spacing is ~2 nm, optimized for the time spacing of 12.5 ps and reduced crosstalk between adjacent channels. The dispersive media include a 638-m SSMF and a chirped fiber Bragg grating with dispersion of 20 ps/nm. The total dispersion applied is ~30.8 ps/nm. After passing through the dispersive media, 80 GHz time- and wavelength-interleaved pulsed source is generated.

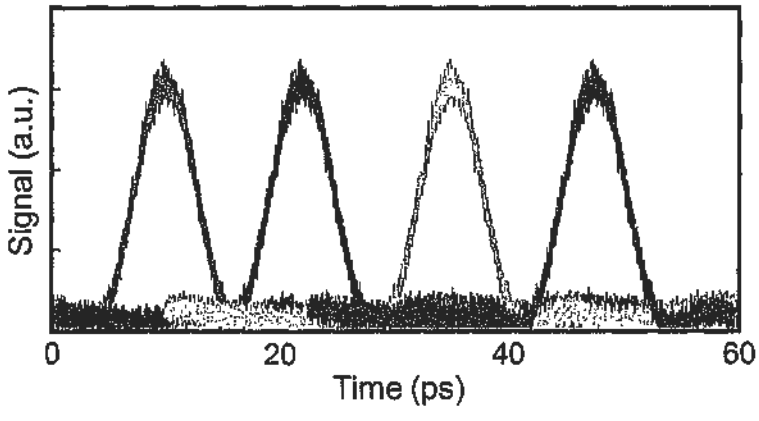

Fig. 3.3.7. *Time profile of the 80 GHz time- and wavelength-interleaved pulsed source. The trace is captured with a 500-GHz optical sampling oscilloscope.*

The generated pulses are detected using a 500-GHz optical sampling oscilloscope. The pulse profile is shown in fig. 3.3.7. The measured pulse width is 5.9 ps. It is worth mentioning that the overlapping between adjacent pulses is not serious. It can be anticipated that the crosstalk between adjacent pulsed channels is be negligible when the pulsed source is applied in nonlinear optical signal processing.

Fig. 3.3.8 shows the spectrum of the 80-GHz pulsed source. The pulses are generated at 1547.18, 1549.26, 1551.35, and 1553.42 nm respectively. The 3-dB bandwidth of an individual channel is 0.63 nm. As a result, the calculated TBP is 0.464, close to the theoretical value of 0.44 considering a Gaussian pulse profile. The pulsed source is nearly transformed-limited. To further increase the speed of the

pulsed source, several issues should be considered. Firstly, as shown in Fig. 3.3.8, spectral overlapping is not yet a problem at this repetition rate. However, when the repetition rate goes over 100 GHz, the wavelength spacing should be further increased to avoid spectral overlapping. The wide spectrum may also lead to walk-off effect during nonlinear optical signal processing. The research on the signal processing issues using high-speed pulses will be an important future direction.

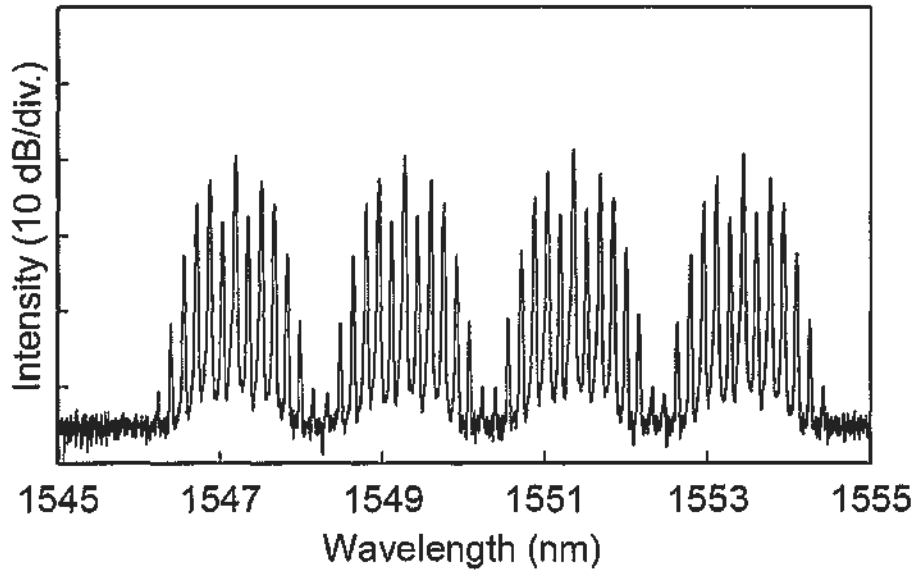

Fig. 3.3.8. *Optical spectrum of the 80 GHz time- and wavelength-interleaved pulsed source.*

3.4 Summary

In this chapter, we demonstrated three different approaches for generation of 40 GHz time- and wavelength-interleaved pulses. The generation methods and characterization of pulses have been discussed in details. The following table concludes the three approaches:

***Table 3.4.1**: Comparison among three generation schemes*

	XAM in EAM and GVD by LCFBG	Phase modulation with GVD	Phase and amplitude modulation with GVD
Cost	High	Low	Low
Pulse width	Depends on MLFL	Depends on modulation depth and modulator properties	Depends on modulation depth and modulator properties
Required optical power	High	Low	Low
Power consumption	High (due to the use of MLFL)	Low	Low
Polarization Sensitivity	Low	High	High
Insertion loss	High	Low	Low
TBP	0.472	0.558	0.596

Although EAM can provide advantages of low polarization sensitivity and small size, the insertion loss and required optical power are much larger than that of phase modulator and DDMZM. Comparing phase modulator and DDMZM, the latter can generate pulses with better pulse profile. Although the pulse width generated by DDMZM is larger than that by the phase modulator, using a dual-drive approach can help to further reduce the pulse width.

Moreover, we successfully generated nearly transformed-limited 80 GHz time- and wavelength-interleaved pulses using DDMZM and chirp compensation. A

very short pulse width of 5.9 ps is achieved and further extension to the processing of 80 Gb/s data is ready.

After the generation of time- and wavelength-interleaved laser source, in following chapters we will discuss the applications of the pulsed source and their respective performance.

3.5 References

[1] M. Nakazawa, K. Suzuki, and Y. Kimura, "Transform-limited pulse generation in the gigahertz region from a gain-switched distributed-feedback laser diode using spectral windowing," *Opt. Lett.*, vol. 15, pp. 715 – 717, June 1990.

[2] C. Wu and N. K. Dutta, "High-repetition-rate optical pulse generation using a rational harmonic mode-locked fiber laser," *IEEE J. Quantum Electron.*, vol. 36, pp. 145 – 150, February 2000.

[3] H. Schmeckebier, G. Fiol, C. Meuer, D. Arsenijević, and D. Bimberg, "Complete pulse characterization of quantum dot mode-locked lasers suitable for optical communication up to 160 Gbit/s," *Opt. Express*, vol. 18, pp. 3415 – 3425, February 2010.

[4] C. X. Yu, H. A. Haus, E. P. Ippen, W. S. Wong, and A. Sysoliatin, "Gigahertz-repetition-rate mode-locked fiber laser for continuum generation," *Opt. Lett.*, vol. 25, pp. 1418 – 1420, October 2000.

[5] T. Morioka, K. Mori, S. Kawanishi, and M. Saruwatari, "Multi-WDM-channel, Gbit/s pulse generation from a single laser source utilizing LD-pumped supercontinuum in optical fibers," *IEEE Photon. Technol. Lett.*, vol. 6, no. 3, pp.365 – 368, March 1994.

[6] K. Vlachos, K. Zoiros, T. Houbavlis, and H. Avramopoulos, "10 × 30 GHz pulse train generation from semiconductor amplifier fiber ring laser," *IEEE Photon. Technol. Lett.*, vol. 12, no. 1, pp.25 – 27, January 2000.

[7] J. Yao, J. Yao, and Z. Deng, "Multiwavelength actively mode-locked fiber ring laser with suppressed homogeneous line broadening and reduced supermode noise," *Opt. Express,* vol. 12, pp. 4529 – 4534, September 2004.

[8] W. J. Tomlinson, R. H. Stolen, and C. V. Shank, "Compression of optical pulses chirped by self-phase modulation in fibers," *J. Opt. Soc. Am. B*, vol. 1, pp. 139 – 148, April 1984.

[9] A. O. J. Wiberg, C.-S. Brès, B. P. P. Kuo, J. X. Zhao, N. Alic, and S. Radic, "Pedestal-free pulse source for high data rate optical time-division multiplexing based on fiber-optical parametric processes," *IEEE J. Quantum Electron.*, vol. 45, pp. 1325 – 1330, November 2009.

[10] T. B. Iredale, M. D. Pelusi, and B. J. Eggleton , "40 GHz sub-picosecond pulse generation from a Mach-Zehnder modulator and its application to 320 Gb/s OTDM," *in OSA Tech. Digest, OFC/NFOEC 2009*, San Diego, CA, paper OWS6.

[11] T. Komukai, T. Yamamoto, and S. Kawanishi, "Optical pulse generator using phase modulator and linearly chirped fiber Bragg gratings," *IEEE Photon. Technol. Lett.*, vol. 17, pp. 1746 – 1748, August 2005.

[12] K. R. Tamura and M. Nakazawa, "54-fs, 10-GHz soliton generation from a polarization-maintaining dispersion-flattened dispersion-decreasing fiber pulse compressor," *Opt. Lett.*, vol. 26, pp. 762 – 764, June 2001.

[13] A. C. Scott, F. Y. F. Chu, and D. W. McLaughlin, "The soliton: A new concept in applied science," *Proc. of the IEEE*, vol. 61, no. 10, pp. 1443 – 1483, October 1973.

[14] L. F. Mollenauer and R. H. Stolen, "The soliton laser," *Opt. Lett.*, vol. 9, pp. 13 – 15, January 1984.

[15] K. L. Lee, C. Shu, and H. F. Liu, "Subharmonic pulse-gating in self-seeded laser diodes for time- and wavelength-interleaved picosecond pulse generation," *IEEE J. Quantum Electron.*, vol. 40, pp. 205 – 213, March 2004.

[16] K. L. Lee and C. Shu, "Switching-wavelength pulse source constructed from a dispersion-managed SOA fiber ring laser," *IEEE Photon. Technol. Lett.*, vol. 15, pp. 513 – 515, April 2003.

[17] A. H. Gnauck, R. M. Jopson, R. W. Tkach, C. J. McKinstrie, and S. Radic, "Serial-to-parallel demultiplexing using WDM sampling pulses," *IEEE Photon. Technol. Lett.*, vol. 21, pp. 97 – 99, Jan. 2009.

[18] P. J. Almeida, P. Petropoulos, F. Parmigiani, M. Ibsen, and D. J. Richardson, "OTDM add-drop multiplexer based on time-frequency signal processing," *J. Lightwave Technol.*, vol. 24, pp. 2720 – 2732, July 2006.

[19] K. K. Chow and C. Shu, "All-optical signal regeneration with wavelength multicasting at 6×10 Gb/s using a single electroabsorption modulator," *Opt. Express*, vol. 12, pp. 3050 – 3054, June 2004.

[20] E. J. M. Verdurmen, Y. Liu, G. D. Khoe and H. de Waardt, "Study on the limits of all-optical time-domain demultiplexing using cross-absorption modulation in an electroabsorption modulator," *IEE Proc. Optoelectron.* , vol. 153, pp. 75 – 83, April 2006.

[21] T. E. Murphy, "10-GHz 1.3-ps pulse generation using chirped soliton compression in a Raman gain medium," *IEEE Photon. Technol. Lett.*, vol. 14, pp. 1424 – 1426, October 2002.

[22] L. Huo, Y. Yang, Y. Nan, C. Lou, and Y. Gao, "A study on the wavelength conversion and all-optical 3R regeneration using cross-absorption modulation in a bulk electroabsorption modulator," *J. Lightwave Technol.*, vol. 24, pp. 3035 – 3044, August 2006.

[23] T. Kobayashi, H. Yao, K. Amano, Y. Fukushima, A. Morimoto, and T. Sueta, "Optical pulse compression using high-frequency electrooptic phase

modulation," *IEEE J. Quantum Electron.*, vol. 24, pp. 382 – 387, February 1988.

[24] B. J. Bortnik and H. R. Fetterman, "High-speed photonically assisted analog-to-digital conversion using a continuous wave multiwavelength source and phase modulation," *Opt. Lett.*, vol. 33, pp. 2230 – 2232, October 2008.

[25] T. Sakamoto, T. Kawanishi, and M. Tsuchiya, "10 GHz, 2.4 ps pulse generation using a single-stage dual-drive Mach–Zehnder modulator," *Opt. Lett.*, vol. 33, pp. 890 – 892, April 2008.

[26] I. Morohashi, T. Sakamoto, H. Sotobayashi, T. Kawanishi, I. Hosako, and M. Tsuchiya, "Widely repetition-tunable 200 fs pulse source using a Mach–Zehnder-modulator-based flat comb generator and dispersion-flattened dispersion-decreasing fiber," *Opt. Lett.*, vol. 33, pp. 1192 – 1194, June 2008.

[27] K. Wang and J. Li, "160 Gbit/s OTDM system based on 40 GHz optical pulses generated using simultaneous two-arm modulation of a Mach-Zehnder modulator," *in 35th European Conference and Exhibition on Optical Communication (ECOC)*, September 2009, Vienna, Austria, paper P2.12.

4 Sampling of Analog Signals Using Time- And Wavelength-Interleaved Pulses

In Chapter 3, we introduced the generation of time- and wavelength-interleaved pulses. As mentioned before, the pulsed source can help to reduce the bandwidth requirement on electronics. For high-speed optical signals, it is difficult to directly analyze the information using traditional electronic devices. Also it is difficult to process the high-speed signals using low-speed semiconductor devices such as SOA and EAM. By using time- and wavelength-interleaved pulses, wavelength-division all-optical sampling and photonic analog-to-digital conversion (ADC) for analog signals can be achieved.

In Section 4.1 we mainly focus on the principle of all-optical sampling and discuss the performance of the approach. In Section 4.2 we briefly describe the principle of a photonic ADC.

4.1 All-Optical Sampling

High-speed all-optical sampling is of importance in optical communications owing to its uniqueness in real-time signal monitoring and performance evaluation. Different approaches have been demonstrated to achieve optical sampling. Examples are four-wave mixing (FWM) in a semiconductor optical amplifier (SOA) [1], two-photon absorption in a semiconductor cavity [2], and sum frequency generation in a periodically poled $LiNbO_3$ crystal [3]. All-optical sampling has been widely adopted for use in different applications, including eye-diagram measurement [4], high-speed optical time-division-multiplexed signal measurement [5], and photonic analog-to-digital converter [6]. Apart from communications, optical sampling is also used in other areas including microwave amplifier analysis [7] and THz resonator array characterization [8]. In this chapter, we will discuss how time- and wavelength-interleaved laser source plays its role in all-optical sampling application.

4.1.1 Introduction

As discussed in Chapter 3, different approaches have been proposed to generate the time- and wavelength-interleaved pulses. In this experiment, the pulses are generated by multiwavelength cross-absorption modulation (XAM) in an electro-absorption modulator (EAM) together with group velocity dispersion in a linearly chirped fiber Bragg grating (LCFBG). We demonstrate 40 GSample/s (GS/s) all-optical sampling of an arbitrary optical waveform using four-wave mixing (FWM) in a 64-m highly nonlinear photonic crystal fiber (PCF) [10]. The time separation between adjacent wavelengths is governed by the group velocity dispersion provided by the LCFBG. This approach does not depend on multiple fiber delay lines that often require precise trimming of fibers to match the relative delay times. Owing to the small dispersion and dispersion slope of the PCF, a wide FWM bandwidth is obtained. As a result, multiwavelength FWM is supported over a large wavelength range. The sampled outputs are distributed sequentially among four wavelengths, each operated at a frequency of 10-GHz. By combining data obtained from the four channels, 40 GS/s all-optical wavelength division sampling is achieved.

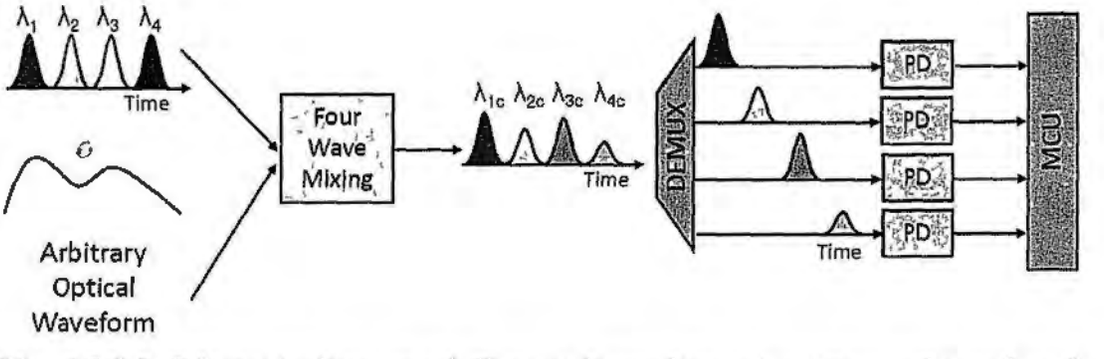

Fig. 4.1.1.1. *Schematic diagram of all-optical sampling using time- and wavelength-interleaved pulses. PD: photodetector. DEMUX: demultiplexer. MCU: microprocessor*

The schematic diagram of the approach is shown in Fig. 4.1.1.1. The time- and wavelength-interleaved pulses are combined with an arbitrary optical waveform. After four-wave mixing, the amplitudes of the wavelength-converted pulses are modified by the arbitrary waveform. By using a wavelength demultiplexr or arrayed-waveguide grating, individual channels are detected by low-speed photodetector, while the overall sampling is four times of the individual channel. The data of the four channels are combined in a computer or microprocessor and the original waveform can be reconstructed.

4.1.2 Experimental Setup

The experimental for all-optical sampling is shown in Fig. 4.1.2.1. Four CW lasers with adjacent wavelength spacing of 1.25 nm and operated around 1550 nm are obtained from a WDM optical source. The outputs are combined with optical couplers. The combined output has a power of 4.8 dBm and is directed to a 10-GHz EAM biased at -1.8V. A 1564-nm 10-GHz mode-locked fiber laser (MLFL) with an average power of 13.1 dBm is fed to the other port of the EAM via an optical circulator. XAM takes place between the counter-propagating CW lights and the mode-locked pulses at the EAM. The MLFL pulses generate electron-hole pairs that screen the applied electric field, thus allowing the CW lights to transmit through the EAM. Therefore, the CW inputs are modulated at 10 GHz and a non-inverting 10-GHz multiwavelength pulsed source is obtained.

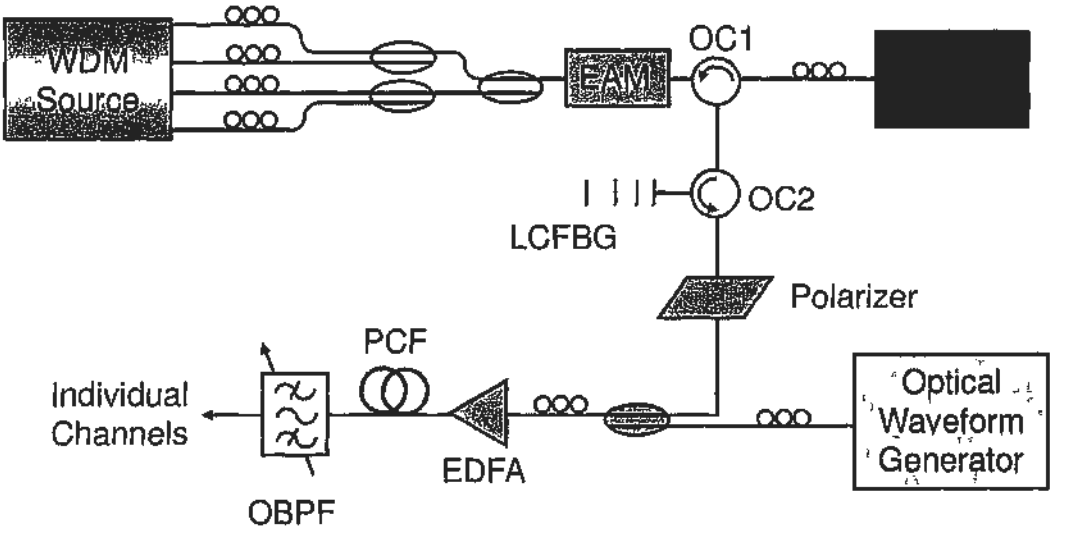

Fig. 4.1.2.1. *Experimental setup. WDM: wavelength division multiplexing; EAM: electro-absorption modulator; MLFL: mode-locked fiber laser; LCFBG: linearly chirped fiber Bragg grating; EDFA: erbium-doped fiber amplifier; PCF: photonic crystal fiber; BPF: optical bandpass filter; OC1, OC2: optical circulator;*

The pulsed source is directed to the LCFBG through another optical circulator. With the 20 ps/nm chirp introduced by the LCFBG, a temporal separation of 25 ps is introduced between the 1.25 nm-spaced channels. The separation corresponds to a 40-GHz pulsed source. The output is then used as the sampling laser source for our experiment.

It is worth mentioning that the polarizations of the MLFL and the four CW laser sources are set to be orthogonal. A polarizer has been used to block the residual MLFL pulses from the generated time- and wavelength-interleaved laser source. The sampling source is combined with an arbitrary optical waveform using an optical coupler. The average power of the waveform is set to be at 10 dB higher than that of the sampling source. The combined signal is then launched to an erbium-doped fiber amplifier (EDFA). The total average power of the amplified output is 17 dBm. The output is directed to a 64-m highly nonlinear, dispersion-flattened PCF to introduce FWM. Four new wavelength components are generated, each carrying information of the arbitrary waveform at different time slots. The sampled data at individual wavelengths are obtained using an optical bandpass filter. The data from the four wavelength components are combined to reconstruct the arbitrary waveform.

4.1.3 Experimental Results and Discussions

Fig. 4.1.3.1(a) shows the generated 4×10-GHz time- and wavelength-interleaved laser output. The wavelength of the pulsed source switches sequentially from λ_1 (1548.07 nm) to λ_4 (1551.86 nm) in a repetitive manner. The spacing between adjacent channels is 1.25 nm. The average power is -17.7 dBm. By transmitting the laser output through a polarizer, residual light of the MLFL at 1562 nm is suppressed as shown in Fig. 4.1.3.1(b). The suppression reduces the noise in the sampling source and the sampled output. A slight non-uniformity is observed in the pulse amplitude and is caused by the variation in the reflectivity of the LCFBG. The pulses at individual wavelengths have been filtered, showing a full-width-half-maximum of ~20 ps as limited by the 10 GHz response limit of the EAM.

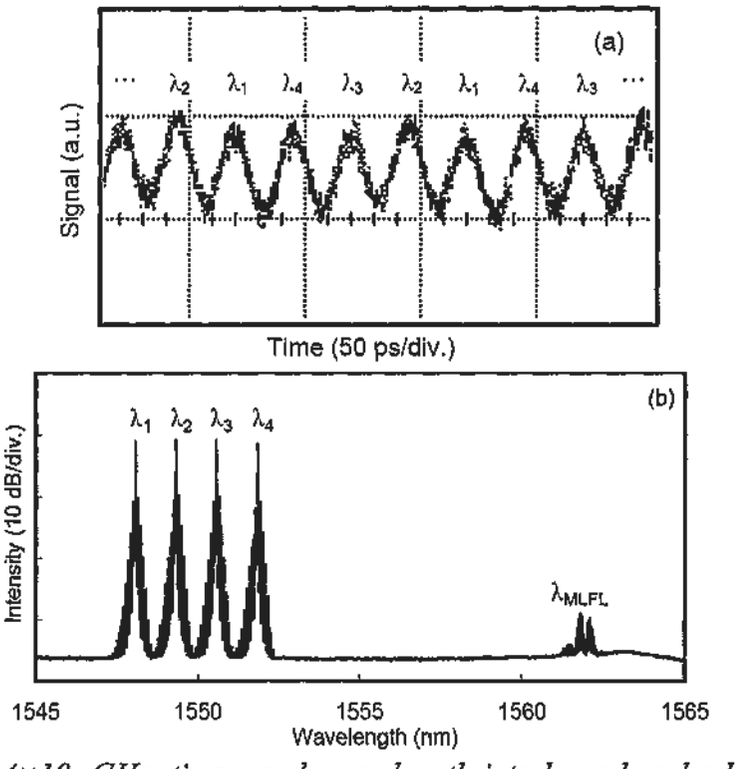

Fig. 4.1.3.1. *4×10 GHz time- and wavelength-interleaved pulsed source. (a) Temporal profile (b) Optical spectrum. MLFL: mode-locked fiber laser.*

An arbitrary optical waveform is generated at 1553.79 nm with an average power of -7.15 dBm. FWM takes place between the sampling pulse and the optical

signal in the 64-m highly nonlinear, dispersion-flattened PCF. The nonlinear coefficient γ of the PCF is 11 /W•km. The PCF has a dispersion coefficient of -1.3 ps/(km•nm) at 1550 nm and the dispersion slope is ~10^{-3} ps/(km•nm^2). The 3-dB FWM conversion bandwidth is 20 nm. The optical spectrum of the sampled output is shown in Fig. 4.1.3.2. The converted wavelength components are denoted by λ_{4c} (1555.71 nm) to λ1c (1559.55 nm). The conversion efficiency is about -14 dB.

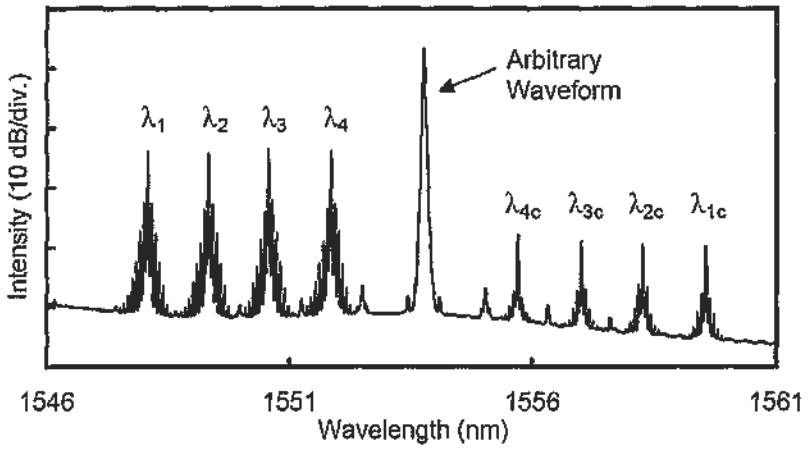

Fig. 4.1.3.2. *Optical spectrum of the FWM output showing all-optical sampling at 4 different wavelengths.*

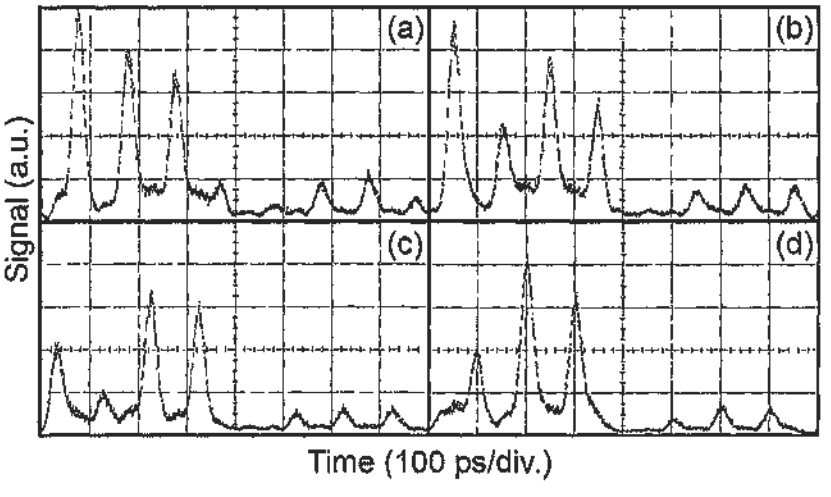

Fig. 4.1.3.3. *Waveforms of the sampled data from individual channels. (a) –(d): data obtained from λ_{1c} to λ_{4c}.*

Each of the wavelengths is individually detected and the results are shown in Fig. 4.1.3.3 (a) to (d). It can be observed that the amplitudes of the wavelength-

converted components have been modified by the arbitrary optical waveform. To reconstruct the original waveform, the four channels are combined together as shown in Fig. 4.1.3.4. During the superposition process, a square root operation is needed as the amplitude relationship between the input signal and the wavelength-converted single is a quadratic function [9]. The process is governed by the equation

$$\hat{E}_{FWM} = \kappa[\hat{E}_p \cdot \hat{E}_s^*]\hat{E}_p \qquad [4.1]$$

where E_{FWM} is the field amplitude of the output signal and E_p is that of the input signal. The data from individual channels are processed in computer and the original signal is reconstructed by combining data from the four interleaved channels. As shown in Fig. 4.1.3.4, the result matches well with the input arbitrary signal represented by the black solid curve in the figure.

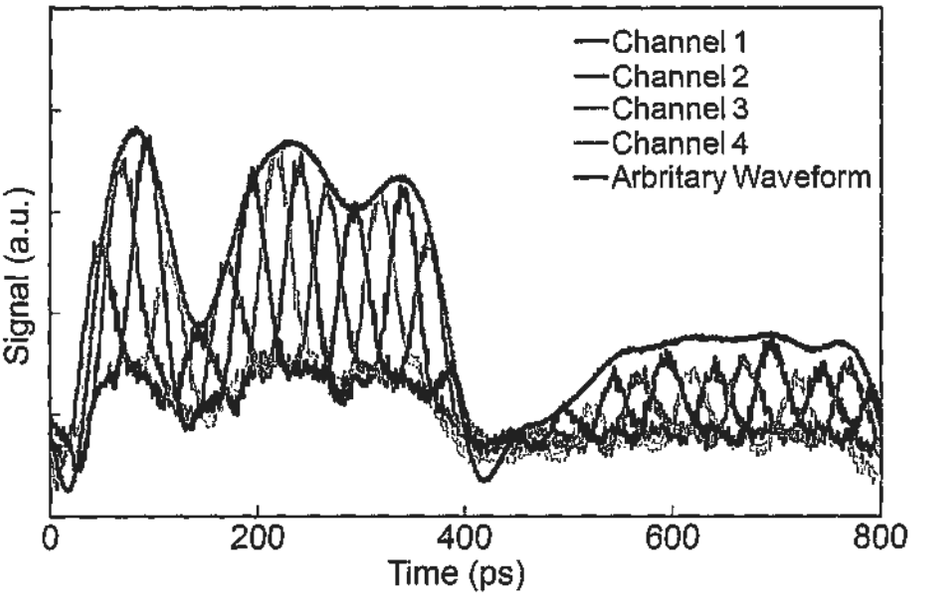

Fig. 4.1.3.4. *Reconstructed Waveform. Channel 1 – 4: data obtained from λ_{1c} to λ_{4c}.*

Instead of sampling a repetitive signal, our approach can also be used to sample a single-shot signal. Real-time signal monitoring is therefore supported. To increase the sampling rate, one can use a higher frequency MLFL together with reduced wavelength spacing among the channels or a lower LCFBG dispersion. The number of wavelengths in the sampling source can also be increased as long as they

fall within the operating bandwidth of the EAM and the reflection bandwidth of the LCFBG. A total sampling rate of 100 Gb/s can be realized when 10 channels are operating each at 10 Gb/s. Thus, the required bandwidth of the components is only 10 GHz.

In conclusion, we experimentally demonstrate 40-GS/s all-optical wavelength division sampling of an arbitrary optical signal using a time- and wavelength-interleaved laser pulsed source. The laser source is generated by multiwavelength cross-absorption modulation in an EAM followed by group velocity dispersion in a LCFBG. The sampling is performed in a 64-m highly nonlinear, dispersion-flattened PCF using four-wave mixing. Individual wavelength channels are filtered and calibrated. The sampled outputs are combined and the arbitrary waveform is successfully reconstructed. Compared with commercial optical sampling oscilloscope, our approach is potentially to be developed to a real-time oscilloscope with reduced required electronics bandwidth. Current commercial products can only sample repetitive waveforms at single wavelength. We can further develop our approach to sample real-time signals at multiple wavelengths using our time- and wavelength-interleaved pulse laser source. Further optimization on the post-processing algorithm can help to enhance the performance of our optical sampling scheme.

4.2 Photonic Analog-to-Digital Conversion

Analog-to-digital converters (ADC) play important role in electronic systems. It is a device which converts a continuous quantity to a discrete time digital representation. It is an important device to communication between analog and digital systems. However, because of the limits of electronics speed and fabrication process, the best electronic ADC in the world can support sampling rate of around 40 GSample/s (GSa/s). For future development with signals over 100 GHz, electronic components can hardly handle the operation.

The development in photonic devices can be a solution for the mentioned bottleneck. In recent years, much research efforts have been paid to assist electronic ADC with optical waves. Photonics devices can help in different ways. As mentioned in [11], there are four classes of photonic ADCs 1) photonic assisted ADC in which a photonic device is added to an electronic ADC to improve performance, 2) photonic sampling and electronic quantizing ADC, 3) electronic sampling and photonic quantizing ADC, and 4) photonic sampling and quantizing ADC.

In this section we will briefly describe an ADC with photonic sampling with electronic quantizing. The photonic sampling is assisted by time- and wavelength-interleaved laser source. The speed requirement of electronic quantizing can be reduced using our proposed approach.

4.2.1 Architecture

Fig. 4.2.1.1 shows the proposed photonic ADC assisted by time- and wavelength-interleaved laser source. The sampler can be an optical phase modulator or amplitdue modulator. The electrical signal is input to the RF port of the modulator. A time- and wavelength-interleaved laser source is directed to the input of the modulator. An amplitude modutator is used for simple illustration. After the modulator, the amplitudes of the time- and wavelength-interleaved pulses are modified by the input RF signal. The pulses are then separated into different channels using a wavlenegth demultiplexer. Each channel contains a photodetector and an electronic ADC. The speed of the electronic ADC is determined by the input RF signal and the number of pulsed channels:

$$F = Fs / N$$

Where F is the required sampling speed, Fs is the speed of input RF signal and N is the number of pulsed channels.

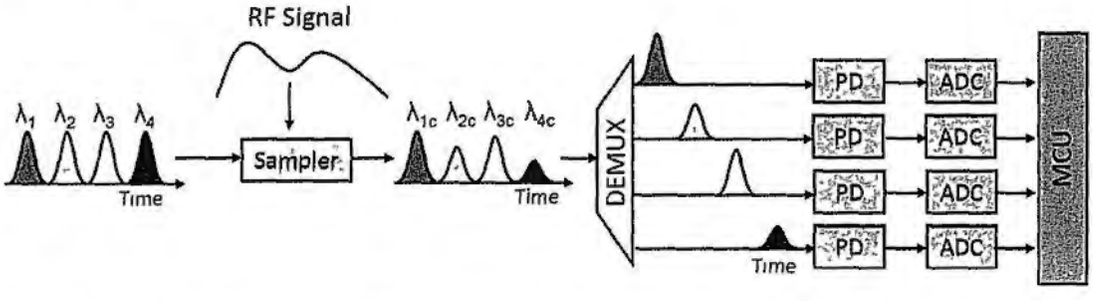

Fig. 4.2.1.1. *Architecture of the proposed photonic ADC. Sampler: either a phase or amplitude modulator; DEMUX: wavelength demultiplexer; PD: photodetector; ADC: electronic analog-to-digital converter;*

After processing by electronic ADC, the data are recombined in a computer or micro-controller unit. The reconstructed sampled waveform can be obtained after processing.

It is obvious that using the time- and wavelength-interleaved pulses can help to reduce the electronic ADC requirement. By Nyquist theorem, the minimum sampling rate for a specific signal of frequency F should be 2F. For example, a 40 GSa/s ADC is needed to sample a 20 GHz signal. However, with our proposed scheme, only 10 GSa/s electronic ADCs are needed for sampling a 20 GHz signal when four 10 GHz pulsed channels are used. The cost for the whole system can be reduced and the capability of low speed ADC is enhanced.

To evaluate the photonic ADC, different parameters can be accessed, including the total harmonic distortion, spurious-free dynamic range, effective number of bits, and signal-to-noise and distortion ratio. These parameters can be obtained using RF spectrum analyzer and software processing.

The limitations of this scheme are the bandwidth of the modulators and the pulse width of the time- and wavelength-interleaved laser source. For the modulator, bandwidth > 40 GHz is already commercially available, so it is not a big issue. For the pulse width, in Chapter 3 we demonstrated that short pulses can be generated with different methods. Even though there is slight overlapping between adjacent pulses, the crosstalk is not a problem as the proposed scheme does not include any nonlinear processing.

Although the architecture is fully explored, a 10 GSa/s electronic ADC is not available at this moment. So the implementation of the proposed scheme is regarded as a future work of the thesis.

4.3 Summary

In this chapter, we demonstrate all-optical sampling using time- and wavelength-interleaved pulses. The processing speed of the individual channels is 10 GSa/s, while the system processing speed can reach 40GSa/s. The bandwidth requirement on electronics is relieved and the processing speed can be increased with more pulsed channels. Also, we briefly described the architecture of a 40 GSa/s photonic ADC. Only 10 GHz electronic components are needed for sampling a 20 GHz signal. The implementation of the photonic ADC can be achieved when a 10 GSa/s electronic ADC is available.

4.4 References

[1] S. Diez, R. Ludwig, C. Schmidt, U. Feiste, and H. G. Weber, "160 Gbit/s Optical Sampling by a Novel Ultra-Broadband Switch Based on Four-Wave Mixing in a Semiconductor Optical Amplifier," *OFC/IOOC 1999*, San Diego, CA, PD38-1 – PD38-3, February 1999.

[2] P. J. Maguire, L. P. Barry, T. Krug, M. Lynch, A. L. Bradley, J. F. Donegan, and H. Folliot, "All-Optical Sampling Utilising Two-Photon Absorption in Semiconductor Microcavity," *Electron. Lett.*, vol. 41, pp. 489 – 490, April 2005.

[3] S. Nogiwa, N. Yamada, and H. Ohta, "Optical Sampling System Using a PPLN Crystal and Wavelength-Tunable Soliton Pulse," in *Proc. IEEE Lightwave Technologies in Instrumentation & Measurement Conf. 2004*, pp. 73 – 78, 19-20 October, 2004.

[4] H. Ohta, N. Banjo, N. Yamada, S. Nogiwa, and Y. Yanagisawa, "Measuring Eye Diagram of 320 Gbit/s Optical Signal by Optical Sampling Using Passively Modelocked Fibre Laser," *Electron. Lett.*, vol. 37, pp. 1541 – 1542, December 2001.

[5] N. Yamada, S. Nogiwa, and H. Ohta, "640 Gb/s OTDM Signal Measurement With High-Resolution Optical Sampling System Using Wavelength-Tunable Soliton Pulses," *IEEE Photon. Technol. Lett.*, vol. 16, pp. 1125 – 1127, April 2004.

[6] J. C. Twichell and R. Helkey, "Phase-Encoded Optical Sampling for Analog-to-Digital Converters," *IEEE Photon. Technol. Lett.*, vol. 12, pp. 1237 – 1239, September 2000.

[7] M. D. Weiss, M. H. Crites, E. W. Bryerton, J. F. Whitaker, and Z. Popović, "Time-Domain Optical Sampling of Switched-Mode Microwave Amplifiers and Multipliers," *IEEE Trans. Microw. Theory Tech.* vol. 47, pp. 2599 – 2604, December 1999.

[8] C. Janke, M. Först M. Nagel, and H. Kurz, "Asynchronous Optical Sampling for High-Speed Characterization of Integrated THz Resonator Arrays," in *Conf. Lasers and Electro-Optics*, Baltimore, MD, May 2005, Paper CFM7.

[9] K. Inoue, "Four-Wave Mixing in an Optical Fiber in the Zero-Dispersion Wavelength Region," *J. Lightwave. Technol.,* vol. 10, pp. 1553 – 1561, December 1992.

[10] Gordon K. P. Lei, Mable P. Fok, and Chester Shu, "40-GS/s all-optical sampling using four-wave mixing with a time- and wavelength-interleaved laser source," in *Conference on Lasers and Electro-Optics/Quantum Electronics and Laser Science Conference and Photonic Applications Systems Technologies,* OSA Technical Digest (CD) (Optical Society of America, 2008), San Jose, CA, May 2008, paper CTuH6.

[11] G. C. Valley, "Photonic analog-to-digital converters," *Opt. Express*, vol. 15, pp. 1955 – 1982, March 2007.

5 Wavelength Multicasting and Conversion

Wavelength Multicasting is an important process in communications for transmitting identical information to different locations at the same time. It is particularly useful for bandwidth-intensive applications such as Internet Protocol television distribution and teleconferencing in wavelength division multiplexing (WDM) and time division multiplexing (OTDM) networks. Different approaches have been proposed to achieve wavelength multicasting. In this chapter we will discuss the use of time- and wavelength-interleaved pulses for wavelength multicasting operation. Both non-return-to-zero on-off keying (NRZ-OOK) and non-return-to-zero differential phase-shift keying (NRZ-DPSK) signals can be processed using the same pulsed source. Besides, pulse format conversion from non-return-to-zero (NRZ) to return-to-zero (RZ) is achieved at the same time. Performances of the multicasting process will be analyzed. Also the pulse width of the multicast outputs can be tunable, making the scheme suitable for different system requirements.

Instead of broadcasting the data to different locations, sometimes the information is needed to be transmitted to a specific destination. In this case, wavelength conversion plays an important role in a wavelength-routed network. However, for high-speed conversion, low-speed optoelectronic devices cannot handle the operation. The use of time- and wavelength-interleaved pluses can help to reduce the data speed by serial-to-parallel processing and enable the operation by low-speed devices. The operation principle and the performance of conversion will be discussed.

5.1 Wavelength Multicasting of OOK Signals

On-off keying (OOK) signal is one of the most popular formats in optical communication networks due to its simple implementation. In OOK signal, the data is modulated on light by changing its amplitude. Different approaches have been proposed to achieve wavelength multicasting of OOK signals. Examples include cross-absorption modulation in an electro-absorption modulator [1], four-wave mixing in a highly-nonlinear fiber [2], optical parametric amplification aided by self seeding [3], and cross-phase modulation in a semiconductor optical amplifier (SOA) [4]. By using multiple probes, up to 40 multicast channels have been demonstrated using 20 continuous-wave lasers [5]. In future communication networks, the traffic will be carried by data at different pulse and modulation formats. Hence, pulse format conversion is a desirable technology to connect between different networks. In particular, the interface between a WDM and an OTDM network requires inter-conversion between NRZ and RZ formats. Different approaches have been demonstrated to achieve the conversion, including schemes for single and multiple channels [6 – 8]. In this section, we report results on wavelength multicasting of a 10 Gb/s NRZ-OOK signal to 4 × 10 Gb/s RZ-OOK outputs using a time- and wavelength-interleaved laser source [9]. The multicasting is performed by four-wave mixing in a highly nonlinear photonic crystal fiber (PCF), while simultaneous pulse format conversion is achieved using the interleaved pulses. A unique feature of this approach is that the multicast outputs have a common relative delay time and thus can be effectively applied for use in an all-optical tunable delay line [10] and in applications of TDM-WDM traffic grooming [11]. Furthermore, we experimentally demonstrate the tuning of duty cycles by controlling the RF driving power of the phase modulator in the pulse generation stage. It is important to optimize the pulse

width in a transmission link as it can greatly affect the system performance [12, 13]. Eye diagrams of the outputs at different duty cycles are presented to demonstrate the flexibility of our approach. Error-free operations have been obtained for all multicast outputs with a maximum power penalty of 0.5 dB at output pulse width of 19.3 ps.

The schematic diagram of the wavelength multicasting process is shown in Fig. 5.1.1. A 4 x 10 GHz time and wavelength-interleaved pulsed source is combined with a NRZ-OOK data. The pulsed peaks are aligned with the peak amplitude of the data. The two signals undergo four-wave mixing and new wavelength components are generated. By the equation

$$\hat{E}_{FWM} = \kappa[\hat{E}_p \cdot \hat{E}_s^*]\hat{E}_p \qquad [5.1]$$

where E_{FWM} is the field amplitude of the FWM generated idler, E_p is the field amplitude of the pump and E_s is the field amplitude of the signal. From the equation, the FWM-generated idler contains the information of both the pump and signal. In the configuration shown in Fig. 5.1.1, the pulsed source acts as signal and the NRZ-OOK data acts as pump. As a result, all generated idlers contain the information of the NRZ-OOK data. So wavelength multicasting is achieved after the operation.

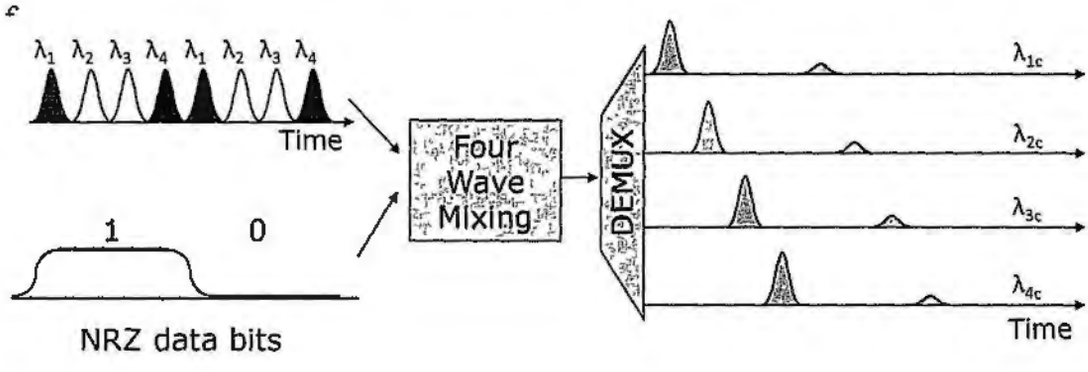

Fig. 5.1.1. *Schematic diagram of the proposed wavelength multicasting scheme.*

5.1.1 Experimental Setup

The experimental setup is shown in Fig. 5.1.1.1. Four CW laser beams with adjacent channel spacing of 1.25 nm are obtained from a WDM source. The laser outputs are combined with optical couplers and connected to the input port of an optical phase modulator. The modulator is driven with a 10 GHz RF signal to introduce frequency chirp on the CW beams. The half-wave voltage V_π of the phase modulator is 5 V. The power of the RF signal is ~ 24 dBm, leading to a modulation index of 2π. The modulated outputs are then connected to 8.4-km single-mode fiber (SMF). As the spectral content in each of the four lasers is now time-dependent, the GVD in the SMF compresses the CW beams to generate short pulses [14]. The time spacing between adjacent channels is ~25 ps, determined by the wavelength spacing between adjacent laser outputs and the GVD of the SMF [14]. As a result, 40 GHz time- and wavelength-interleaved laser pulses are achieved at the output of the SMF. The time spacing between any two wavelength channels should be equal to the difference between the product of the GVD and their wavelength spacing and an integral multiple of the driving period, which is 100 ps in our case.

To generate a 10 Gb/s data stream, a tunable laser is modulated by an electro-optic modulator driven by a 2^{31}-1 pseudorandom binary sequence. The time and wavelength-interleaved pulses and the data stream are then combined with a 50/50 optical coupler. An optical tunable delay line is used in the setup to synchronize the two signals. The coupled lights are subsequently amplified by an erbium-doped fiber amplifier (EDFA) to 26 dBm and are directed to a 64-m PCF. The nonlinear coefficient of the PCF is 11.2 $(W \cdot km)^{-1}$ around 1550 nm. The insertion loss is 2.6 dB. The dispersion is less than 3 ps $(km \cdot nm)^{-1}$ over the C-band, while the dispersion slope is ~10^{-3} ps $(km \cdot nm^2)^{-1}$. The low-dispersion and dispersion-flattened properties

contribute to a wide 3-dB FWM conversion bandwidth of 16 nm, implying that the number of multicast outputs can be potentially increased.

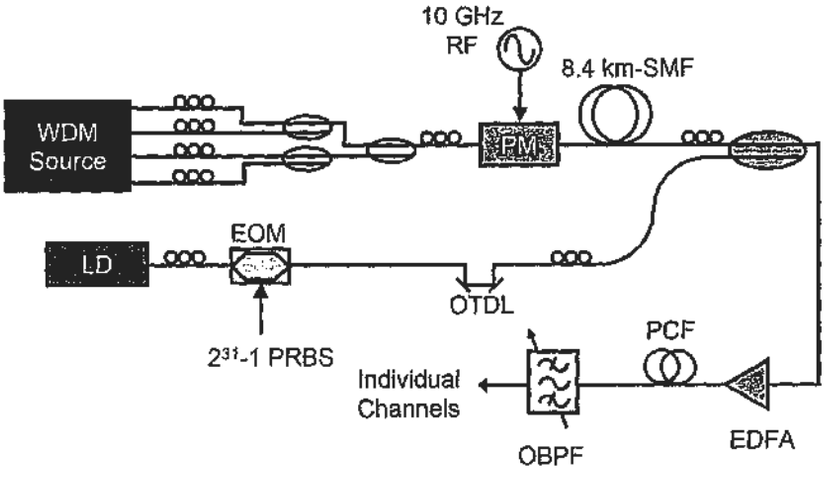

Fig. 5.1.1.1. *Setup for simultaneous wavelength multicasting and pulse format conversion. LD: laser diode; EOM: electro-optic modulator; PRBS: pseudorandom binary sequence; PM: phase modulator; OTDL: optical tunable delay line; EDFA: erbium-doped fiber amplifier; PCF: photonic crystal fiber; OBPF: optical band pass filter.*

FWM takes place in the PCF. The input data stream acts as a pump and interacts with four probes represented by different wavelength components in the interleaved laser pulses. Consequently, new wavelength components are generated and they carry the same data spaced by ~25 ps. By filtering out the four generated components, the multicast outputs are obtained.

5.1.2 Results on Time- and Wavelength-Interleaved Pulses

The waveform and the optical spectrum of the time- and wavelength-interleaved pulses are shown in Fig. 5.1.2.1 (a) and (b), respectively. The repetition rate is 40 GHz. The wavelengths are selected at 1548.20, 1549.55, 1550.80, and 1552.05 nm to produce a time separation of ~25 ps between adjacent pulses. The width of the individual pulses at each center wavelength is ~ 12.5 ps, as confirmed by measurement with a 500-GHz optical sampling oscilloscope. The measured profile of one of the channels is shown in Fig. 5.1.2.2. It is noticed that some pedestals appear next to the pulse peak in the temporal profile. The pedestals are believed to be caused by the nonlinear chirp in the CW light. To reduce the distortion, a better optimization is required on the amount of dispersion and the modulation depth.

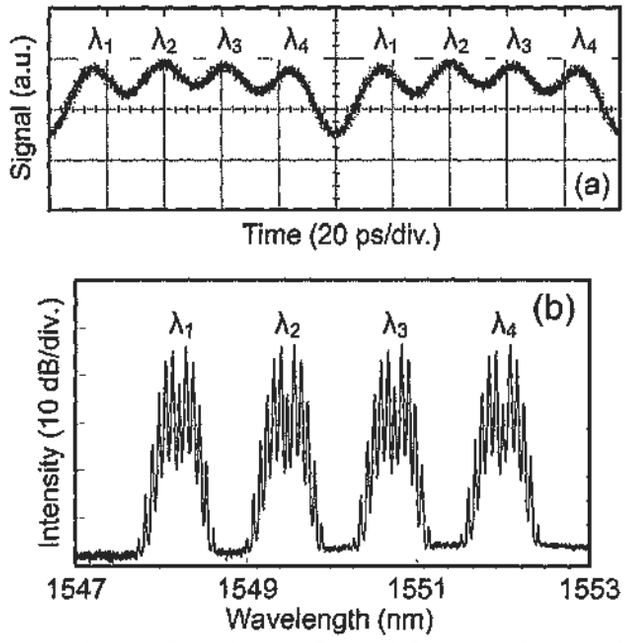

Fig. 5.1.2.1. *Time- and wavelength-interleaved laser pulses. (a) Temporal profile measured with a high-speed photodetector and an electrical sampling oscilloscope. (b) Optical spectrum of the interleaved pulses.*

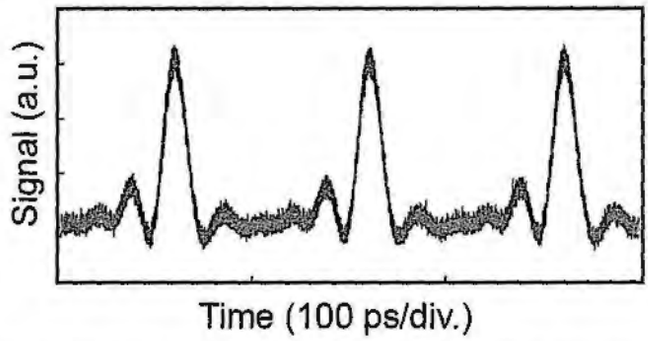

Fig. 5.1.2.2 *Trace of an individual channel at 1548.20 nm obtained with a 500-GHz optical sampling oscilloscope. The actual pulse width is determined to be ~12.5 ps.*

Fig. 5.1.2.3 shows the 10 Gb/s NRZ-OOK data. The PRBS data are generated at 1545.3 nm with a pattern length of 2^{31}-1 bits. Since the rise time of the data is relatively long, we deliberately introduce an offset in one channel of the interleaved pulses to minimize distortions at the eye crossing regions of the input data.

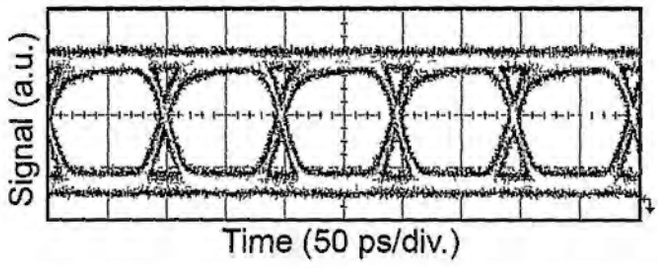

Fig. 5.1.2.3. *Eye diagram of the 10 Gb/s NRZ-OOK input signal.*

5.1.3 Results on Wavelength Multicasting

Wavelength multicasting is achieved by FWM in the PCF. Fig. 5.1.3.1 (a) shows the FWM output spectrum. The multicast outputs are located at the short wavelength side of the spectrum after wavelength conversion. The respective center wavelengths are 1542.50, 1541.34, 1540.00 and 1538.82 nm. The FWM conversion efficiency is ~ -18 dB. The fiber length is much shorter than that in conventional HNLF and the SBS threshold is higher (27 dBm). However, due to the uneven optical gain of the EDFA over the spectral region as shown in Fig. 5.1.3.1 (b), the intensities of the multicast outputs are not identical. To further analyze the performance of multicasting, we filter out the four individual channels from the PCF output using a 0.3-nm optical band pass filter.

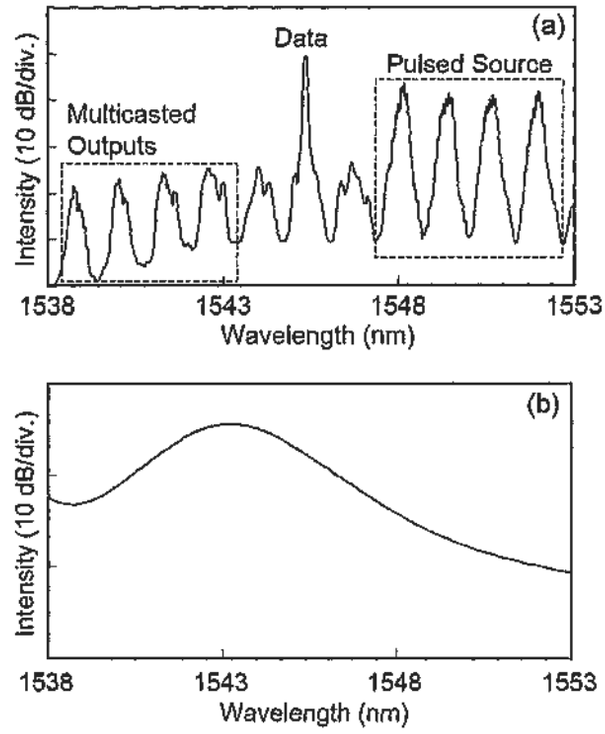

Fig. 5.1.3.1. *(a) Optical spectrum after FWM in the PCF. (b) Amplified spontaneous emission noise spectrum of the EDFA.*

The eye diagrams of the multicast outputs are shown in Fig. 5.1.3.2 (a) – (d) for channels 1 to 4, respectively. The traces are detected using a 32-GHz photodetector with a 50-GHz digital sampling oscilloscope. The response time of the whole detection system is ~ 17 ps. The outputs are in RZ-OOK format. The time spacing between adjacent channels is ~ 25 ps, governed by the pulse separation in the time- and wavelength-interleaved laser source. It is observed that some ripples appear at the ground level of channel 1. The reason is that the eye crossing region has a partial overlap with channel 1 in the laser pulses, resulting in a poorer extinction ratio in the multicast output. The unequal amplitudes of the output eye diagrams are mainly caused by the uneven optical gain in the EDFA as shown in Fig. 5.1.3.1(b).

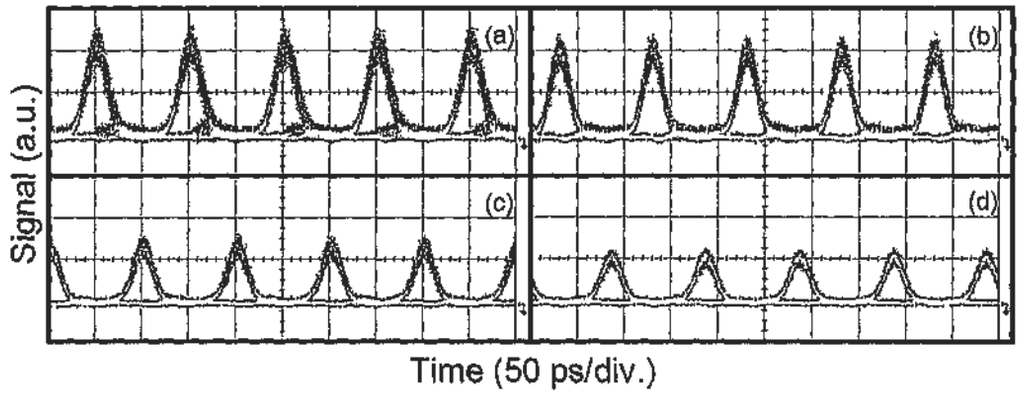

Fig. 5.1.3.2. *(a) – (d). Eye diagrams of the four wavelength-multicast channels with a common delay time. (a) 1542.50 nm, (b) 1541.34 nm, (c) 1540.00 nm and (d) 1538.82 nm.*

To analyze the multicasting performance, we also carry out BER measurements. Error free operations (BER < 10^{-9}) have been achieved in all channels. The results are shown in Fig. 5.1.3.3. The power penalty ranges from -0.5 dB to 0.5 dB at the BER of 10^{-9}. The degraded receiver sensitivity of channel 1 is caused by the appearance of ripples as mentioned above. Also, an error floor is developed at the BER curve of channel 1 but operation with a BER < 10^{-10} can still be obtained. The

improvement on the receiver sensitivity is a consequence of NRZ to RZ pulse format conversion, as the impulsive coding can reduce the effect of inter-symbol interference [20].

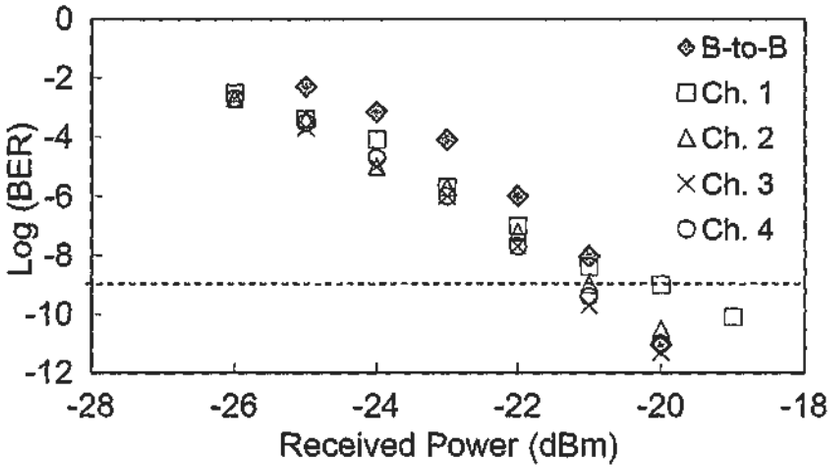

Fig. 5.1.3.3. *BER performance of the 10 Gb/s back-to-back and the 4 multicast outputs. The receiver sensitivities are improved except for channel 1. The dotted line indicates the BER level of* 10^{-9}.

5.1.4 Tuning of Duty Cycle

By controlling the applied voltage on the phase modulator, the width of the time- and wavelength-interleaved pulses can be adjusted. As a result, the duty cycles of the multicast outputs can be tuned. As derived in [15], the relationship between the pulse width and the phase change is given by:

$$\tau \approx 0.7/2(\Delta\theta \times f_m) \qquad [5.2]$$

where τ is the transform-limited pulse width, $\Delta\theta$ is the modulation index, and f_m is the modulation frequency. By changing the modulation index, we can achieve multicast outputs with different pulse widths.

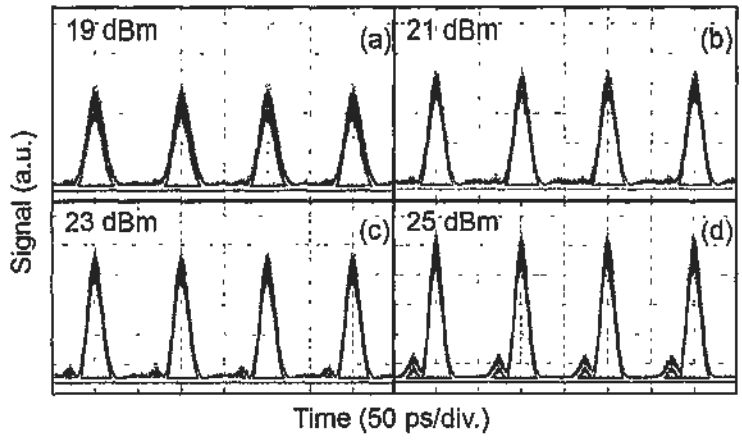

Fig. 5.1.4.1. *Eye diagrams of the multicast output at 1542.50 nm. Different duty cycles are obtained by adjusting the RF power applied to the phase modulator. The traces are captured with a 500-GHz optical sampling oscilloscope.*

Here, we demonstrate the tunability of the pulse width with four different applied RF powers. The eye diagrams are shown in Fig. 5.1.4.1 (a)–(d). Table 5.1.4.1 shows the relationship between the applied RF power, the measured pulse width, and the extinction ratio observed from the eye diagrams.

The tuning range of the pulse width is around 4.3 ps and is limited by the maximum output power of the RF amplifier. Shorter pulse width has been demonstrated with an even larger driving voltage [15]. It is observed that the

extinction ratio of the eye diagrams does not change substantially when the pulse width is adjusted. For the pulses with the shortest width of 17.9 ps, pedestals appear because of nonlinear chirp on the CW light. However, they can in principle be suppressed by a pulse cleaning approach [16].

Table 5.1.4.1. *The relationship between the applied RF power, the multicast output pulse width, and the respective extinction ratios.*

RF power (dBm)	Pulse width (ps)	Extinction ratio (dB)
19	22.2	16.5
21	20.5	16.6
23	19.3	16.1
25	17.9	16

It has been demonstrated that the delay between adjacent channels is an important parameter for multi-wavelength operation, including the control of walk-off between channels in 2R regeneration [17] and the time alignment for WDM and OTDM inter-conversion [18, 19]. Also it is important to have data with different delays for dropping and adding different tributary channels in a WDM-TDM network [21]. Time- and wavelength-interleaved pulses can act as an intermediate tool for the aforementioned operations and provide desirable delays between the WDM channels.

In conclusion, we have demonstrated 4 × 10 Gb/s wavelength multicasting together with NRZ to RZ format conversion. The process is achieved by FWM between a 10 Gb/s NRZ data and a 40 GHz time- and wavelength-interleaved pulse train in a 64-m highly nonlinear PCF. The multicast copies are separated by a common relative delay time of ~25 ps. Error-free operations have been achieved for all multicast outputs with a maximum power penalty of 0.5 dB. Multicast outputs with different duty cycles have also been demonstrated with a tuning range of 4.3 ps in the pulse width. The scheme is potentially scalable to produce additional multicast

channels when more wavelength components are adopted in the interleaved laser pulsed source.

5.2 Wavelength Multicasting of DPSK Signals

Besides OOK signals, phase-shift keying (PSK) is another popular signal format in modern communication systems. Compared with OOK signal which carries data by changing the intensity of the light beam, PSK signal carries data by changing the phase of the light. Usually the differential form of PSK signals are used as it does not require a reference signal. It is called differential phase-shift keying (DPSK) signal. The use of DPSK signals can provide several advantages, including enhancement of receiver sensitivity by 3 dB using balanced detection, higher tolerance to nonlinearity due to constant intensity and also higher spectral efficiency [22]. Fig. 5.2.1 shows a typical DPSK signal. The data is encoded by the differential phase change. When there is a bit "0", no phase change happens. When there is a "1", a 180-degree phase change is added on the light. To retrieve the original information, demodulation is needed before direct detection by photodetector. A fiber-based delay interferometer is used for the demodulation process.

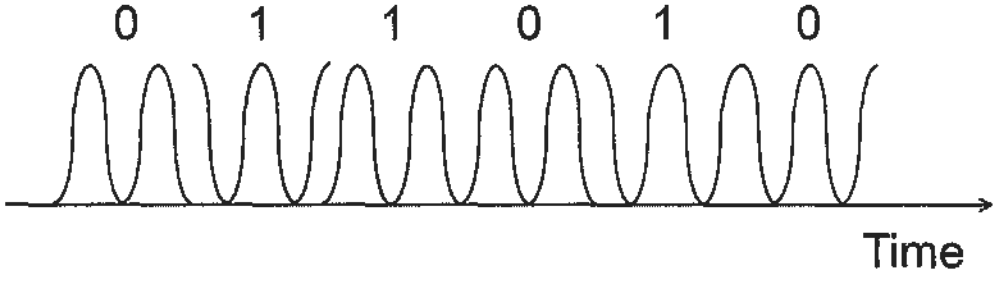

Fig. 5.2.1. *Phase changes in a DPSK signal. Phases are changed by 180 degrees when there is a "1" in the data stream.*

To multicast DPSK signals, one important issue is that the process should be phase-sensitive such that the phase information can be preserved. By using four-wave mixing (FWM) effect and sum frequency generation/difference frequency generation effects, wavelength multicasting of DPSK signals have been

demonstrated in nonlinear optical fibers, semiconductor optical amplifiers, phase sensitive amplifiers and periodically-poled lithium-niobate (PPLN) waveguides [23 – 27]. It is also desirable to demonstrate the capability for simultaneous conversion of signals among different formats according to the specific system requirement [22]. In this section, we experimentally demonstrate wavelength multicasting of DPSK signals with simultaneous NRZ to RZ pulse format conversion [28]. The operation is achieved by FWM of the incoming DPSK signal with a time- and wavelength-interleaved pulsed source. The FWM is performed in a 64-m photonic crystal fiber (PCF). Four multicast channels have been achieved with power penalties ranging from 0.8 dB to 1 dB. The scheme can easily be extended to higher speed by increasing the repetition rate of the pulsed source. Also, the number of multicast outputs can be increased by using up to ten wavelengths in a time- and wavelength-interleaved pulsed source [29].

5.2.1 Experimental Setup

The experimental setup is shown in Fig. 5.2.1.1. Two continuous-wave (CW) laser outputs are obtained at different wavelengths from a pair of tunable distributed feedback lasers. The CW lights are combined with a coupler and directed to a dual-drive Mach-Zehnder modulator driven by a 10 GHz sinusoidal signal. The power of the driving signal is 24 dBm. Both amplitude and phase modulations are achieved with the modulator. The modulated outputs are then launched into an 8.4-km single-mode fiber to further compress the pulses by compensating the frequency chirp. The generated time- and wavelength-interleaved pulses are amplified by an erbium-doped fiber amplifier (EDFA) to 4.7 dBm.

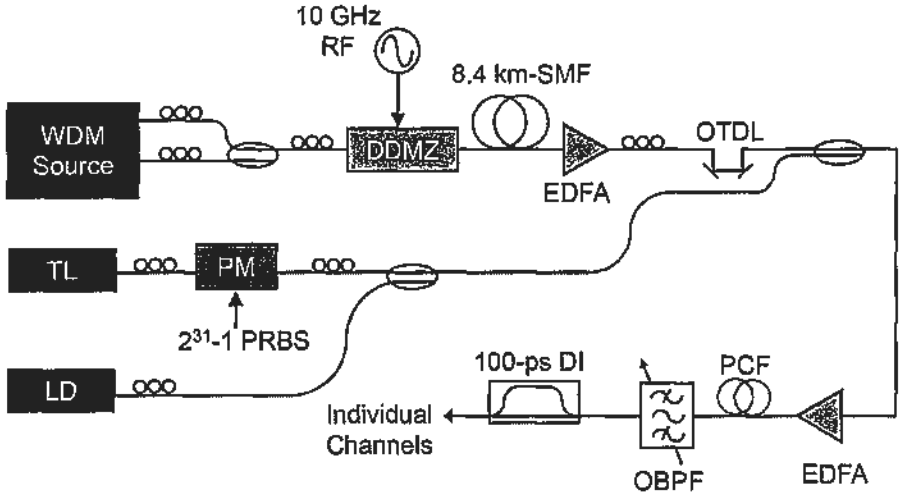

Fig. 5.2.1.1. *Experimental setup for DPSK wavelength multicasting with simultaneous pulse format conversion. DDMZ: dual-drive Mach-Zehnder modulator; SMF: single-mode fiber; EDFA: erbium-doped fiber amplifier; OTDL: optical tunable delay line; TL: tunable laser; PM: phase modulator; LD: laser diode; PCF: photonic crystal fiber; OBPF: optical bandpass filter; DI: delay interferometer.*

To prepare a NRZ-DPSK data signal, the output from a tunable laser is directed to a phase modulator driven by a 10-Gb/s 2^{31}-1 pseudorandom binary

sequence. The NRZ-DPSK data stream is combined with both a CW pump and the time- and wavelength-interleaved pulses. The pulse peaks are temporally aligned to the constant phase region of the NRZ-DPSK signal using an optical tunable delay line. The combined inputs are then amplified to 26 dBm with an EDFA and directed to 64-m highly nonlinear PCF. The nonlinear coefficient of the PCF is 11 $W^{-1}km^{-1}$ and the dispersion coefficient is −1.3 $ps{\cdot}km^{-1}nm^{-1}$ at 1550 nm. The dispersion slope is ~10^{-3} $ps{\cdot}km^{-1}nm^{-2}$. The 3-dB FWM conversion bandwidth is 16 nm. FWM takes place inside the PCF.

The phase transfer process during FWM is illustrated in Fig. 5.2.1.2. The CW pump at ω_p and the data stream at ω_s create an index grating in the PCF by frequency beating. This grating scatters the two pulsed channels at ω_1 and ω_2 and generates new wavelength components at $\omega_{1H,L}=\omega_1\pm(\omega_s-\omega_p)$ and $\omega_{2H,L}=\omega_2\pm(\omega_s-\omega_p)$. The phases of these generated idlers are $\Phi_{1H,L}=\Phi_1\pm(\Phi_s-\Phi_p)$ and $\Phi_{2H,L}=\Phi_2\pm(\Phi_s-\Phi_p)$, respectively. As the CW and pulsed pumps do not contain data information, the phase changes in the pulsed idlers follow that of the NRZ-DPSK data stream. As a result, NRZ-to-RZ format conversion is achieved simultaneously with wavelength multicasting. The four multicast outputs are extracted using a tunable optical filter before they are individually analyzed.

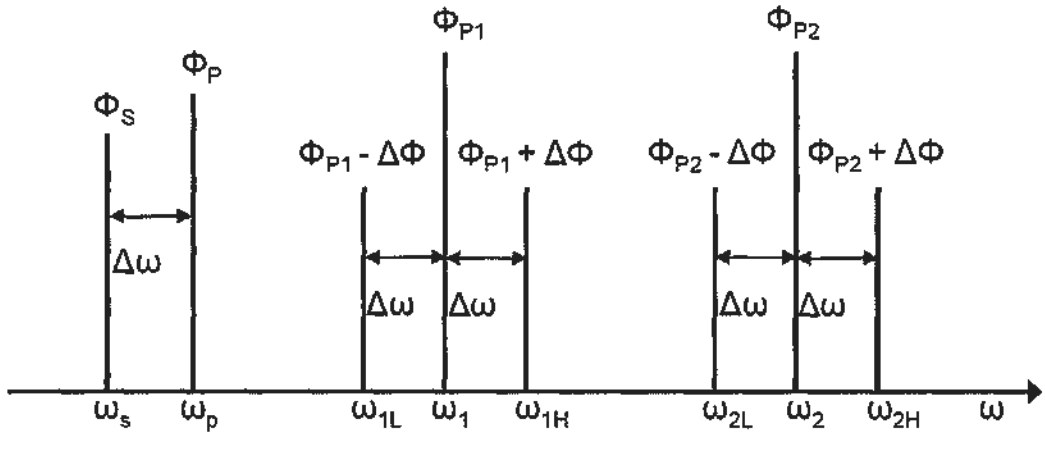

Fig. 5.2.1.2. *Phase transfer diagram during four-wave mixing. $\Delta\Phi$: Φ_P - Φ_S.*

5.2.2 Experimental Results

The time- and wavelength-interleaved pulses are measured with a high-speed photodetector and a sampling oscilloscope with a system response time of ~17 ps. The result is shown in Fig. 5.2.2.1 (a). Since the pulses are not well resolved, a 500-GHz optical sampling oscilloscope is used to accurately determined the pulse width that is found to be ~ 14 ps. The pulses are generated at 1548.1 nm and 1550.8 nm. The time separation between pulses at the two center wavelengths is ~ 21 ps. The NRZ-DPSK data signal is generated at 1557.4 nm while the CW pump is obtained at 1556.5 nm. Fig. 5.2.2.1 (b) shows the eye diagram of the demodulated NRZ-DPSK signal. A 100-ps delay interferometer is used for the demodulation. It is observed that the limited response time of the phase modulator used in this experiment restricts the number of multicast channels.

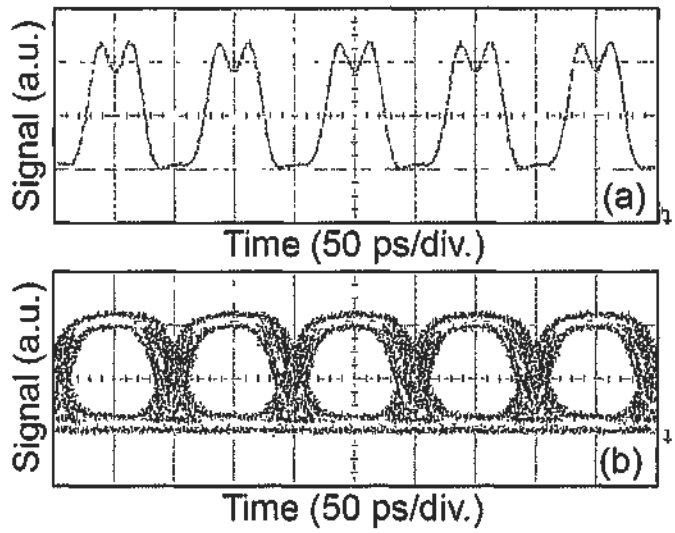

Fig. 5.2.2.1. *(a) Profile of the time- and wavelength-interleaved pulses measured with a high-speed photodetector and oscilloscope with a system response of 17 ps. The pulse width is determined to be ~14 ps with a 500-GHz optical sampling oscilloscope. (b) Eye diagram of the demodulated NRZ-DPSK signal.*

After FWM in the PCF, the multicast outputs are obtained. The spectrum after FWM in the PCF is shown in Fig. 5.2.2.2. Although there are several high-order FWM products, no obvious crosstalk is observed. Multicast outputs are filtered out and examined individually.

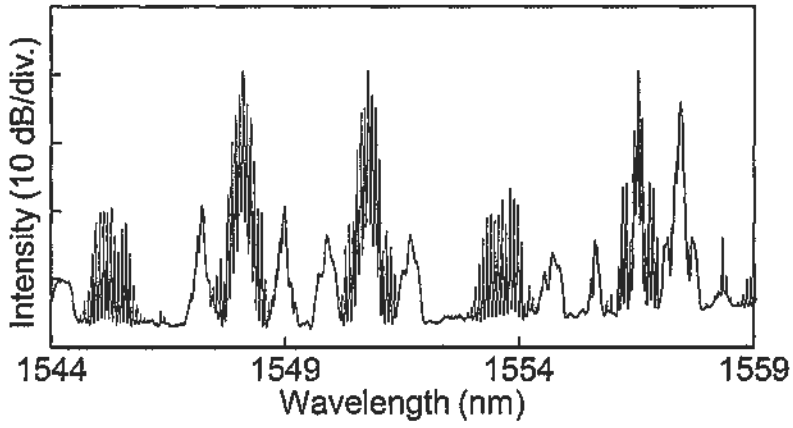

Fig. 5.2.2.2. *Optical spectrum after FWM in PCF.*

The outputs are again demodulated with a 100-ps delay interferometer. Fig. 5.2.2.3 (a) to (d) show the eye diagrams of the multicast outputs obtained at 1547.2, 1549.0, 1549.9 and 1551.7 nm, respectively. Clear eye diagrams have been achieved for all multicast channels. Also, the pulse format has been converted from NRZ to RZ. The amplitude non-uniformity can be reduced by further optimizing the optical filtering process.

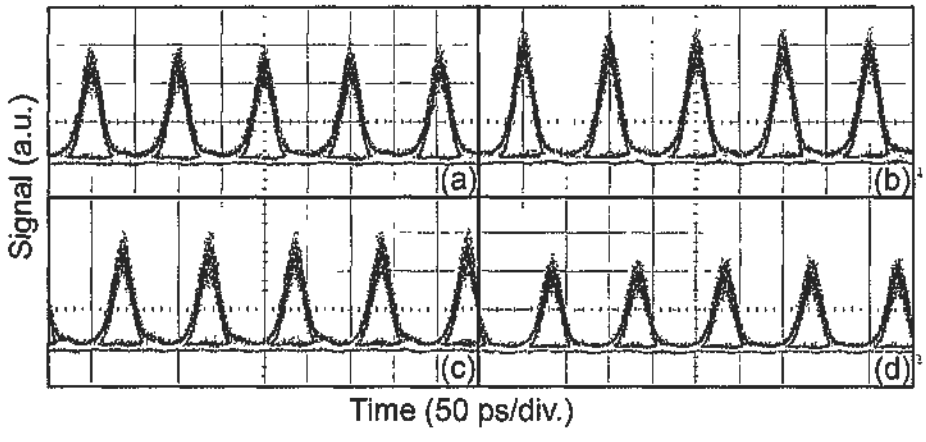

Fig. 5.2.2.3. *(a) – (d) Eye diagrams of the four multicast outputs. (a) 1547.2 nm; (b) 1549.0 nm; (c) 1549.9 nm; (d) 1551.7 nm.*

To characterize the performance of the multicast operation, bit error rate measurements have been performed on the output channels. The measurement results are shown in Fig. 5.2.2.4. Error-free operations are achieved for all the outputs with power penalties ranging from 0.8 dB to 1 dB. The power penalty is mainly caused by amplified spontaneous emission noise in the EDFAs and the noise introduced during FWM.

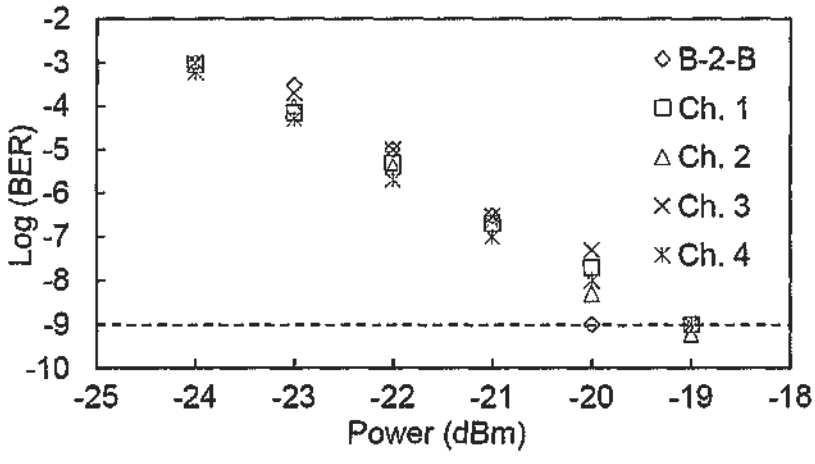

Fig. 5.2.2.4. *BER measurement results. B-2-B: NRZ-DPSK input signal. Ch.1 to Ch.4: RZ-DPSK multicast outputs. The dotted line indicates the BER level of* 10^{-9}.

In conclusion, we have experimentally demonstrated wavelength multicasting of DPSK signals with simultaneous NRZ-to-RZ format conversion. The scheme is achieved by FWM of the DPSK signal with time- and wavelength-interleaved pulses in a 64-m nonlinear photonic crystal fiber. Four multicast channels have been achieved with power penalties ranging from 0.8 dB to 1 dB. The scheme can be easily upgraded to operate at a higher speed and with additional output wavelength channels. Up to 10 wavelength channels have been demonstrated in [29]. The number of multicast channels is limited by the pulse width and also the interactions among the pulse channels. Careful wavelength arrangement is needed for expansion to more channel count.

5.3 Wavelength Conversion of High-Speed Data Signal Using Optoelectronic Devices of Limited Speed

In the previous chapter, we discussed the processing of optical analog signal using time- and wavelength-interleaved pulses. The concept can be extended to digital signal with the same pulsed source for high-speed optical signal processing. High-speed optical signal processing is important as the transmission rate of communication system continues to increase. In recent years, different approaches have been proposed to process high-speed optical signals, including the use of nonlinearity in optical fibers [30], high-speed semiconductor devices [31] and parallel processing approach [32]. For the parallel processing approach, it is necessary to divide an incoming high-speed signal into different branches. By the interaction between time- and wavelength-interleaved pulses and a high-speed optical signal, multiple lower speed branches can be generated thus parallel processing can be achieved. The use of parallel processing can help to reduce the bandwidth requirement of the optoelectronic devices. Also the scheme can be easily scalable to higher operation speed if multiple channels are used. Moreover, the carrier dynamics in the optoelectronic devices can be fully recovered, thus increasing the extinction ratios of the processed signals.

5.3.1 Introduction

With the time-wavelength mapping characteristic of the time- and wavelength-interleaved pulses, high-speed optical signal can be divided into multiple lower speed branches at different wavelengths. The schematic diagram is shown Fig. 5.3.1.1.

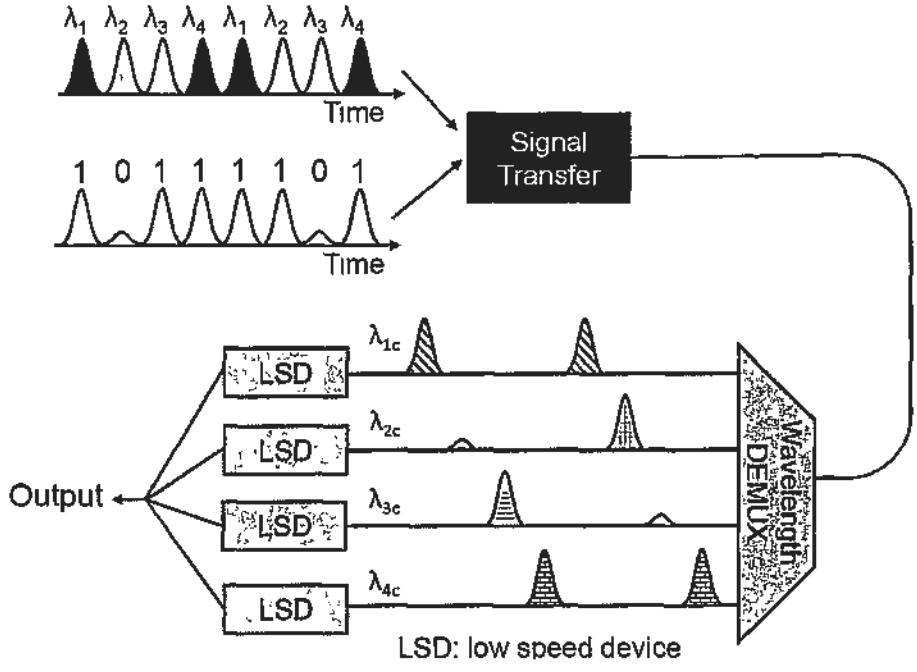

Fig. 5.3.1.1. *Schematic diagram for high-speed parallel processing. λ_1 to λ_4 :Channel 1 – 4 of time- and wavelength-interleaved pulses; λ_{1c} to λ_{4c} :demultiplexed data.*

The time- and wavelength-interleaved pulses interact with a train of high-speed data. They undergo a signal transfer process such that the data are now carried by pulses of different center wavelengths. Therefore, by a wavelength demultiplexer, the data can be split into multiple channels with a reduced operation speed. For each path, an optoelectronic device such as a low-speed electro-absorption modulator (EAM) or a semiconductor optical amplifier (SOA) can be used for different types of optical processing, including wavelength conversion, 3R regeneration and logic

operation. The processed signals from the four branches can be combined again to reconstruct the high-speed signal.

As a proof-of-concept experiment, we demonstrate the use of a 10 GHz EAM to perform wavelength conversion on a 10 Gb/s data channel demultiplexed from a 40 Gb/s OTDM data [33]. The demultiplexing is performed by four-wave mixing (FWM) between the OTDM data and the time- and wavelength-interleaved pulses. Error-free operations have been achieved for both the demultiplexing process and the wavelength conversion operation, with a total power penalty of less than 5 dB.

5.3.2 Experimental Setup

The experimental setup is shown in Fig. 5.3.2.1. Four continuous-wave (CW) laser beams obtained from a WDM source are combined with optical couplers and directed to a phase modulator. The phase modulator is modulated by a 10 GHz sinusoidal signal. As a result, the light beams are chirped and different frequency components are generated. The chirped lights are then directed to an 8.4-km single-mode fiber. As different frequency components propagate at different speeds inside the optical fiber, the chirped CW lights are then compressed into pulses. The time separation between adjacent channels is determined by the wavelength spacing and is 25 ps in this work. 40 GHz time- and wavelength-interleaved pulses are achieved at the output of the single-mode fiber. The pulses are then amplified to 20.9 dBm by an erbium-doped fiber amplifier (EDFA).

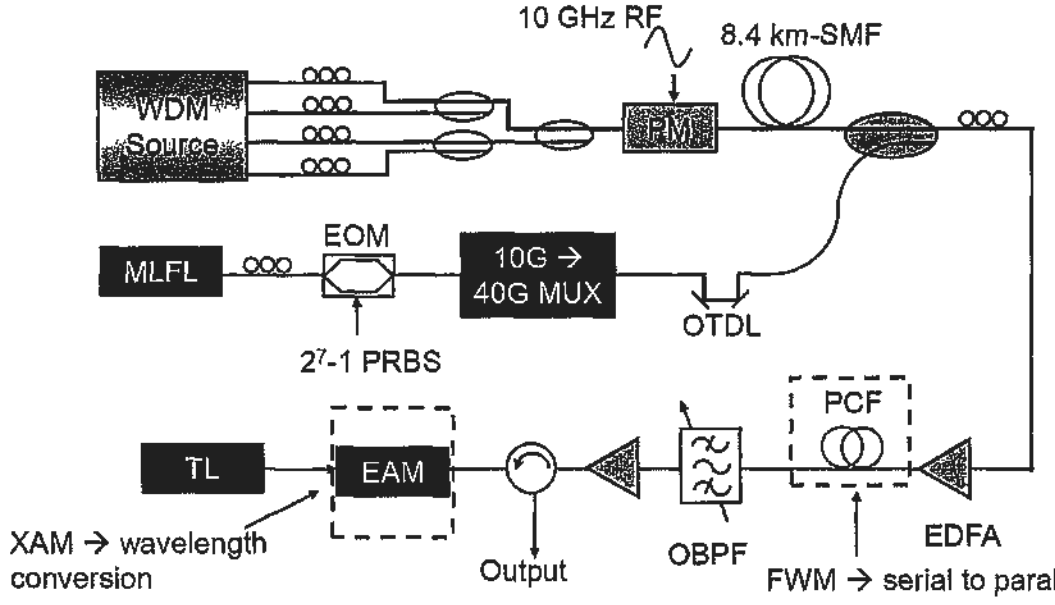

Fig. 5.3.2.1. *Experimental setup. PM : phase modulator; EDFA: erbium-doped fiber amplifier; PRBS: pseudorandom binary sequence; MUX: optical multiplexer; OTDL: optical tunable delay line; PCF: photonic crystal fiber; EAM: electro-absorption modulator; TL: tunable laser.*

To generate a 40 Gb/s OTDM signal, the output from a mode-locked fiber laser with a full-width half maximum pulse width of 10 ps is modulated by a 2^7-1 pseudorandom binary sequence in an electro-optic modulator. The wavelength of the fiber laser is ~1545.00 nm. The sequence length is limited by the commercial optical multiplexer that is used subsequently to multiply the bit-rate by a factor of 4. A 40 Gb/s OTDM data stream is thus achieved. The data stream is amplified by another EDFA to 27.5 dBm and combined with the interleaved pulses using an optical coupler. An optical tunable delay line is used to synchronize the two branches. Polarization controllers are used to optimize the states of polarization during the operation. The combined signals are then directed to a 64-m photonic crystal fiber where FWM takes place. As a result, the data are transferred to four new wavelength components, each operating at 10 Gb/s. They can then be separated by an arrayed-waveguide grating into four branches. In the experiment, we use a 0.3-nm band-pass filter instead of the grating to investigate the performance of each channel separately.

After being demultiplexed, the baseband signal is amplified to 13 dBm and directed to the input of an EAM through an optical circulator. The EAM is biased at -2.1 V. Meanwhile, a CW light at 1560 nm is obtained from a tunable laser and is connected to another input port of the EAM. Cross-absorption modulation occurs inside the EAM and the data are copied to the CW light. The output is obtained through an optical circulator.

5.3.3 Experimental Results and Discussions

The waveform of the time- and wavelength-interleaved pulses and its optical spectrum are shown in Fig. 5.3.3.1 (a) and (b), respectively. The repetition rate is 40 GHz, while the exact FWHM pulse width is determined by a 500-GHz optical sampling oscilloscope to be ~14 ps. The wavelength separation between adjacent channels is 1.6 nm. The wavelengths of the pulses are switched sequentially in time. As a result, after FWM in the PCF, each wavelength component carries information of an individual baseband channel in the OTDM data stream.

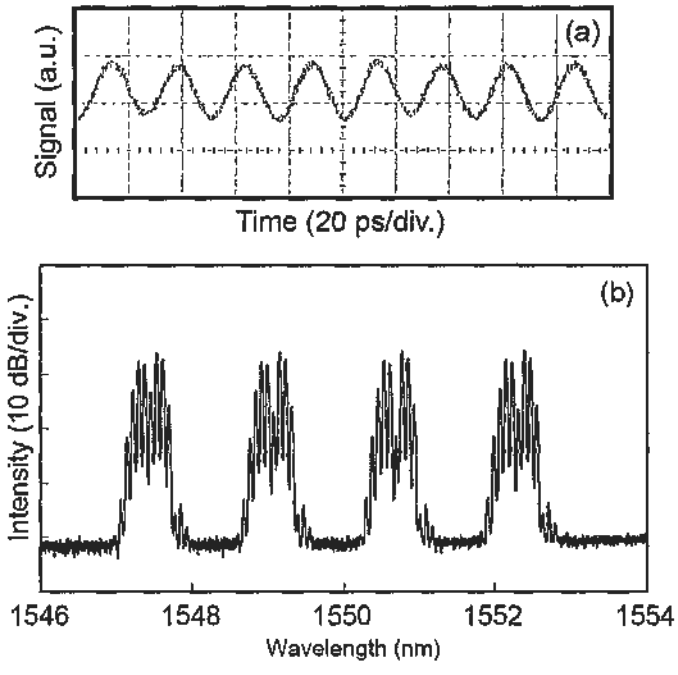

Fig. 5.3.3.1. *(a) Waveform of the time- and wavelength-interleaved pulses (b) optical spectrum. The wavelengths are selected at 1547.50 nm, 1549.08 nm, 1550.70 nm, and 1552.35 nm.*

The waveform and the optical spectrum of one demultiplexed channel are shown in Fig. 5.3.3.2 (a) and (b), respectively. Clear eye diagrams have been obtained for all channels with similar performance [34]. The spacing of the peaks in Fig. 5.3.3.2 (b) is 0.08 nm, confirming that the channel is operating at 10 Gb/s. As

mentioned above, each channel is converted to another wavelength through cross absorption modulation (XAM) in the EAM.

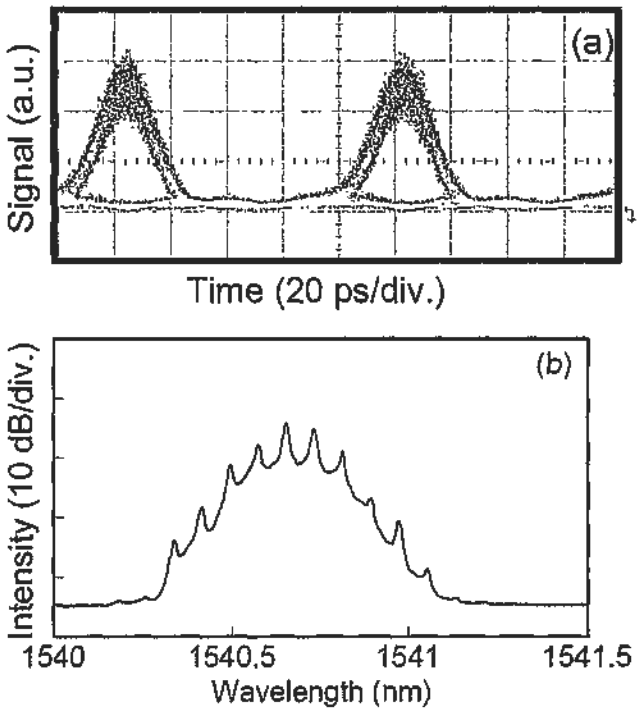

Fig. 5.3.3.2. *(a) Measured eye diagram of one demultiplexed channel (b) optical spectrum.*

Fig. 5.3.3.3 (a) to (d) show the wavelength converted outputs. It is observed that the ripples at bit zero are flattened due to the S-shape of the EAM transfer function. However, time jitter appears at the trailing edges. The jitter is believed to originate from noises inside the EAM. The response time limit of the EAM also increases the pulse width of the demultiplexed channel. However, as each channel is operating at the baseband, there is sufficient time for the distribution and density of electrical carriers to recover to its original state inside the EAM. Before combining the four channels, pulse compression should be performed to ensure that there is no overlapping between adjacent channels. By passing the converted outputs through a red-shifted filter, the distortion at the trailing edges can be reduced [35].

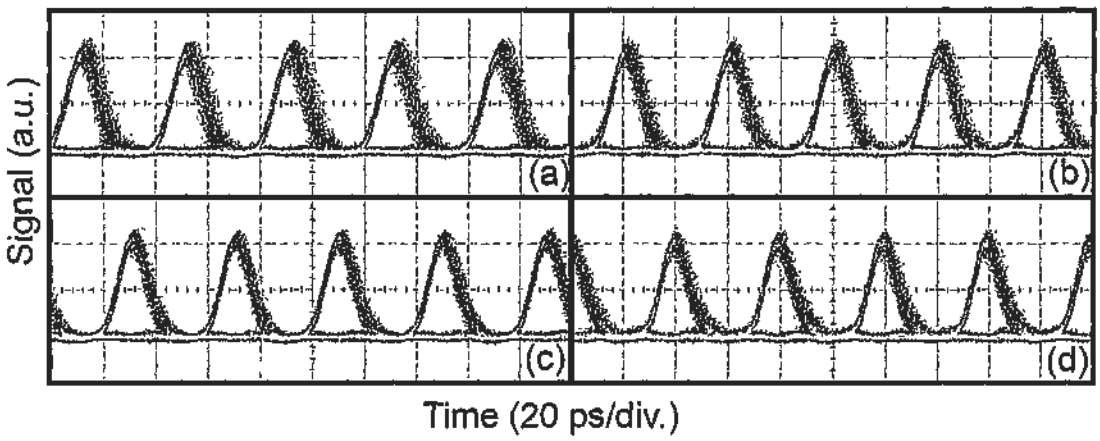

Fig. 5.3.3.3. *Waveforms of the wavelength-converted outputs from channel 1 to channel 4.*

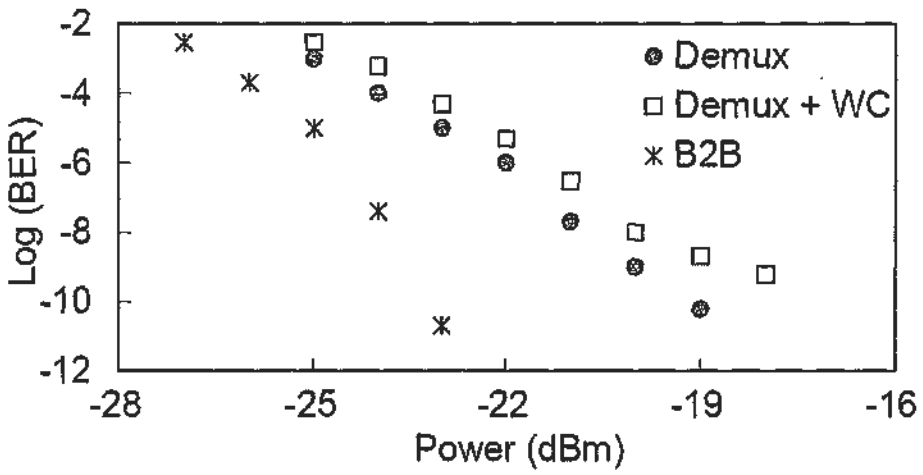

Fig. 5.3.3.4. *BER measurement. B2B: 10 Gb/s data before optical multiplexing; Demux: 10 Gb/s data after four-wave mixing-based demultiplexing; Demux + WC: 10 Gb/s wavelength-converted output with XAM in EAM.*

Bit error rate measurements are performed on the 10 Gb/s back-to-back signal before multiplexing, the demultiplexed channel, and the wavelength-converted (WC) output. The measurement results are shown in Fig. 5.3.3.4. The power penalty for the demultiplexed output is ~3 dB at a BER of 10^{-9}, while the wavelength conversion process adds another 1 dB penalty. Although there is a slight signal degradation, it is worth mentioning that a 10 GHz EAM cannot otherwise process a 40 Gb/s data without the serial-to-parallel conversion stage.

In conclusion, we demonstrate the use of a 10 GHz EAM to perform wavelength conversion of a demultiplexed channel obtained from FWM of a 40-Gb/s OTDM data with time- and wavelength-interleaved pulses. Error-free operations have been achieved for both the demultiplexing and the wavelength conversion operations. The architecture is applicable for high-speed signal processing using optoelectronic devices of limited speed performance.

5.4 Summary

In this chapter, we have experimentally demonstrated wavelength multicasting using time- and wavelength-interleaved pulses and four-wave mixing in photonic crystal fiber. Both OOK and DPSK signals can be processed using similar approaches. Four multicast channels have been achieved for both data formats. Also, we demonstrated a scheme to use optoelectronic devices of limited speed to perform wavelength conversion of high-speed data signal by serial-to-parallel processing. Error-free operations have been achieved in all of the above demonstrations.

5.5 References

[1] K. K. Chow and C. Shu, "All-optical signal regeneration with wavelength multicasting at 6×10 Gb/s using a single electroabsorption modulator," *Opt. Express*, vol. 12, pp. 3050 – 3054, June 2004.

[2] Y. Wang, C. Yu, T. Luo, L. Yan, Z. Pan, and A. E. Willner, "Tunable all-optical wavelength conversion and wavelength multicasting using orthogonally polarized fiber FWM," *J. Lightw. Technol.*, vol. 23, pp. 3331 – 3338, October 2005.

[3] C.-S. Brès, A. O. J. Wiberg, B. P.-P. Kuo, N. Alic, and S. Radic, "Wavelength multicasting of 320-Gb/s channel in self-seeded parametric amplifier," *IEEE Photon. Technol. Lett.*, vol. 21, pp. 1002 – 1005, July 2009.

[4] M. Matsuura, N. Kishi, and T. Miki, "Broadband regenerative wavelength conversion and multicasting using triple-stage semiconductor-based wavelength converters," *Opt. Lett.*, vol. 32, pp. 1026 – 1028, May 2007.

[5] C.-S. Brès, J. M. C. Boggio, N. Alic, and S. Radic, "1-to-40 10-Gb/s channel multicasting and amplification in wideband parametric amplifier," *IEEE Photon. Technol. Lett.*, vol. 20, pp. 1417 – 1419, August 2008.

[6] B. Wu, S. Fu, J. Wu, P. Shum, N. Q. Ngo, K. Xu, X. Hong, and J. Lin, "40 Gb/s multifunction optical format conversion module with wavelength multicast capability using nondegenerate four-wave mixing in a semiconductor optical simplifier," *J. Lightw. Technol.*, vol. 27, pp. 4446 – 4454, October 2009.

[7] B. P.-P. Kuo, P. C. Chui, and K. K.-Y. Wong, "All-optical tunable delay with NRZ-to-RZ format conversion capability based on optical Kerr switch and

pulse pre-chirping," *J. Lightw. Technol.*, vol. 26, pp. 3770 – 3775, December 2008.

[8] C. H. Kwok and C. Lin, "Simultaneous 4 × 10 Gb/s NRZ-to-RZ modulation format conversion in nonlinear optical loop mirror With a photonic crystal fiber," IEEE *Photon. Technol. Lett.*, vol. 19., pp.1825 – 1827, November 2007.

[9] G. K. P. Lei and C. Shu, "4 × 10 Gb/s time and wavelength multicasting with NRZ to RZ format conversion using four-wave mixing in a highly nonlinear photonic crystal fiber ," in *OSA Tech. Dig., OFC/NFOEC*, San Diego, CA, March 2010, paper JWA49.

[10] P. Seddighian and L. R. Chan, "Discretely tunable optical delay based on wavelength multi-casting and dispersion," *14th OptoElectronics and Communications Conference*, Hong Kong, July 2009, paper FE5

[11] J. Wang, Z. Bakhtiari, Y. Xiao-Li, O. F. Yilmaz, S. Nuccio, X. Wu, H. Huang, J.-Y. Yang, Y. Yue, I. Fazal, R. W. Hellwarth, and A. E. Willner, "Experimental demonstration of data traffic grooming of a single 10-Gbit/s TDM tributary channel between two 160-Gbit/s WDM channels," in *OSA Tech. Dig., OFC/NFOEC*, San Diego, CA, March 2010, paper OWF1.

[12] C. Yu, L.-S. Yan, T. Luo, Y. Wang, Z. Pan, and A. E. Willner, "Width-Tunable Optical RZ Pulse Train Generation Based on Four-Wave Mixing in Highly Nonlinear Fiber," *IEEE Photon. Technol. Lett.*, vol. 17 pp. 636 – 638, March 2005.

[13] H. Nguyen-Tan, M. Matsuura, and N. Kishi, "Transmission performance of a wavelength and NRZ-to-RZ format conversion with pulsewidth tunability by combination of SOA- and fiber-based switches," *Opt. Express.*, vol. 16, pp. 19063–19071, November 2008.

[14] B. J. Bortnik and H. R. Fetterman, "High-speed photonically assisted analog-to-digital conversion using a continuous wave multiwavelength source and phase modulation," *Opt. Lett.*, vol. 33, pp. 2230 – 2232, October 2008.

[15] T. Kobayashi, H. Yao, K. Amano, Y. Fukushima, A. Morimoto, and T. Sueta, "Optical pulse compression using high-frequency electrooptic phase modulation," *IEEE J. Quantum Electron.*, vol. 24, pp. 382 – 387, February 1988.

[16] W. S. Wong, S. Namiki, M. Margalit, H. A. Haus, and E. P. Ippen, "Self-switching of optical pulses in dispersion-imbalanced nonlinear loop mirrors," *Opt. Lett.*, vol. 22, pp. 1150 – 1152 August 1997.

[17] L. Provost, P. Petropoulos, and D. J. Richardson, "Optical WDM regeneration: status and future prospects," in *OSA Tech. Dig., OFC/NFOEC*, San Diego, CA, March 2009, paper OWD7.

[18] X. Wu, A. Bogoni, O. F. Yilmaz, S. R. Nuccio, J. Wang, and A. E. Willner, "8-fold 40-to-320-Gbit/s phase-coherent WDM-to-TDM multiplexing and 320-to-40-Gbit/s demultiplexing using highly nonlinear fibers," in *OSA Tech. Dig., OFC/NFOEC*, San Diego, CA, March 2010, paper OThV4.

[19] G. K. P. Lei, C. Shu, and M. P. Fok, "All-optical OTDM to WDM signal conversion using cross absorption modulation with time- and wavelength-interleaved short pulse," *IEEE Photon. Technol. Lett.*, vol. 22, pp. 571-573, April 15, 2010.

[20] P. J. Winzer and A. Kalmár, "Sensitivity enhancement of optical receivers by impulsive coding," *J. Lightw. Technol.*, vol. 17, pp. 171 – 177, February 1999.

[21] E. Modiano and P. J. Lin, "Traffic grooming in WDM networks," *IEEE Commun. Mag.*, vol. 39, pp. 124 – 129, July 2001.

[22] P. J Winzer. and R.-J. Essiambre, "Advanced optical modulation formats," *Proceedings of the IEEE*, vol. 94, pp. 952 – 985, May 2006.

[23] M. P. Fok and C. Shu, "Multipump four-wave mixing in a photonic crystal fiber for 6 × 10 Gb/s wavelength multicasting of DPSK signals," *IEEE Photon. Technol. Lett.*, vol. 19, pp. 1166 – 1168, August 2007.

[24] O. F. Yilmaz, S. R. Nuccio, S. Khaleghi, J.-Y. Yang, L. Christen, and A. E. Willner, "Optical multiplexing of two 21.5 Gb/s DPSK signals into a single 43 Gb/s DQPSK channel with simultaneous 7-fold multicasting in a single PPLN waveguide," in *OSA Tech. Dig., OFC/NFOEC*, 2009, San Diego, CA, March 2009, paper OThM4.

[25] R. Slavik, J. Kakande, F. Parmigiani, L. Gru□ner-Nielsen, D. Jakobsen, S. Herstrøm, P. Petropoulos, and D. J. Richardson, "All-optical phase-regenerative multicasting of 40 Gbit/s DPSK signal in a degenerate phase sensitive amplifier," in *36th European Conference and Exhibition on Optical Communication (ECOC)*, Torino, Italy, September 2010, paper Mo.1.A.2.

[26] D. Wang, T.-H. Cheng, Y.-K. Yeo, Z. Xu, Y. Wang, G. Xiao, and J. Liu, "Performance comparison of using SOA and HNLF as FWM medium in a wavelength multicasting scheme with reduced polarization sensitivity," *J. Lightw. Technol.*, vol.28, pp. 3497 – 3505, December 2010.

[27] Y. Dai and C. Shu, "Polarization-insensitive wavelength multicasting of RZ-DPSK signal based on four-wave mixing in a photonic crystal fiber with residual birefringence," in *OSA Tech. Dig., OFC/NFOEC*, 2010, San Diego, CA, March 2010, paper OWP7.

[28] Gordon K. P. Lei, Yongheng Dai, Jiangbing Du, and Chester Shu, "Wavelength multicsting of DPSK signal with NRZ-to-RZ format conversion," *Electron. Lett.*, vol. 47, issue 17, pp. 808 – 810, July 2011.

[29] K. L. Lee, C. Shu, and H. F. Liu, "Subharmonic Pulse-Gating in Self-Seeded Laser Diodes for Time- and Wavelength-Interleaved Picosecond Pulse Generation," *IEEE J. Quantum Electron.*, vol. 40, pp. 205 – 213, March 2004.

[30] H. Hu, E. Palushani, M. Galili, H. Mulvad, A.T. Clausen, L.K. Oxenlowe, and P. Jeppesen,"1.28 Tb/s wavelength conversion for polarisation multiplexed RZ-DPSK signals," *in OSA Tech. Dig., OFC/NFOEC*, San Diego, CA, March 2010, paper OWP1.

[31] G. Contestabile, A. Maruta, S. Sekiguchi, K. Morito, M. Sugawara, and K.-i. Kitayama, "Cross-Gain Modulation in Quantum-Dot SOA at 1550 nm," *IEEE J. Quant. Electron.*, vol. 46, no. 12, pp. 1696 – 1703, December 2010.

[32] Y. Han and B. Jalali, "Continuous-time time-stretched analog-to-digital converter array implemented using virtual time gating," *IEEE Trans. Circuits and Syst.—I*, vol. 52, pp. 1502-1507, August 2005.

[33] Gordon K. P. Lei and Chester Shu, "Performance investigation of processing high-speed optical signals using time- and wavelength-interleaved pulses and low-speed optoelectronics," *in Asia Communications & Photonics Conference & Exhibition 2010*, Shanghai, China, Dec. 2010, paper SuH2.

[34] G. K. P. Lei, C. Shu, and M. P. Fok, "All-optical OTDM to WDM signal conversion using cross absorption modulation with time- and wavelength-interleaved short pulse," *IEEE Photon. Technol. Lett.*, vol. 22, pp. 571-573, April 2010.

[35] N. El Dahdah, R. Coquillé, B. Charbonnier, E. Pincemin, C. Kazmierski, J. Decobert, A. Vedadi, G. Aubin, and A. Ramdane, "All-optical wavelength conversion by EAM with shifted bandpass filter for high bit-rate networks," *IEEE Photon. Technol. Lett.*, vol. 18, pp. 61–63, January 2006.

6 All-Optical OTDM-to-WDM Conversion

To increase the capacity in the optical fiber, different multiplexing techniques can be adopted. Some examples are optical time-division multiplexing (OTDM), wavelength-division multiplexing (WDM) and polarization-division multiplexing (PDM). In different optical networks, different multiplexing techniques can be used. For example, in long-haul transmission, OTDM has many potential advantages [1, 2] while WDM is popular in metro networks [3 – 6]. To bridge networks with different multiplexing schemes, an all-optical conversion is desirable as the data rates of these networks are usually over the bandwidth limit of electronics. By performing all-optical demultiplexing and wavelength conversion, an OTDM signal can be converted to a number of lower-speed WDM channels. In this chapter, we will introduce two approaches to perform OTDM-to-WDM conversion with the time- and wavelength-interleaved pulses. In Section 6.1, the conversion using cross-absorption modulation (XAM) in electro-absorption modulator (EAM) is achieved. In Section 6.2, four-wave mixing (FWM) in photonic crystal fiber (PCF) is performed instead. We will discuss the experimental results and the comparison between these two approaches will be given in details.

6.1 OTDM-to-WDM Conversion by Cross-Absorption Modulation in an Electro-Absorption Modulator

All-optical conversion between optical time division multiplexing (OTDM) and wavelength division multiplexing (WDM) signals has been a subject of intense research. By performing all-optical demultiplexing and wavelength conversion, an OTDM signal can be converted to a number of lower-speed WDM channels. Examples of the approaches include wavelength conversion in a Mach-Zehnder interferometer [7] and cross-phase modulation (XPM) in a nonlinear optical loop mirror (NOLM) [8] or a semiconductor optical amplifier (SOA) [9]. The above approaches rely on precise time delay among individual laser branches or complicated source generation scheme, making them unattractive for application in a system with large channel count. OTDM to WDM conversion has also been demonstrated using four-wave mixing (FWM) with WDM sampling pulses in a highly non-linear fiber [10] or spectral slicing of data-signal-induced supercontinuum light source [11]. However, the setups are relatively bulky, polarization sensitive, and are dependent on high-power operation. In this demonstration [12, 13], we generate 40-GHz time- and wavelength-interleaved pulses by XAM of four laser beams in an electro-absorption modulator (EAM) followed by dispersion in a linearly chirped fiber Bragg grating (CFBG). We then applied the pulses for 40-Gb/s OTDM to 4 × 10-Gb/s WDM signal conversion, again through XAM. The setup is compact, potentially integrable, and operates at moderate optical power levels. Bit-error rate measurement shows error-free operation with power penalties ranging from 4 to 6 dB.

The operation principle is illustrated in Fig. 6.1.1. A time- and wavelength-interleaved pulsed source is directed to a reversely biased EAM. All the light pulses

are absorbed at this stage. An OTDM data stream is input to the EAM at another input port via an optical circulator. When a bit "0" in the data stream is fed into the EAM, the time- and wavelength-interleaved pulses are absorbed by the EAM and no light can pass through the device. When a bit "1" is input to the EAM, the intense light screens the electric field applied to the EAM. During this time window, the time- and wavelength-interleaved pulses can pass through the EAM and be observed from the output port of the optical circulator. An example is shown in Fig. 6.1.1 with data bits "1001". As the "1" bits are time aligned with λ_1 and λ_4, the pulses of these two wavelengths can pass the EAM while λ_2 and λ_3 are absorbed. The data are thus correctly copied to the pulses. By the time-to-wavelength mapping of the pulsed source, different channels can be separated using a WDM filter or arrayed-waveguide grating. OTDM-to-WDM conversion is thus achieved.

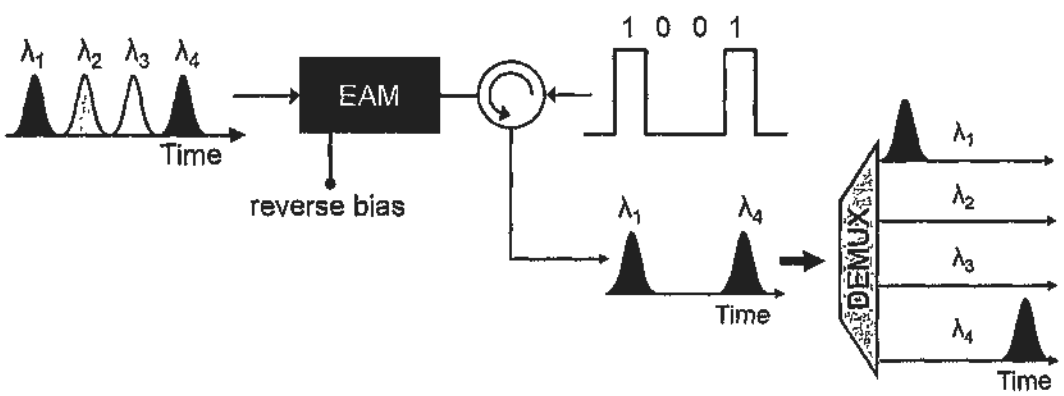

Fig. 6.1.1. *Operation principle of OTDM-to-WDM conversion with XAM in EAM.*

6.1.1 Experimental Setup

The experimental setup is shown in Fig. 6.1.1.1. Four continuous-wave (CW) lasers are obtained from a WDM source. The wavelength spacing is 1.3 nm. The laser outputs are combined with optical couplers before they are connected to the input port of EAM1. Another input port of EAM1 is connected to a 10-GHz mode-locked fiber laser (MLFL) via an optical circulator. The MLFL is centered at 1536.41 nm. The intensity FWHM pulse width measured with a 500-GHz optical sampling oscilloscope is 12 ps. The pulse shape is squared hyperbolic secant.

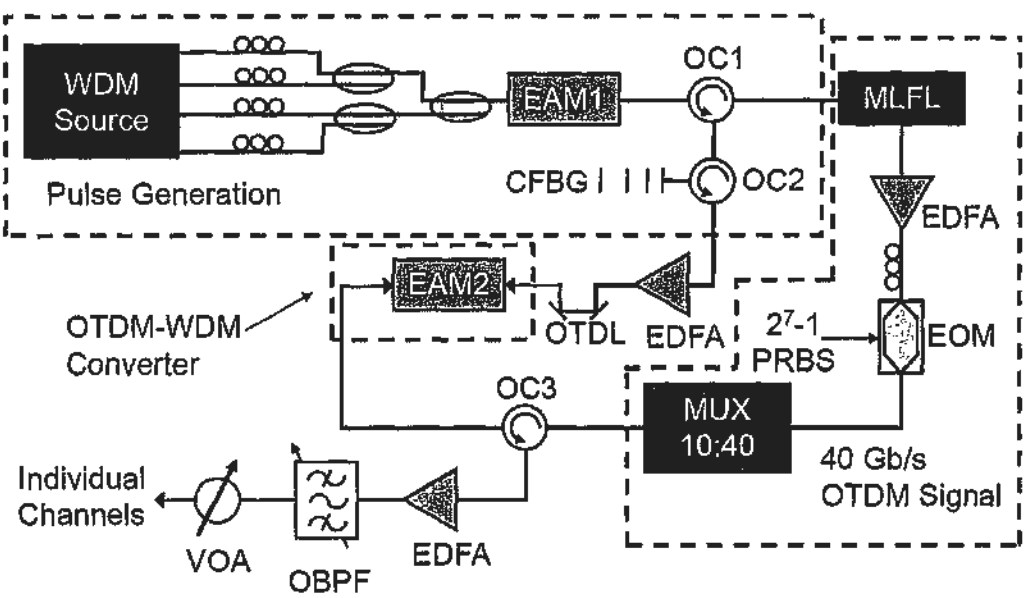

Fig. 6.1.1.1. *Experimental setup for OTDM to WDM conversion. EAM1, EAM2: electro-absorption modulator; OC1, OC2 and OC3: optical circulator; MLFL: mode-locked fiber laser; CFBG: linearly chirped fiber Bragg grating; EDFA: erbium-doped fiber amplifier; OTDL: optical tunable delay line; EOM: electro-optic modulator; PRBS: pseudorandom binary sequence; MUX: optical multiplexer; OBPF: optical band pass filter; VOA: variable optical attenuator.*

EAM1 is biased at -3 V to maximize the absorption of the CW lasers in the absence of the MLFL. When the MLFL is applied, XAM takes place and the four CW lasers are modulated. The modulated lasers are then reflected by the CFBG via

another optical circulator. The dispersion of the CFBG is ~20 ps/nm and introduces a 25-ps separation between adjacent pulses. The 3-dB bandwidth of the CFBG is ~30 nm and is centered at 1550 nm, enabling a wideband operation. 40-GHz time- and wavelength-interleaved pulses are thus achieved. The pulses are amplified to 9.8 dBm by an erbium-doped fiber amplifier before it is directed to EAM2.

To generate a 40-Gb/s OTDM signal, a 10-GHz pulsed source is obtained from another output port of the MLFL. In practice, a separate pulsed source should be used. The laser pulses are modulated by an electro-optic modulator with a 2^7-1 pseudorandom binary sequence (PRBS). The pattern length is limited by the delay of the optical multiplexer. The modulated signal is multiplexed to 40 Gb/s and amplified to 16 dBm. The signal enters EAM2 via an optical circulator. An optical tunable delay line is used to ensure the time synchronization between the OTDM signal and the interleaved pulses. XAM is performed in EAM2 and the output is obtained from OC3. The output is amplified by another EDFA to achieve the minimum detection power. It is worth mentioning that the polarization sensitivities for both EAMs are within 0.5 dB, providing a polarization-insensitive property for the whole process.

6.1.2 Experimental Results on EAM

To optimize the conversion performance, we first investigate the characteristics of the EAM utilized in the experiment. The static characteristic of EAM2 from 1540 to 1560 nm is shown in Fig. 6.1.2.1. It is observed that the EAM absorption efficiency is wavelength-dependent, agreeing with the results in [14, 15]. The absorption changes rapidly at a reverse bias voltage of around -1.5 V.

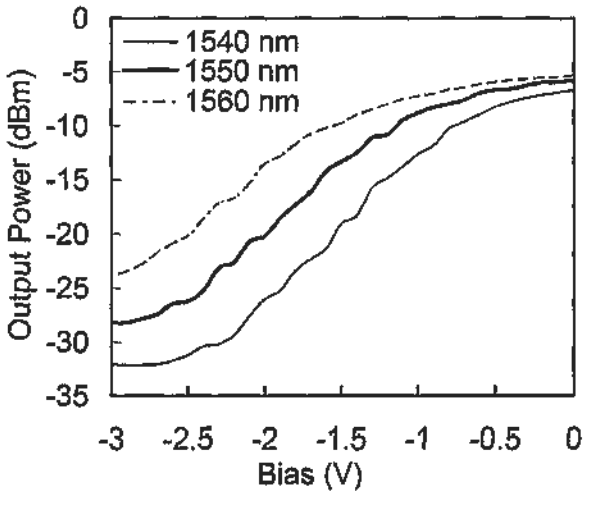

Fig. 6.1.2.1. *Output power against bias voltage of EAM2 at different input wavelengths. The input optical power is 0 dBm.*

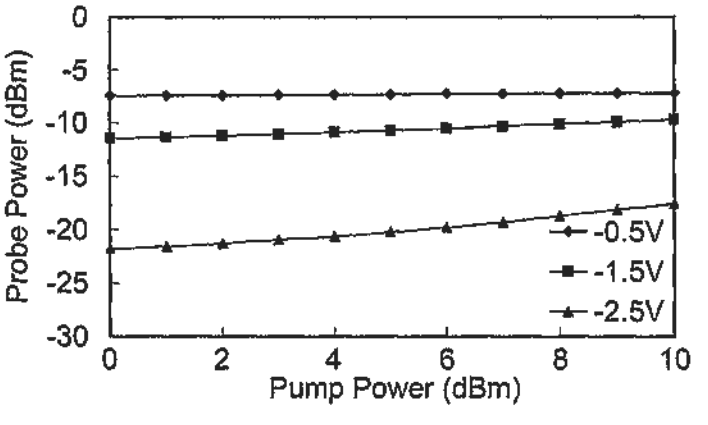

Fig. 6.1.2.2. *Output probe power against pump power at different bias voltages.*

The XAM performance at different bias is plotted in Fig. 6.1.2.2. In the measurement, both probe and pump lights are CW and they counter-propagate inside the EAM2. As the design of the EAM2 is not optimized for XAM operation, a 10 dB

change in pump power can only induce a ~ 2 dB change in the probe power at the bias voltage of -1.5 V. We can anticipate that the on-off ratio of the demultiplexed channels is not very high. It is worth mentioning at the bias voltage of -2.5 V, a 5 dB change in probe power can be achieved, which in principle can lead to better performance in OTDM-to-WDM conversion. However, the optical loss is too high and additional amplification decreases the signal-to-noise ratio. During the experiment, both the extinction ratio of the cross-absorption modulated pulses and the output power are optimized to obtain the largest eye-opening after the conversion.

6.1.3 Experimental Results on OTDM-to-WDM Conversion

The waveforms of different channels in the time- and wavelength-interleaved pulses are shown in Fig. 6.1.3.1 (a) to (d). The repetition rate at each channel is 10 GHz and the pulse width is around 20 ps. The contrast ratio of the pulses is 25 dB. The time-bandwidth product of the pulses is ~ 0.524, showing that the pulses are slightly chirped. The measured optical spectrum is shown in Fig. 6.1.3.1 (e). The pulse width is limited by the pulse width of the MLFL, which is 12 ps in this experiment. The pulse width of the time- and wavelength-interleaved source can be reduced if a separate MLFL is used to optimize each stage of XAM.

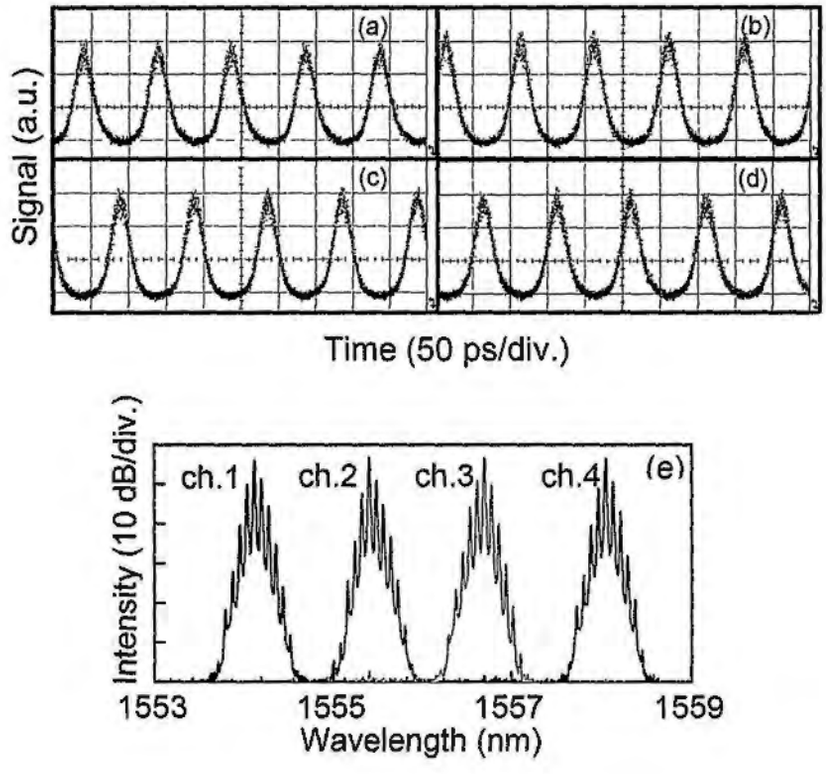

Fig. 6.1.3.1. *(a) – (d)Waveforms of the four channels of the time- and wavelength-interleaved pulses. (e) Optical spectrum of the interleaved pulses. The center wavelengths of the four channels are 1554.10, 1555.40, 1556.70, and 1558.05 nm respectively.*

The eye diagram of the 40 Gb/s OTDM data is shown in Fig. 6.1.3.2. The data stream is generated at 1536.00 nm. The data acts as pump to screen out the electric field applied to EAM2.

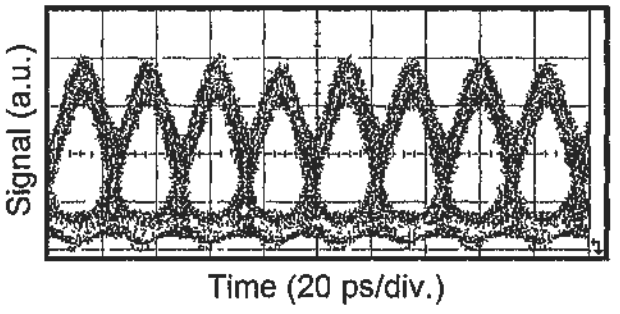

Fig. 6.1.3.2. *Eye diagram of the 40 Gb/s OTDM data.*

After XAM in EAM, we filter out the four individual channels from the EAM output using a 0.3-nm optical band pass filter. In principle, an arrayed waveguide grating can be used to separate all the channels simultaneously.

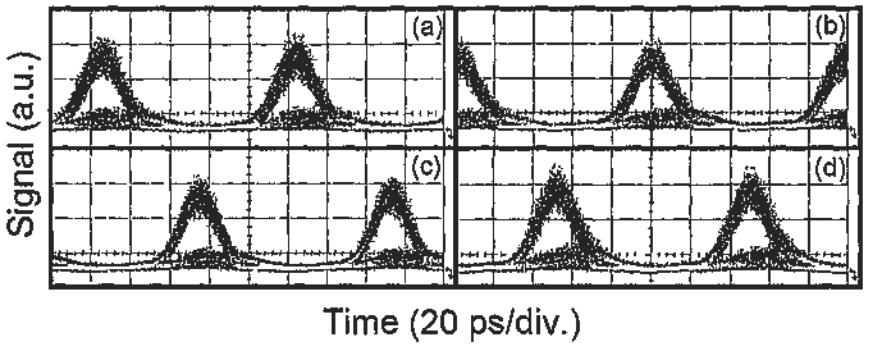

Fig. 6.1.3.3. *(a) – (d) Eye diagrams of the four demultiplexed channels, from ch.1 to ch. 4.*

Figure 6.1.3.3 (a) – (d) show the eye diagrams of the four demultiplexed channels. The traces are detected using a 50-GHz digital oscilloscope with a 32-GHz photodetector. The response of the whole detection system is ~ 17 ps. We observe some amplitude noise together with a slight reduction in the extinction ratio. The degradation occurs as a result of channel overlapping in the interleaved pulses shown in Fig. 6.1.3.1. When an OTDM bit "1" opens an optical gate in the EAM for the corresponding pulse in the interleaved source, the pulses at adjacent channels can

also be partially transmitted due to the channel overlapping. As a result, the signal-to-noise ratio of the output is reduced.

The BER performances of the four channels are shown in Fig. 6.1.3.4. Error-free operations (BER<10^{-9}) are obtained in all channels. However, a relatively large power penalty of 4 to 6 dB is observed. The penalty is mainly caused by channel overlapping of the interleaved pulses as described above. An additional cause for the degradation is the reduction of optical signal-to-noise ratio in the EAMs and additional amplified spontaneous emission (ASE) noise from the EDFA. The power penalty varies slightly among the four channels owing to power fluctuation in the WDM laser source. An error floor appears in the converted outputs, suggesting that an optical regenerator such as a Mamyshev-based regenerator [16] or EAM-based regenerator [17] may be needed to improve the system performance.

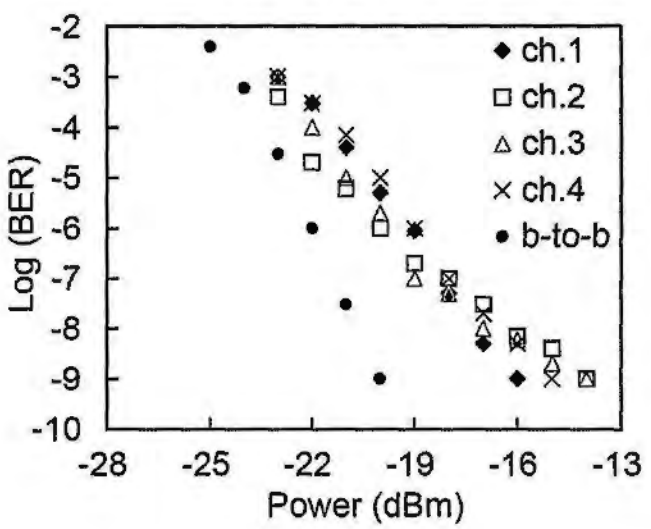

Fig. 6.1.3.4. *BER performance of the 10 Gb/s back-to-back and the 4 demultiplexed WDM signals.*

In conclusion, a new scheme for all-optical OTDM to WDM signal conversion has been demonstrated using XAM in an EAM with time- and wavelength-interleaved pulses. The time separation between pulses at different wavelengths is determined by wavelength mapping of the pulses. No adjustment is

needed on the optical delay of individual laser branches. We have successfully applied the scheme for 40 Gb/s OTDM to 4×10 Gb/s WDM conversion. The power penalty is 4 – 6 dB and is limited by temporal overlapping of the interleaved pulses and additional ASE noise. The system can be further improved to operate at higher bit rates by accommodating more channels in the setup. The compact setup is potentially integrable and provides a polarization insensitive solution to address all-optical data conversion in future photonic networks.

6.2 OTDM-to-WDM Conversion by Four-Wave Mixing in Photonic Crystal Fiber

In last section, we have demonstrated OTDM-to-WDM conversion by XAM in EAM. However, the power penalties are relatively large due to the large pulse widths and the limited speed of EAM. For higher speed operation up to 80 Gb/s or even 160 Gb/s, expensive semiconductor devices are needed, such as quantum-dot semiconductor optical amplifier (QD-SOA) [18] and quantum-dash mode-locked laser diode (QD-MLLD) [19]. Instead, the use of nonlinearity in specialty fiber can help to reduce the cost and enhance the bandwidth a lot. For the application of OTDM-to-WDM conversion, different approaches have been proposed to achieve the operation in specialty fibers including time-domain Fourier transform [20], self-phase modulation with a single optical gate [21] and optical parametric amplification [22]. Other than these effects in specialty fibers, in recent years, pump-modulated FWM has been rigorously pursued for all-optical signal processing. The regenerative property of the approach has been previously demonstrated [23, 24]. By the regenerative properties, the performance of the OTDM-to-WDM conversion is expected to improve compared with the previous approach using XAM in EAM. In this section, we experimentally demonstrate the conversion of 40 Gb/s OTDM data to 4 × 10 Gb/s WDM channels by pump-modulated four-wave mixing with a time- and wavelength-interleaved pulsed source in a highly nonlinear photonic crystal fiber (PCF) [25]. With the regenerative property of pump-modulated FWM, the extinction ratios of the demultiplexed channels are enhanced compared with that of the 40 Gb/s OTDM input data.

The operation principle is illustrated in Fig. 6.2.1. A time- and wavelength-interleaved pulsed source is combined with the OTDM data and directed to the PCF.

FWM occurs inside the PCF. During the FWM process, four idlers are generated. The information of the individual idlers is governed by the following equation:

$$\hat{E}_{FWM} \propto [\hat{E}_p \cdot \hat{E}_s^*]\hat{E}_p \qquad [6.1]$$

where E_{FWM} is field amplitude of the FWM-generated idler, E_p is the field amplitude of the pump and E_s is the field amplitude of probe pulses. It is worth mentioning that the OTDM data acts as a pump during the FWM process. As a result, the field amplitudes of the idlers have a quadratic relationship with the field amplitude of the OTDM data. In consequence, the extinction ratios of the idlers are enhanced compared with the input data stream.

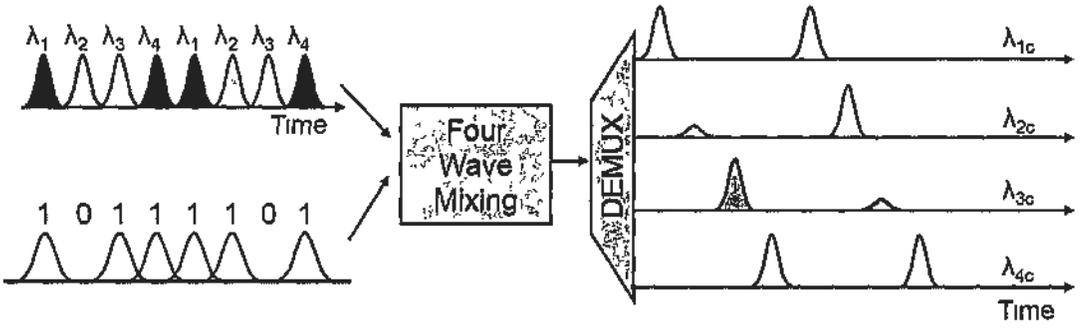

Fig. 6.2.1. *Operation principle of OTDM-to-WDM conversion with FWM in PCF*

Moreover, as different wavelength components reside at different time slots in the time- and wavelength-interleaved pulsed source, each converted wavelength component contains information in a particular channel of the OTDM data. By filtering out the four generated components, four WDM channels are obtained. As a result, the OTDM to WDM conversion is achieved.

6.2.1 Experimental Setup

The experimental setup is shown in Fig. 6.2.1.1. Four CW laser outputs are obtained from a WDM source. The four branches are combined with couplers and directed to the input of a phase modulator. The phase modulator is driven by a 10 GHz RF signal, introducing a 10 GHz chirp on the CW lights. The CW lights are then transmitted in an 8.4 km single-mode fiber (SMF), introducing a dispersion of -142 ps•nm^{-1}. Owing to frequency chirp introduced in the phase modulator, different portions of the CW lights are of different instantaneous frequencies. As a result, group delay occurs for the CW lights and short pulses are generated through group velocity dispersion in the SMF. At the same time, since the four CW lights are of different wavelengths, inter-channel time delay occurs between adjacent channels. By optimizing the phase modulation depth, the wavelength spacing and the dispersion, a 4 × 10 GHz time- and wavelength-interleaved pulsed source is achieved.

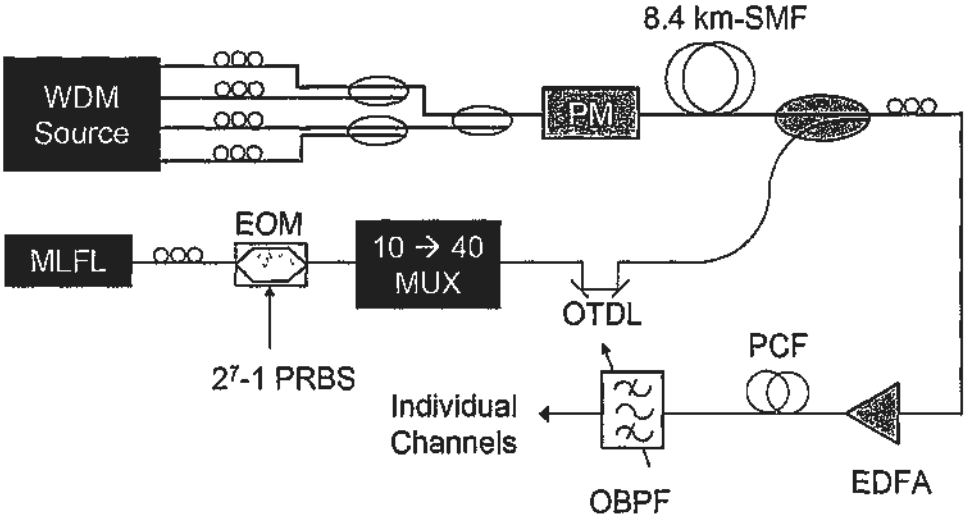

Fig. 6.2.1.1. *Experimental setup. EDFA: erbium-doped fiber amplifier; EOM: electro-optic modulator; MLFL: mode-locked fiber laser; MUX: multiplexer; OBPF: optical band-pass filter; OTDL: optical tunable delay line; PCF: photonic crystal fiber; PM: phase modulator; PRBS: pseudorandom binary sequence; SMF: single mode fiber.*

To generate a 40 Gb/s OTDM signal, a 10-GHz pulsed source is obtained from the output port of a mode-locked fiber laser (MLFL). The laser pulses are then modulated by an electro-optic modulator with a 2^7-1 pseudorandom binary sequence (PRBS) and optically multiplexed to 40 Gb/s. The sequence length is limited by the maximum delay provided by the optical multiplexer. The 40 Gb/s OTDM data are then combined with the time- and wavelength-interleaved pulses. A tunable optical delay line is added after the multiplexer to ensure synchronization between the two light branches. The combined signal is directed to an EDFA through a polarization controller and is then amplified to 27 dBm. FWM occurs inside the PCF and four new wavelengths are generated. The individual channels are filtered out for further investigation.

6.2.2 Experimental Results on Extinction Ratio Enhancement

The waveform of the time- and wavelength-interleaved pulses is measured with a 32-GHz photodetector connected to a 50-GHz digital sampling oscilloscope with a measurement response time of ~ 17 ps. The result is shown in Fig. 6.2.2.1. With an optical sampling oscilloscope, the width of the laser pulses is determined to be 14.4 ps as shown in Fig. 6.2.2.2. The wavelength spacing between adjacent channels is 1.25 nm. The wavelengths of the pulsed source range from 1548.40 nm to 1552.24 nm. The pulsed source acts as probes during FWM.

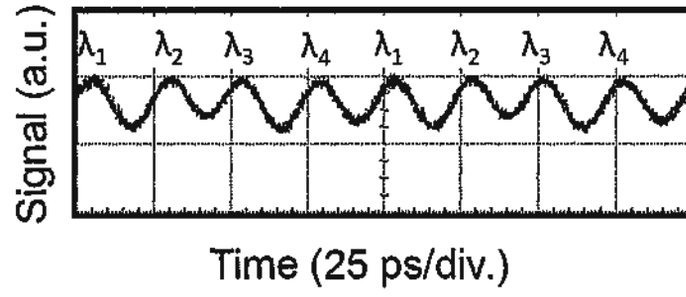

Fig. 6.2.2.1. *Temporal profile of the time- and wavelength-interleaved pulses. The center wavelengths of the four channels are 1548.40, 1549.76, 1550.92, and 1552.24 nm, from λ_1 to λ_4 respectively.*

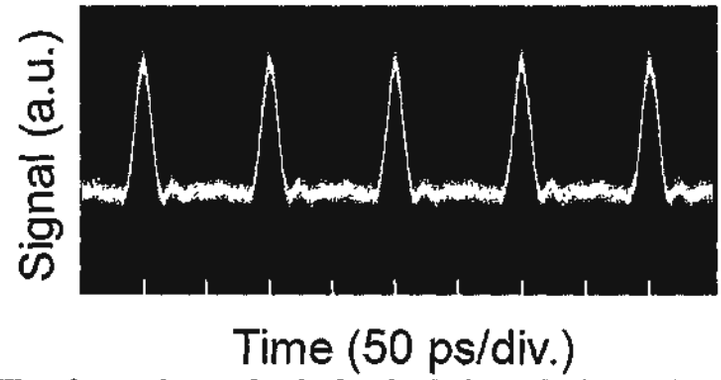

Fig. 6.2.2.2. *Waveform of an individual pulsed channel, detected using a 500-GHz optical sampling oscilloscope.*

The eye diagram of the 40 Gb/s OTDM data is shown in Fig. 6.2.2.3. The quality of the data is distorted intentionally by applying an offset bias to the electro-

optic modulator. The extinction ratio is 8.6 dB. Four-wave mixing occurs in a 64-m, highly nonlinear, low-dispersion, and dispersion-flattened PCF. The nonlinear coefficient γ is equal to 11 $W^{-1}km^{-1}$, with a dispersion of < 3 $ps{\bullet}km^{-1}nm^{-1}$ over the C-band and a dispersion slope of 10^{-3} $ps{\bullet}km^{-1}nm^{-2}$. The 3-dB conversion bandwidth of the PCF is 16 nm. The wide conversion bandwidth ensures similar conversion efficiencies for all pulsed channels.

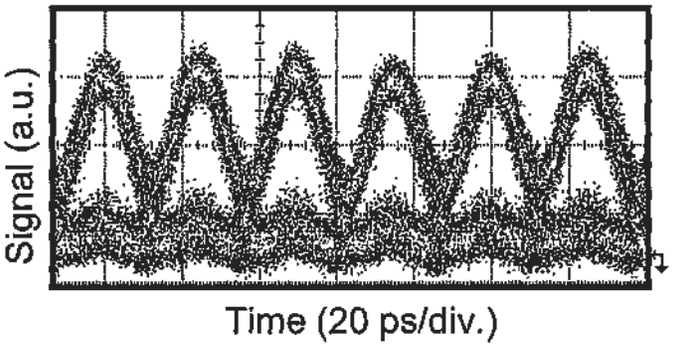

Fig. 6.2.2.3. *Eye diagram of the distorted 40 Gb/s OTDM data stream. The extinction ratio is 8.6 dB.*

After FWM in PCF, the OTDM data are demultiplexed into four WDM channels. To examine the property of extinction ratio enhancement, we filter out the idler generated by FWM between the data pump and the pulsed probe at 1548.40 nm. The eye diagram of the filtered channels is shown in Fig. 6.2.2.4.

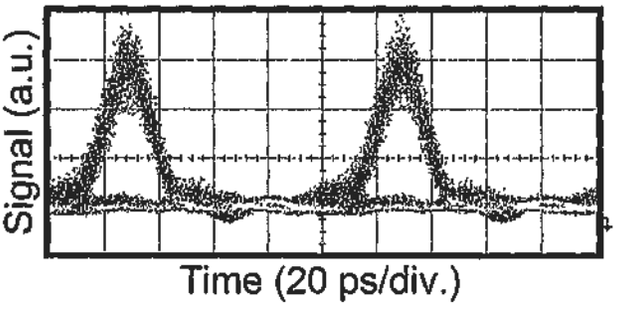

Fig. 6.2.2.4. *Eye diagram of one demultiplexed channel. The extinction ratio is enhanced to be 11.2 dB.*

A widely opened eye with an extinction ratio of 11.2 dB is obtained, showing a 2.6 dB improvement compared with the original 40 Gb/s OTDM data. The noise on bit "0" is also suppressed. We observe channel crosstalk at the leading and trailing

edges that can be attributed to pulse pedestal observed in Fig. 6.2.2.2. The pedestal can be eliminated with further compression of the pulses and additional pulse cleaning process [26]. However, as both the OTDM data and demultiplexed channels are too noisy, bit-error rate measurement cannot be performed. To further investigate the performances of the OTDM-to-WDM converter, an error-free OTDM data is used instead of a noisy one.

6.2.3 Experimental Results on OTDM-to-WDM Conversion

The eye diagram of the error-free 40 Gb/s OTDM data is shown in Fig. 6.2.3.1. The wavelength of the data is at 1545.5 nm. The extinction ratio of the data stream is over 11 dB. The optical spectrum after FWM in PCF is shown in Fig. 6.2.3.2. The conversion efficiency, defined as the peak intensity ratio between the generated idler and the input probe, is ~ -20 dB. Also, it is observed that the conversion efficiencies of the FWM components generated among the pulsed channels are less than -25 dB, proving that the slight overlapping between adjacent pulses does not introduce serious crosstalk among the WDM channels.

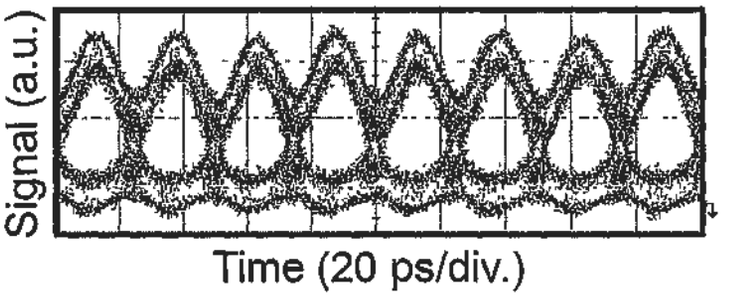

Fig. 6.2.3.1. *Eye diagram of a normal 40 Gb/s OTDM data stream. The extinction ratio is over 11 dB.*

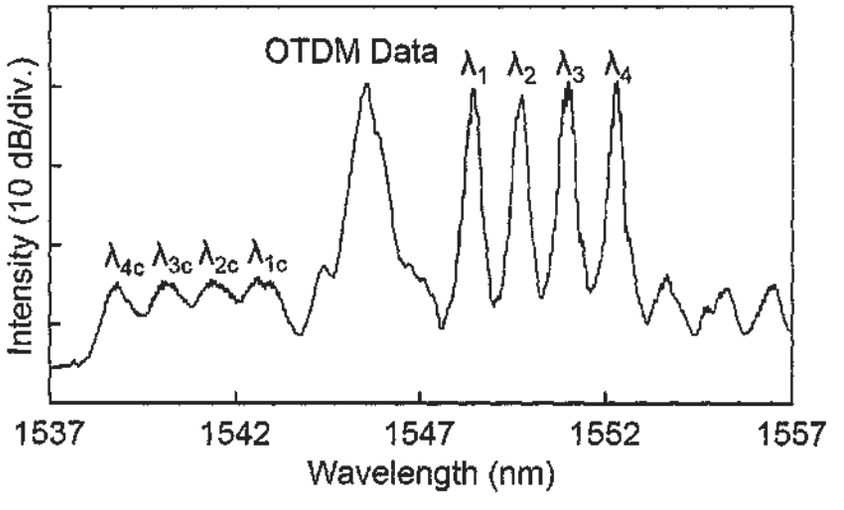

Fig. 6.2.3.2. *Optical spectrum after FWM in PCF.*

The waveforms of the filtered idlers are shown in Fig. 6.2.3.3 (a) – (d). . The idlers are generated at 1542.6, 1541.24, 1540.08, and 1538.76 nm, respectively. Non-uniform amplitudes are observed for the four channels. The reason is that the EDFA used in the experiment has a non-flattened gain over its spectrum.

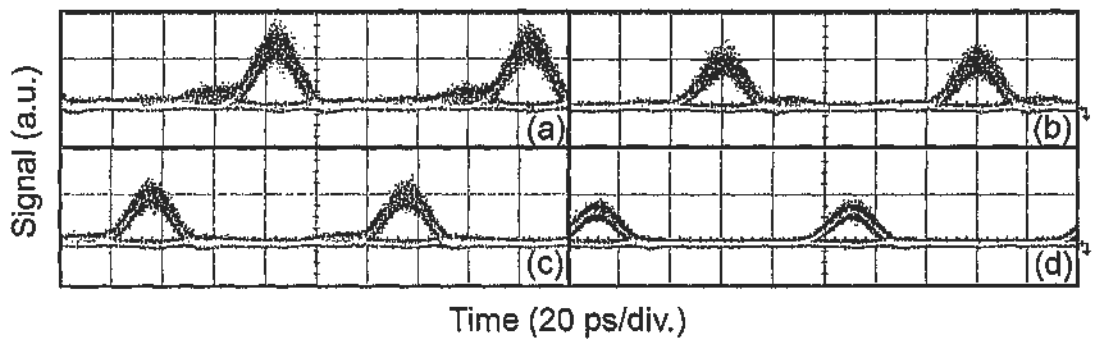

Fig. 6.2.3.3. *(a) – (d) Eye diagrams the demultiplexed channels, from λ_{1c} to λ_{4c} respectively.*

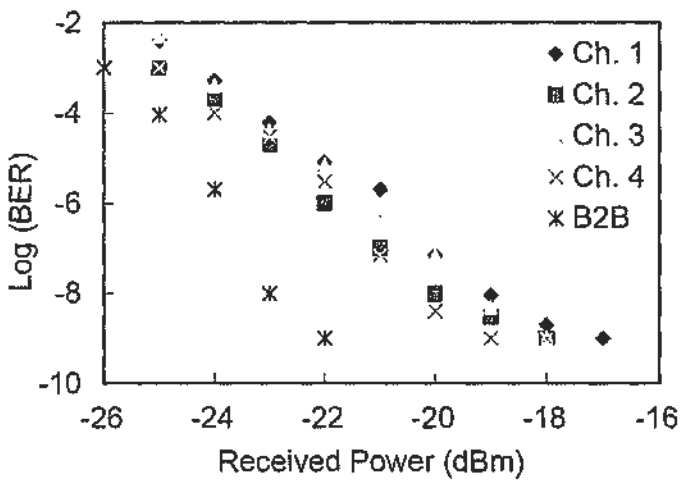

Fig. 6.2.3.4. *BER measurement. B2B: back-to-back measurement on 10 Gb/s before optically multiplexed to 40 Gb/s OTDM data.Ch.1 to Ch. 4: demultiplexed channels from λ_{1c} to λ_{4c}.*

Finally, bit-error rate measurements are performed on the demultiplexed channels. The back-to-back curve indicates the 10 Gb/s RZ-OOK signal before optical multiplexing. Error-free operations have been achieved for all channels. The power penalties range from 3 dB to 5 dB. The power penalties are believed to be caused by the pump-to-idler intensity noise during the FWM process and additional

ASE noise. The poorer performance of channel 1 is attributed to the large ASE noise at the gain peak of the EDFA around 1543 nm.

In conclusion, we experimentally demonstrate the conversion from 40 Gb/s OTDM to 4 x 10 Gb/s WDM channels using pump-modulated four-wave mixing in a 64-m PCF with a time- and wavelength-interleaved pulsed source. Error-free operations have been achieved for all demultiplexed channels with power penalties ranging from 3 dB to 5 dB. With the bit-rate transparency of FWM, the system can potentially be operated at higher speeds with additional channels.

6.3 Summary

In this chapter, we have demonstrated two approaches for OTDM-to-WDM conversion using time- and wavelength-interleaved pulses. The first one is by XAM in EAM, and the second one is by FWM in PCF. The following table concludes the comparison between these two approaches.

	XAM in EAM	FWM in PCF
Response limit	~ 1 ps [27]	Several fs [28]
Compactness	Integrable	Bulky
Polarization Sensitivity	Low (by proper design)	High
Cost	Moderate (expensive for high speed)	Moderate
Required Optical Power	Low	High

In [27], the proposed transmitter is an electro-absorption modulated laser (EML) operating at 100 Gb/s. As a result, it is believed that the response time for XAM is at the ps region.

To conclude, for the OTDM-to-WDM conversion, the two proposed approaches have their pros and cons. Depending on the budget and system requirement, either EAM or PCF can be used for the operation, both offering satisfactory system performances.

6.4 References

[1] B. Mikkelsen, G. Raybon, and R.-J. Essiambre, "160 Gb/s transmission systems," *Proc. of ECOC*, Munich, Germany, 2000, Inv. Paper 6.1.1.

[2] G. Raybon, B. Mikkelsen, R.-J. Essiambre, A. J. Stentz, T. N. Nielsen, D. W. Peckham, L. Hsu, L. Gruner-Nielsen, K. Dreyer, and J. E. Johnson, "320 Gbit/s single channel pseudo-linear transmission over 200 km of nonzero-dispersion fiber," *Proc. of ECOC*, Munich, Germany, 2000, Paper PD29-1.

[3] G. R. De Los Santos, M. Urueña, M., J. A. Hernández, D. Larrabeiti, "On providing metro ethernet services over transparent WDM optical rings," *IEEE Network*, vol. 25, no. 1, pp. 14 – 19, January-February 2011.

[4] R. S. Tucker, "Optical packet-switched WDM networks-a cost and energy perspective," *in Proc. Opt. Fiber Commun. Conf. Expo.* (OFC 2008), San Diego, CA, 2008 paper OMG1.

[5] R. S. Tucker, R. Parthiban, J. Baliga, K. Hinton, R. W. A. Ayre, W.V. Sorin, , "Evolution of WDM Optical IP Networks: A Cost and Energy Perspective," *J. Lightwave Technol.*, vol. 27, no. 3, pp. 243 – 252, February 2009.

[6] A. A. M. Saleh and J. M. Simmons, "Evolution toward the next-generation core optical network," *J. Lightwave Technol.*, vol. 24, no. 9, pp. 3303 – 3321, September 2007.

[7] St. Fischer, M. Duelk, M. Puleo, R. Girardi, E. Gamper, W. Vogt, W. Hunziker, E. Gini, and H. Melchior, "40-Gb/s OTDM to 4 × 10 Gb/s WDM conversion in monolithic InP Mach–Zehnder interferometer module," *IEEE Photon. Technol. Lett.*, vol. 11, pp. 1262 – 1264, October 1999.

[8] P. Vorreau, F. Parmigiani, K. Mukasa, M. Ibsen, P. Petropoulos, D. J. Richardson, A. Ellis, W. Freude, and J. Leuthold, "TDM-to-WDM conversion from 130 Gbit/s to 3 × 43 Gbit/s using XPM in a NOLM switch," *in Proc. Int. Conf. on Transparent Optical Netw.* 2008, Athens, Greece, June 2008, paper Th.PD.2.

[9] H. Hu, J. Yu, L. Zhang, A. Zhang, W. Wang, J. Wang, Y. Jiang, and E. Yang, "40-Gb/s all-optical serial-to-parallel conversion based on a single SOA," *IEEE Photon. Technol. Lett.*, vol. 13, pp. 1181 – 1183, July 2008.

[10] A. H. Gnauck, R. M. Jopson, R. W. Tkach, C. J. McKinstrie, and S. Radic, "Serial-to-parallel demultiplexing using WDM sampling pulses," *IEEE Photon. Technol. Lett.*, vol. 21, pp. 97 – 99, January 2009.

[11] H. Sotobayashi, W. Chujo, and K. Kitayama, "Photonic gateway: TDM-to-WDM-to-TDM conversion and reconversion at 40 Gbit/s (4 channels × 10 Gbits/s)," *J. Opt. Soc. Am. B*, vol. 19, pp. 2810 – 2816, November 2002.

[12] G. K. P. Lei, C. Shu, and M. P. Fok, "All-optical OTDM to WDM signal conversion using cross absorption modulation with time- and wavelength-interleaved short pulse," *IEEE Photon. Technol. Lett.*, vol. 22, pp. 571-573, April 15, 2010.

[13] G. K. P. Lei, M. P. Fok, and C. Shu, "Simultaneous Conversion of 40 Gb/s OTDM to 4 × 10 Gb/s WDM Signals Using a Time- and Wavelength-Interleaved Pulsed Source," *in OSA Tech. Dig., OFC/NFOEC*, San Diego, CA, March 2009, paper OThM2.

[14] J. D. Dow and D. Redfield, "Electroabsorption in semiconductors: the excitonic absorption edge," *Phys. Rev. B*, vol. 1, no. 8, pp. 3358 – 3371, April 1970.

[15] D. A. B. Miller, D. S. Chemla, T. C. Damen, A. C. Gossard, W. Wiegmann, T. H. Wood, and C. A. Burrus, "Band-edge electroabsorption in quantum well structures: the quantum-confined Stark effect," *Phys. Rev. Lett.*, vol. 53, no. 22, pp. 2173 – 2176, November 1984.

[16] L. Provost, F. Parmigiani, P. Petropoulos, D. J. Richardson, K. Mukasa, M. Takahashi, J. Hiroishi, and M. Tadakuma, "Investigation of four-wavelength regenerator using polarization- and direction-multiplexing," *IEEE Photon. Technol. Lett.*, vol. 20, no. 20, pp. 1676 – 1678, October 2008.

[17] K. K. Chow and C. Shu, "All-optical signal regeneration with wavelength multicasting at 6 × 10 Gb/s using a single electroabsorption modulator," *Opt. Express*, vol. 12, pp. 3050 – 3054, June 2004.

[18] G. Contestabile, A. Maruta, S. Sekiguchi, K. Morito, M. Sugawara, and K.-i. Kitayama, "All-optical wavelength multicasting in a QD-SOA," *IEEE J. Quantum Electron.*, vol. 47, no. 4, pp. 541 – 547, April 2011.

[19] M. Costa e Silva, A. Lagrost, L. Bramerie, M. Gay, P. Besnard, M. Joindot, J.-C. Simon, A. Shen, and G. H. Duan, "Up to 427 GHz all optical frequency down-conversion clock recovery based on quantum-dash fabry–perot mode-locked Laser," *J. Lightwave Technol.*, vol. 29, no. 4, pp. 609 – 615, February 2011.

[20] H. C. Hansen Mulvad, E. Palushani, M. Galili, J. Xu, H. Hu, A. T. Clausen, L. K. Oxenløwe, and P. Jeppesen, "OTDM-WDM conversion based on time-domain optical Fourier transformation with spectral compression," *in OSA Tech. Digest, OFC/NFOEC 2011*, Los Angeles, CA, paper OThN2.

[21] R. Morais, R. Meleiro, P. Monteiro, and P. Marques, "OTDM-to-WDM conversion based on wavelength conversion and time gating in a single optical

gate," *in OSA Tech. Digest, OFC/NFOEC 2008*, San Diego, CA, March 2008, paper OTuD5.

[22] C.-S. Brès, A. O. J. Wiberg, B. P.-P. Kuo, J. M. Chavez-Boggio, C. F. Marki, N. Alic, and S. Radic, "Optical demultiplexing of 320 Gb/s to 8 × 40 Gb/s in single parametric gate," *IEEE J. Lightw. Technol.*, vol. 28, pp. 434 – 442, February 2010.

[23] K. K. Chow, C. Shu, C. Lin, and A. Bjarklev, "All-optical wavelength multicasting with extinction ratio enhancement using pump-modulated four-wave mixing in a dispersion-flattened nonlinear photonic crystal fiber," *IEEE J. Sel. Topics. Quantum Electron.*, vol. 12, pp. 838 – 842, July/August 2006.

[24] A. Bogris and D. Syvridis, "Regenerative properties of a pump-modulated four-wave mixing scheme in dispersion-shifted fibers," *J. Lightw. Technol.*, vol. 21, pp. 1892 – 1902, September 2003.

[25] Gordon K. P. Lei and Chester Shu, "Conversion of 40 Gb/s OTDM to 4×10 Gb/s WDM channels with extinction ratio enhancement by pump-modulated four-wave mixing using time- and wavelength-interleaved laser pulses," *OECC 2009*, Hong Kong, Jul. 2009, paper FK4.

[26] W. S. Wong, S. Namiki, M. Margalit, H. A. Haus, and E. P. Ippen, "Self-switching of optical pulses in dispersion-imbalanced nonlinear loop mirrors," *Opt. Lett.*, vol. 22, pp. 1150 – 1152 August 1997.

[27] M. Chaciński, U. Westergren, L. Thylén, B. Stoltz, J. Rosenzweig, R. Driad, R. E. Makon, J. Li, and A. Steffan, "ETDM transmitter module for 100-Gb/s Ethernet," *IEEE Photon. Technol. Lett.*, vol. 22, no. 2, pp. 70 – 72, January 2010.

[28] G. P. Agrawal, "Nonlinear fiber optics," 4th edition, *Academic Press*, 2006.

7 Regenerative Optical Signal Processing in Optical Parametric Amplifier

The research on optical parametric amplifier (OPA) has been a hot topic in recent years. It exploits nonlinear optical properties of optical fibers. The main nonlinear effect utilized is the third order susceptibility χ^3 in silica fibers. Compared with the common optical amplifiers, OPA can provide some interesting properties as listed below [1]:

- Gain bandwidth increasing with pump power
- Arbitrary pump wavelength
- Large gain
- Wavelength conversion
    - Spectral inversion
    - Phase conjugation
    - High-speed optical signal processing
- Low noise figure
- Unidirectional gain and spontaneous emission

Much research has been focused on the gain, bandwidth and the noise figure in the OPA [1, 2]. Besides acting as an optical amplifier, OPA has attracted much interest for applications in nonlinear optical signal processing due to its wavelength conversion properties and also fast response of the optical gain.

For the wavelength conversion property, different applications have been demonstrated using OPA including all-optical demultiplexing [3], wavelength multicasting [4], 3R regeneration [5], all-optical tunable delay [6], and applications in microwave photonics [7]. Due to the gain in OPA, the performances are better

compared with results obtained from traditional four-wave mixing approach and other nonlinearities in optical fibers and semiconductor devices.

In this chapter, we will discuss the applications of time- and wavelength-interleaved pulses in an OPA. In Section 7.1, the principles of one-pump OPA and the pump depletion effect will be discussed. In Section 7.2, reconfigurable all-optical demultiplexing will be demonstrated. The operation is achieved by a data-pumped OPA interacting with a time- and wavelength-interleaved pulsed source. The power penalties of the demultiplexed channels are less than 0.6 dB, which is very small compared with the results obtained in previous chapter. In Section 7.3, some preliminary results on two-channel signal amplitude noise reduction will be discussed. Amplitude noises of two RZ-DPSK signals can be achieved simultaneously in a CW-pumped OPA. We will discuss how the proposed regenerator can be more channel count and other advanced modulation format.

7.1 Introduction of Optical Parametric Amplifier

Although OPA can provide a lot of advantages as mentioned previously, there are several requirements to realize an OPA. They are:

- High nonlinear coefficient γ
- Constant zero-dispersion wavelength for phase matching
- Pump source with high peak power

Although it was difficult to achieve the above requirements in 1990s, the development in fiber fabrication and optical amplifiers in recent years makes it possible to achieve OPA easily. Nowadays optical fiber with nonlinear coefficient γ larger than 10 $W^{-1}km^{-1}$ is commercially available. Also the dispersion wavelength can be controlled accurately along the fiber. For high power pump source, EDFA is widely available and the price for a 1-W EDFA has become affordable. Thus, it is not difficult to achieve a high power laser source, either in CW mode or pulsed mode. As a result, the popularity of OPA has been increasing dramatically in the first decade of the 21^{st} century.

For different applications, various pump configurations can be adopted to achieve OPA with different gain spectra and gain bandwidths. In this chapter, we focus on the discussion of one-pump OPA which will be utilized in Section 7.2 and 7.3. Also we will describe the effect of pump depletion in OPA.

7.1.1 One-Pump Optical Parametric Amplifier

As mentioned in the last section, OPA has a property of working with arbitrary pump wavelength. Also OPA can be pumped by either single pump or multiple pumps. In one-pump OPA, there are two categories: OPA with pump located in the normal dispersion region and OPA with pump located in anomalous dispersion region. The main differences between these two configurations are the shape of the gain spectrum and the phase-matching condition inside the nonlinear fiber.

Fig. 7.1.1.1 (a) shows a typical wavelength assignment in the case of one-pump OPA. The pump ω_p is located at the anomalous dispersion region (frequency lower than zero-dispersion frequency ω_0). The signal at ω_p is also located at the anomalous dispersion region to maintain phase-matching condition throughout the HNLF. Fig. 7.1.1.1 (a) also represents the case for the pump and signal before directing to a highly nonlinear fiber (HNLF). After HNLF, OPA occurs and the situation is shown in Fig. 7.1.1.1 (b). An idler is generated at $\omega_i = 2\omega_p - \omega_s$. The pump energy is redistributed and transferred to the signal and the idler during the OPA process. As a result, the signal at ω_s experiences gain while the pump energy is depleted. The property of pump depletion is very important to the applications that will be demonstrated in Section 7.2 and 7.3.

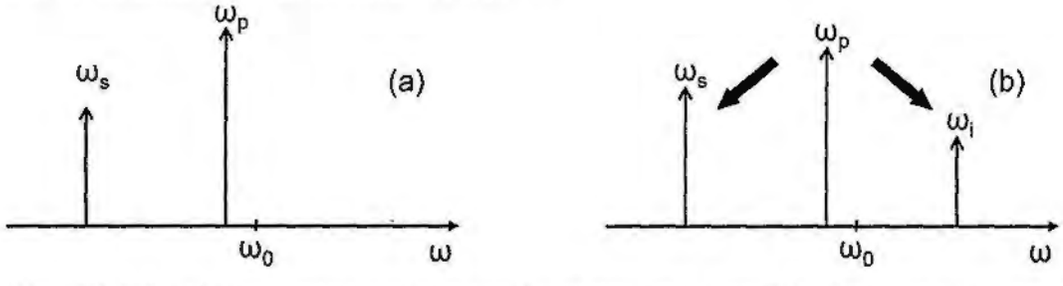

Fig. 7.1.1.1. *(a) Frequency assignment for pump and signal in the case of one-pump OPA, pump wavelength at anomalous dispersion region. (b) Frequency assignment after parametric process in HNLF.*

Fig. 7.1.1.2 shows a typical gain spectrum when the pump is located in the anomalous dispersion region. The pump is a 40 Gb/s data with a pulsed with of 10 ps. The use of a data pump is needed to investigate the properties of a pump-modulated OPA. The pump wavelength is 1551 nm. The pump power is 17.5 dBm. The HNLF has a nonlinear coefficient of 11.7 $W^{-1}km^{-1}$ around 1550 nm. The zero dispersion wavelength of the HNLF is 1549 nm, while the dispersion slope is less than 0.02 $ps•km^{-1}nm^{-2}$ at 1550 nm. The gain spectrum is of M-shape. The gain bandwidth and the amount of gain change when the spacing between the zero-dispersion wavelength and the pump wavelength is changed. For pump depletion application, the signal should align with the gain peak to achieve best performance.

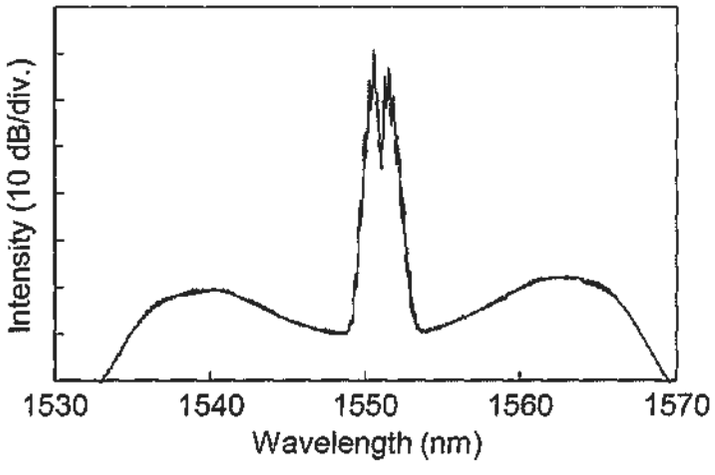

Fig. 7.1.1.2. *A typical gain spectrum of a one-pump OPA with pump wavelength in anomalous dispersion region.*

7.1.2 Pump Depletion in Optical Parametric Amplifier

During amplification in an OPA, as mentioned before the pump energy is redistributed to the signal and the idler. As a result, the pump energy is decreased. This phenomenon is named pump depletion. For pump depletion operation, usually the pump should be of high peak power to achieve reasonable gain on the probe wavelength. As a result, it is easier to achieve pump depletion with pulsed pump rather than CW pump.

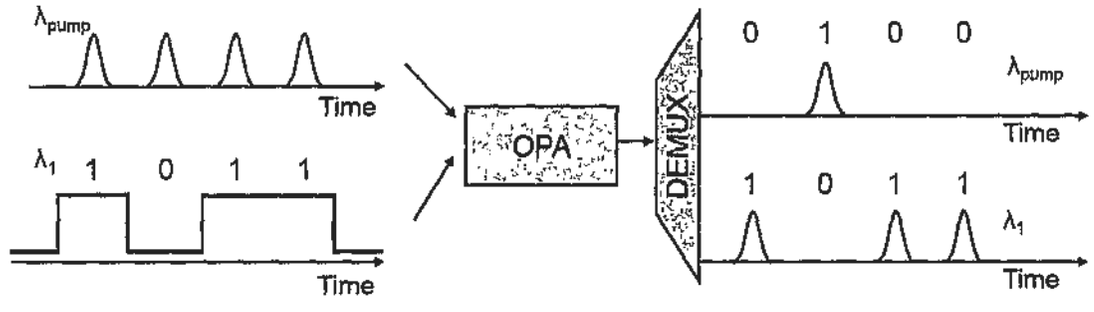

Fig. 7.1.2.1. Operation principle of depletion in a pulsed-pump OPA.

As a proof-of-concept experiment, we demonstrate the pump depletion effect with a clock-pumped OPA and a non-return-to-zero (NRZ) fixed-pattern data. The principle is shown in Fig. 7.1.2.1. A pulse train at λ_{pump} acts as the pump in the OPA, while a fixed-pattern data at λ_1 acts as the probe. When there is a bit "1", the data experiences the gain provided by the pulse train. So the pulse format of the fixed-pattern data is converted from NRZ to return-to-zero (RZ). Also the pulses are depleted (or representing a bit "0"). When there is a bit "0", the correspondent pulse is not depleted (or representing a bit "1"). As a result, the waveform of the pulse train is always an inverse version of the data pattern, which is a NOT gate operation. It is a side-product of pump depletion in a pulsed-pump OPA.

Fig. 7.1.2.2 (a) shows the fixed-pattern non-return-to-zero (NRZ) data with bits "10110110". The data acts as probe in OPA. Fig. 7.1.2.2 (b) shows a 10 GHz clock with a pulse width of 18 ps. It acts as the pump in OPA.

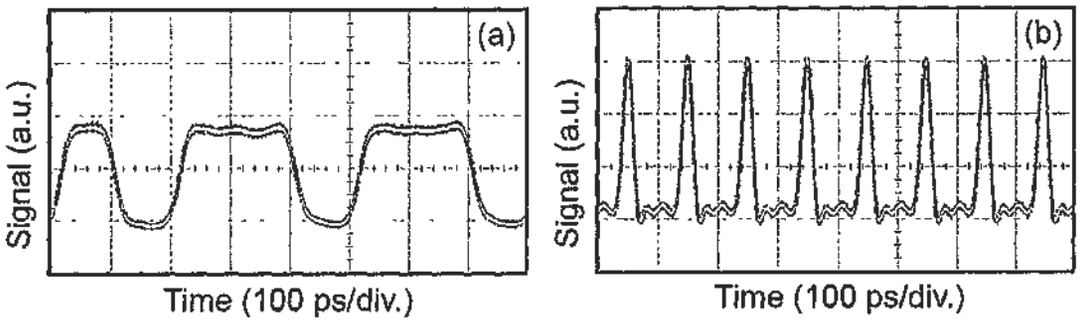

Fig. 7.1.2.2. *Waveforms of (a) Fixed pattern data "10110110". (b) 10 GHz pulses*

After pump depletion in OPA, the energies of the pulses are depleted when the data obtains gain. Fig. 7.1.2.3 (a) shows the amplified data with NRZ-to-RZ format conversion. The pulse width of the RZ data follows that of the pulsed pump. The waveform of the pulsed pump after pump depletion is shown in Fig. 7.1.2.3 (b). The pulses which are aligned with the bits "1" in the data stream are depleted, while those aligned with the bits "0" remain. So the resulting bit pattern is "01001001" which equals a NOT operation on the original data pattern. The experimental results show the pump depletion effect is efficient in a pulsed-pumped OPA, which is suitable for OTDM data add/drop multiplexing.

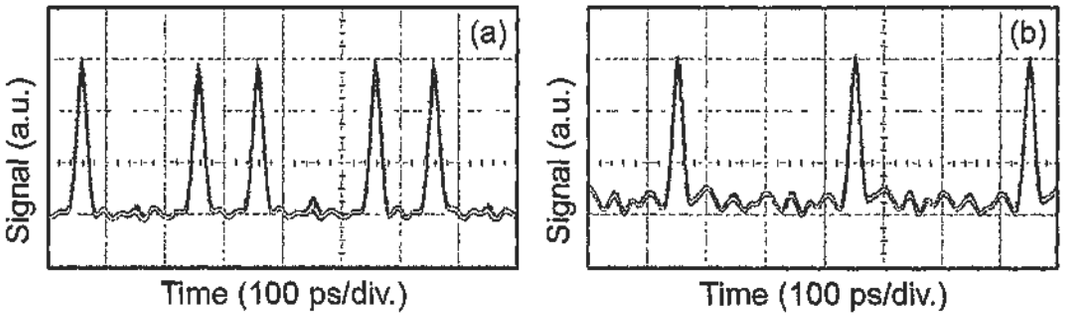

Fig. 7.1.2.3. *Waveforms of (a) format-converted pattern and (b) depleted pulses.*

7.2 All-Optical Demultiplexing by Pump Depletion in an Optical Parametric Amplifier

Optical add/drop multiplexing is an important process in the communication networks for routing data to different destinations. For a wavelength-division multiplexing (WDM) network, the implementation is relatively straightforward using wavelength-selective devices such as fiber Bragg gratings and different types of filters. However, for an optical time-division multiplexing (OTDM) network, a time gating mechanism is required to extract one or more tributaries from the multiplexed data stream. The ability of reconfigurable operation is also a desirable characteristic for an add/drop multiplexer as dynamic routing or bandwidth reallocation is required in optical networks. Several approaches have been proposed to achieve add/drop multiplexing through the use of integrated devices [8] and fiber devices [9-11]. Recently, the applications of optical parametric amplifier (OPA) have been widely explored [12], and different functionalities such as wavelength multicasting [13], optical demultiplexing [14, 15], and 10 Gb/s add/drop multiplexing [16] have been demonstrated. With the use of a multi-wavelength pulsed source, additional functionalities are expected to be achieved with OPA.

In previous chapters, we discussed OTDM-to-WDM conversion by XAM in EAM and FWM in PCF. However, the power penalties were relatively large due to degradation in the optical signal-to-noise ratio (SNR) in the two approaches. To improve the performance, the SNR of the demultiplexed channels should be enhanced. In this section, we use the pump depletion effect in an OPA to achieve reconfigurable two-channel demultiplexing from a 40 Gb/s OTDM data stream [17]. Owing to saturated gain in the OPA, the SNR has been improved compared with the

results in [18] and the power penalties have been reduced. Regeneration properties of OPA have been reported in [19, 20]. Instead of using the conventional pulsed pump configuration, we use the multiplexed data directly as the OPA pump. This pump-modulated OPA achieves channel drop through depletion of the pump (data) power by probe pulses obtained from a time- and wavelength-interleaved laser source. Two 10 Gb/s OTDM tributaries have been successfully dropped from a 40 Gb/s multiplexed data stream with error-free operations and reconfigurable channel selection. Droppings of both adjacent and alternate channels have been demonstrated with measured power penalties less than 0.6 dB. With the wavelength-interleaved probe pulses, the demultiplexed channels can subsequently be wavelength-routed to different destinations. Our scheme allows fast reconfiguration through wavelength tuning instead of relying on complicated length adjustment in multiple delay lines. Moreover, the system can be potentially upgraded to an OTDM-to-WDM converter when two extra pulsed channels are added.

7.2.1 Experimental Setup

The setup is shown in Fig. 7.2.1.1. Two continuous-wave (CW) lasers with a wavelength spacing of 2 nm are obtained from a WDM source. The laser outputs are combined by an optical coupler connected to a dual-drive Mach-Zehnder modulator. The modulator is driven with a 10 GHz sinusoidal signal on one of the arms to introduce chirp and amplitude modulation on the CW lights. The power of the driving signal is 22 dBm. The outputs are then directed to 8.4-km single-mode fiber (SMF). As the frequency components contained in both lasers are now time-dependent, group velocity dispersion (GVD) in the SMF can be used to further compress the pulses [21, 22]. The time spacing between adjacent channels is ~25 ps, governed by the wavelength spacing and the GVD in the SMF. An EDFA is used after the SMF to compensate for the loss. Consequently, a time- and wavelength-interleaved laser source is achieved at the EDFA output.

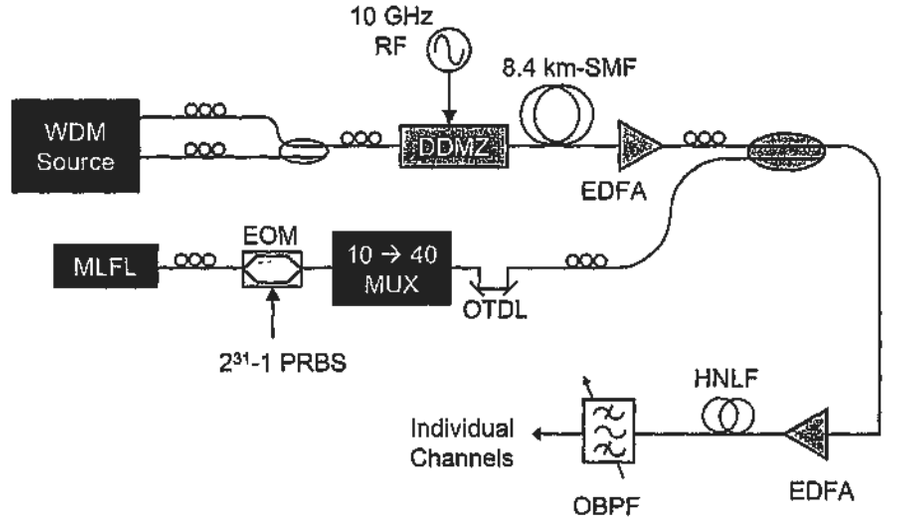

Fig. 7.2.1.1. *Setup for pump-modulated OPA demultiplexing. MLFL: mode-locked fiber laser; EOM: electro-optic modulator; PRBS: pseudorandom binary sequence; DDMZ: dual-drive Mach-Zehnder modulator; RF: radio frequency; OTDL: optical tunable delay line; EDFA: erbium-doped fiber amplifier; HNLF: highly nonlinear fiber; OBPF: optical band pass filter;*

To generate a 40 Gb/s data stream, the output from a 10 GHz mode-locked fiber laser is modulated by an electro-optic modulator driven by a 10 Gb/s 2^{31}-1 pseudorandom binary sequence. The data is directed to an optical multiplexer and the bit rate is increased to 40 Gb/s. The multiplexed data is combined with the time- and wavelength-interleaved pulses using a 90/10 optical coupler. An optical tunable delay line is used to provide synchronization between the two branches. The coupled lights are subsequently amplified by an EDFA to 17.5 dBm and are directed to a 1-km highly nonlinear fiber (HNLF) with a nonlinear coefficient of 11.7 $W^{-1}km^{-1}$ around 1550 nm. The zero dispersion wavelength of the HNLF is 1549 nm, while the dispersion slope is less than 0.02 $ps \cdot km^{-1}nm^{-2}$ at 1550 nm.

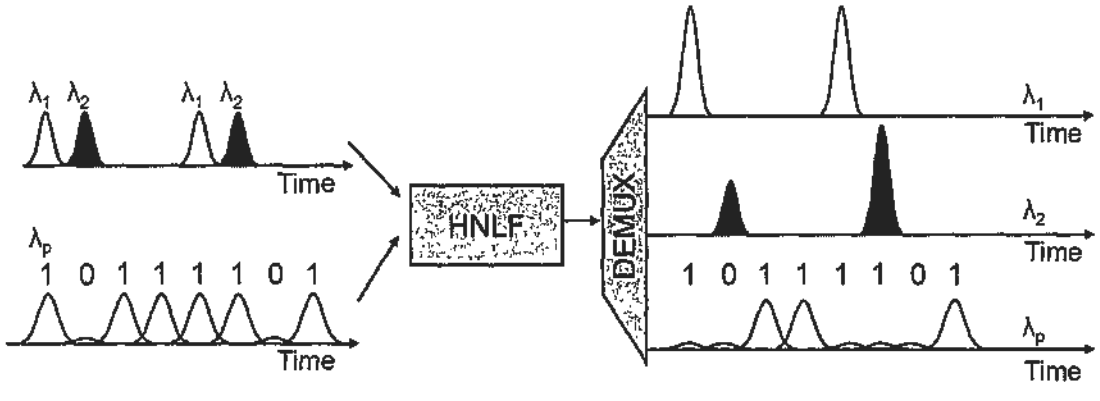

Fig. 7.2.1.2. *Principle of add/drop operation of OTDM data by pump depletion in optical parametric amplifier. The amplitudes of the pulses after DEMUX are for illustration only but not of true values. DEMUX: wavelength demultiplexer; HNLF: highly nonlinear fiber optimized for OPA process.*

Optical parametric amplification takes place inside the HNLF. The principle is illustrated in Fig. 7.2.1.2. The input data stream serves as the pump at λ_p to amplify probe pulses at λ_1 and λ_2. When a bit "1" in the data stream is aligned to a probe pulse, the respective pulse is amplified and the energy is thus transferred to the probe wavelength. The corresponding bit in the data stream is suppressed due to pump

depletion. By this mechanism, the data are transferred to the probe wavelength and channel drop operation is achieved. With multiple pulse channels interacting with the modulated pump, multi-channel demultiplexing can be achieved. Also, by controlling the number and the delay of the probe pulses in the time- and wavelength-interleaved source, reconfigurable operation becomes possible.

7.2.2 Experimental Results and Discussions

The waveform and the optical spectrum of the time- and wavelength-interleaved probe pulses are shown in Fig. 7.2.2.1 (a) and (b), respectively. The wavelengths are selected at 1557.20 and 1559.20 nm to produce a time separation of ~25 ps between the generated pulses. The pulse width is measured with a 500-GHz optical sampling oscilloscope and is found to be ~ 19 ps. The pulse width is optimized for removal of pedestals on the pulses.

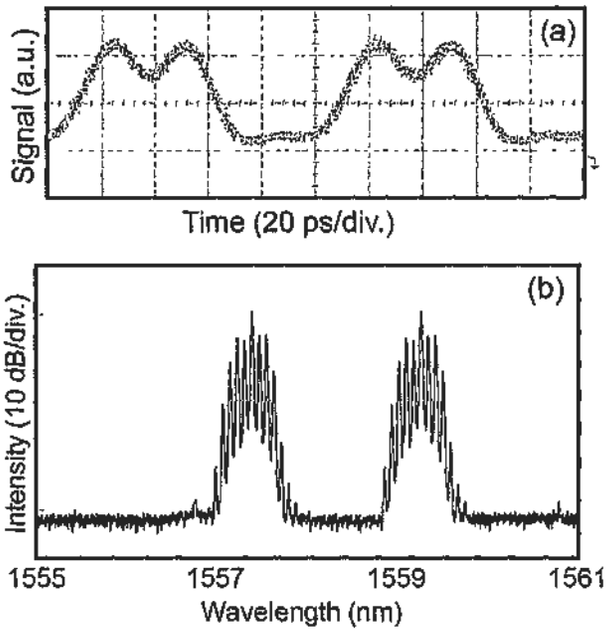

Fig. 7.2.2.1. *Time- and wavelength-interleaved laser pulses. (a) Temporal profile. Adjacent pulses appear to be overlapped due to finite response of the measurement system. The actual pulse widths are determined to be ~18 ps using a 500-GHz optical sampling oscilloscope. (b) Optical spectrum. The two probe pulses are centered at 1557.20 and 1559.20 nm. Resolution: 0.02 nm.*

Fig. 7.2.2.2 shows the eye diagram of 40 Gb/s RZ-OOK data at 1553 nm. The data and the probe wavelengths are all located in the anomalous dispersion region of the HNLF. Fig. 7.2.2.3 shows the optical spectrum measured after the HNLF.

Although there are some undesired four-wave mixing products in the spectrum, they have no effects on the pulsed probes and the data pump.

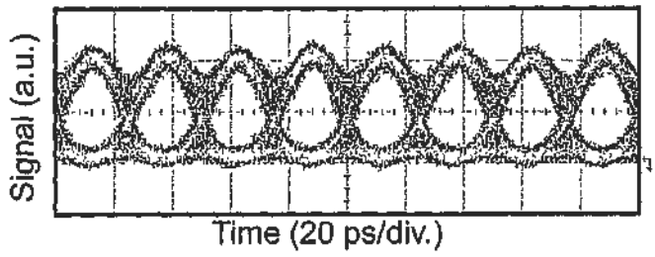

Fig. 7.2.2.2. *Eye diagram of 40 Gb/s OTDM data stream at 1553 nm.*

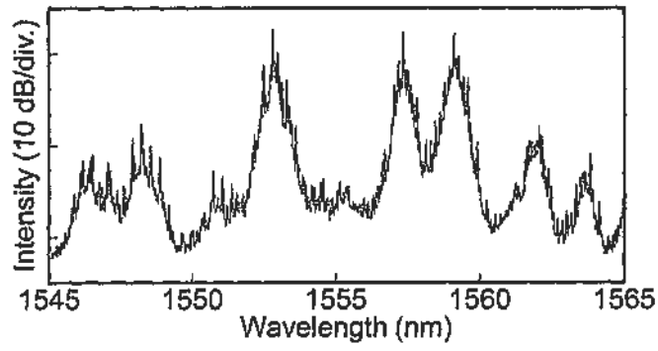

Fig. 7.2.2.3. *Optical spectrum measured after pump depletion in the HNLF. Resolution: 0.1 nm.*

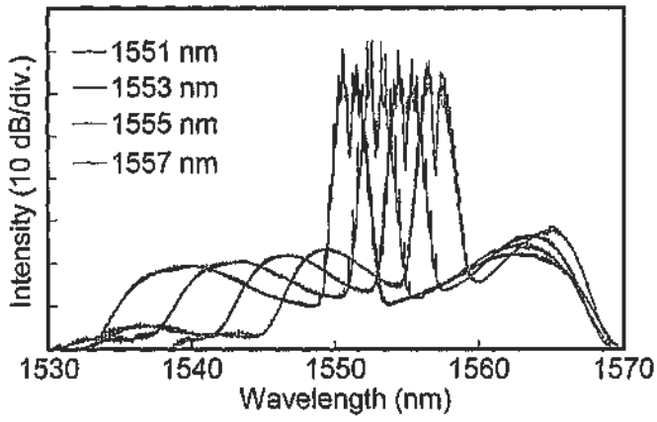

Fig. 7.2.2.4. *OPA gain spectra at different pump wavelengths. Resolution: 0.1 nm.*

Fig. 7.2.2.4 shows the gain spectra of the optical parametric amplifier at different pump wavelengths. For multi-channel operation, it is desirable to optimize the gain bandwidth and the gain profile. When the pump is tuned from 1551 to 1557 nm, the gain bandwidth is observed to decrease while the peak gain increases. To draw a balance between the spectral width and the gain, we choose a pump

wavelength of 1553 nm for the parametric amplification. The gain peak is located at 1563 nm.

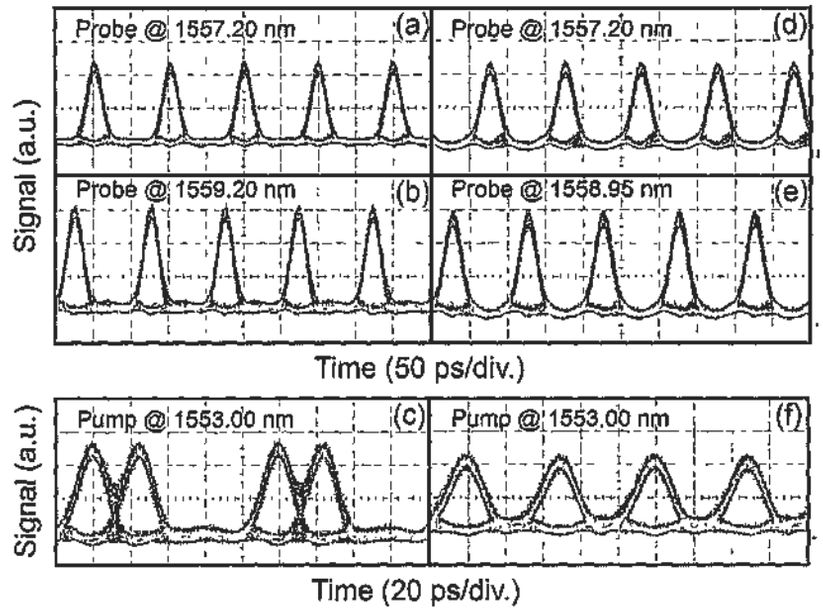

Fig. 7.2.2.5. *(a) – (f) Eye diagrams of the dropped and through channels. (a)-(c) Dropped channels and through channel with interleaved probe pulses separated by 25 ps. (d)-(f) Dropped channels and through channel with interleaved probe pulses separated by 50 ps.*

The demultiplexed outputs are filtered out for analysis. The eye diagrams of the two dropped channels are shown in Fig. 7.2.2.5 (a) and (b) while that of the through channel is shown in Fig. 7.2.2.5 (c). Widely opened eye diagrams have been obtained. In the through channel, the data bits that have been aligned with the probe pulses are depleted in power. The extinction ratios of the through channels are ~11 dB, making it possible to add new channels on the remaining data stream.

By changing the wavelength spacing of the time- and wavelength-interleaved pulses from 2 to 1.75 nm, the time separation between the probe pulses can be tuned to 50 ps. As a result, demultiplexing can be achieved in alternate channels. Fig. 7.2.2.5 (d)-(f) show the corresponding eye diagrams that are again widely opened. The results are comparable to the demultiplexing performance in adjacent channels

shown in Fig. 7.2.2.5 (a)-(c). The extinction ratios of eye diagrams in Fig. 7.2.2.5 (a) and (d) are 13.4 dB, while those in Fig. 7.2.2.5 (b) and (e) are 14 db. It is noted that the channel powers in (b) and (e) are higher than those in (a) and (d) because their wavelengths are closer to the gain peak at 1563 nm.

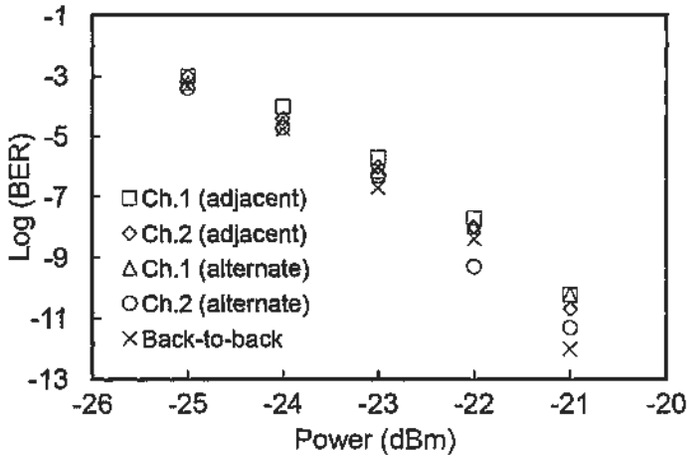

Fig. 7.2.2.6. *BER measurement. Ch.1: dropped channel at shorter wavelength. Ch.2: dropped channel at longer wavelength. Back-to-back: 10 Gb/s data before optical multiplexing.*

To further characterize the performances, bit-error rate measurements are carried out on the demultiplexed outputs for both cases of adjacent and alternate channels. The results are shown in Fig. 7.2.2.6. Ch.1 represents the dropped channel at the shorter wavelength and Ch.2 represents the dropped channel at the longer wavelength. Error-free operations have been achieved for all cases. Power penalties of less than 0.6 dB are obtained for all the dropped channels. The performances of both adjacent and alternate channel demultiplexing are similar, again confirming that the reconfiguration does not introduce additional power penalty to the system.

The fiber-based OPA scheme is applicable for higher speed operation when the repetition rate of the time- and wavelength-interleaved probe pulses is increased. Such pulses have been recently demonstrated at 160 GHz [23], allowing add/drop multiplexing with 4-fold increase in the bit rate. For higher channel count, the main

constraints lie in the limited bandwidth of the OPA and the finite width of the interleaved pulses. To solve the bandwidth limitation, multiple pumps and/or new nonlinear media can be used to increase the gain-bandwidth of the OPA [5]. Also, different pulse compression techniques can be adopted to shorten the pulses and suppress the crosstalk in adjacent channels.

In conclusion, we have demonstrated simultaneous two-channel demultiplexing using pump depletion in an OPA with time- and wavelength-interleaved probe pulses. Error-free operations have been achieved for the dropped channels with power penalties less than 0.6 dB. The setup is relatively simple and the receiver sensitivities have been improved compared with previous approaches. Fast reconfiguration can be achieved by wavelength tuning of the probe pulses. The system can be easily upgraded to operate at a higher speed owing to ultrafast response of OPA. The extension to OTDM-to-WDM converter can also be realized using extra pulse channels in the optical probe.

7.3 Amplitude Noise Reduction by Four-Wave Mixing in an Optical Parametric Amplifier

Signal regeneration is important in communication systems. For traditional regeneration operation in optical networks, optical signals are converted to electrical signals, regenerated by using electronic circuits and devices, and converted back to optical signals. However, for high-speed signal > 100 Gb/s, it is impossible for electronic circuits to handle the signal. Also, the above scheme is format dependent, which cannot be applied to systems with different modulation formats. As a result, all-optical regeneration is desirable for future optical signal regeneration.

Differential phase-shift keying (DPSK) modulation is receiving much attention in recent years because it has superior performances over on-off keying (OOK) modulation on dispersion and nonlinearity tolerance. Different schemes have been proposed for regeneration operations on DPSK signals, including phase-sensitive amplification [24], gain saturation in optical parametric amplifier [25], power saturation in optical saturable absorber [26], and nonlinear optical loop mirror [27].

However, for the above demonstrations, the regenerator can only regenerate a single channel signal. For wavelength division multiplexing (WDM) system, it is desirable to perform optical regeneration on multiple wavelength channels. The main problem for multiple-channel regeneration is the crosstalk among the signal channels. To solve this problem, different techniques have been proposed to reduce the crosstalk problem, including the use of bidirectional operation in a nonlinear optical fiber [28], time-interleaving of signal channels [29], polarization multiplexing [30], multi-channel cross-phase modulation in a dispersion-managed fiber section [31],

and self-phase modulation with inter-channel walk-off control in bidirectional fiber configuration [32]. These demonstrations all focus on OOK signals, but the performances for DPSK signals have not been studied.

In this section, we give a brief demonstration on amplitude noise reduction of DPSK signal. The noise reduction process is performed by four-wave mixing in a highly nonlinear fiber and pump depletion in an OPA. Amplitude noise can be suppressed with this approach. We will report experimental results for single channel amplitude noise reduction of NRZ-DPSK signal in a pulsed pump OPA. Also we demonstrate wavelength multicasting with amplitude noise reduction and format conversion using time- and wavelength-interleaved pulsed pumps. We will describe the background theories, experimental setup and some preliminary experimental results.

7.3.1 Amplitude Limiting Effect in OPA

As mentioned before, wavelength conversion can take place when there is a pump and a probe in an OPA. The process is achieved by four-wave mixing (FWM). During the FWM process, the amplitude of the wavelength-converted output is determined by:

$$\hat{E}_{FWM} = \kappa[\hat{E}_p \cdot \hat{E}_s{}^*]\hat{E}_p \qquad [7.1]$$

where E_{FWM} is the field amplitude of the wavelength converted signal, E_s is the field amplitude of the input signal and E_p is the field amplitude of the pump. However, in an OPA, the pump is depleted during parametric amplification. When the signal power increases, the pump depletion also increases. As a result, the field amplitude of the wavelength converted output reaches a saturation state. The increase in signal power does not increase the amplitude of wavelength converted output because of the drop of pump power. Consequently, different input signal levels map to the same output level. This property is important to signal quality enhancement as the amplitude noise in the input signal can be reduced due to the FWM saturation effect.

7.3.2 DPSK Signal Amplitude Noise Reduction by Four-Wave Mixing Saturation Effect

As mentioned in Chapter 5, DPSK signals play an important role in today's communication systems. During transmission, different impairmnets in the system distort the ampltidue and phase of the DPSK signals. To regenreate DPSK signals, techniques developed for OOK signals such as self-phase modulation and cross-absorption cannot be utilized as the phase information cannot be preseved. FWM is a phase-maintaining process as introudced in Chapter 2. By FWM effect in an nonlinear fiber, we can perform a phase-maintaining wavelength conversion. When the FWM process occurs in an OPA, we can make use of the amplitude limiting effect to regenerate a distorted DPSK signal. By reducing the amplitude noise, the nonlinear phase noise originated from SPM in the fiber link can also be suppressed. As a proof-of-concept experiment, we demonstrate 10 Gb/s NRZ-DPSK amplitude noise reduction by FWM saturation effect in OPA. The OPA is pumped by a 10 GHz pulse train with duty cycyle of 17%. Receiver sensitivity has been imporved by 2.8 dB compared with the input distorted DPSK signal.

Fig. 7.3.2.1 shows the experimental setup. A NRZ-DPSK is generated by phase-modulating the output from a tunable laser with a 10 Gb/s pseudorandom binary sequence. To introduce amplitude noise, the DPSK signal is again modulated by an electro-optic modulator with a 1.25 GHz sinusoidal wave. The DPSK signal is amplified by an EDFA to a power level of 15 dBm to achieve saturation in the OPA. For the pulsed pump generation, a CW light is phase and amplitude modulated by a dual-drive Mach-Zehnder modulator with 10 GHz sinusoidal signal and compressed into pulses by an 8.4-km single-mode fiber. The pulse train is then amplified to 14.5 dBm by another EDFA, coupled with the DPSK signal and directed to a 1-km highly

nonlinear fiber (HNLF) with a nonlinear coefficient of 11.7 $W^{-1}km^{-1}$ around 1550 nm. The zero dispersion wavelength of the HNLF is 1549 nm, while the dispersion slope is less than 0.02 $ps \cdot km^{-1}nm^{-2}$ at 1550 nm. An optical tunable delay line is used for synchronization between the two branches. FWM and optical parametric amplification occur inside the HNLF. New wavelength components are generated after FWM process. An optical bandpass filter is used to filter out the desired wavelength component.

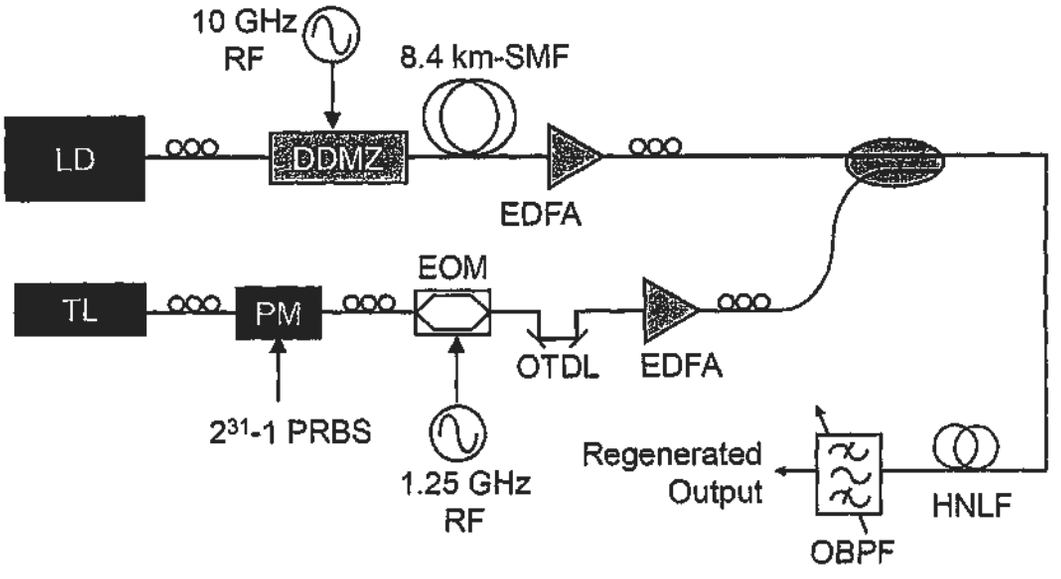

Fig. 7.3.2.1. *Setup for DPSK signal amplitude noise reduction. TL: tunable laser; PM: phase modulator; PRBS: pseudorandom binary sequence; OTDL: optical tunable delay line; LD: laser diode; DDMZ: dual-drive Mach-Zehnder modulator; RF: radio frequency; EDFA: erbium-doped fiber amplifier; HNLF: highly nonlinear fiber; OBPF: optical band pass filter;*

Fig. 7.3.2.2 (a) shows the demodulated DPSK signal with distortion generated at 1557.16 nm. The demodulation is achieved by a 100-ps delay interferometer (DI). It is observed that the bit-1 level has a large amplitude jitter, introduced by the 1.25 GHz sinusoidal wave modulation. Fig. 7.3.2.2 (b) shows the

waveform of the 10 GHz pulse train. The pulse width is ~17 ps and the wavelength is 1553.48 nm. The pulse train acts as a pump during the FWM process.

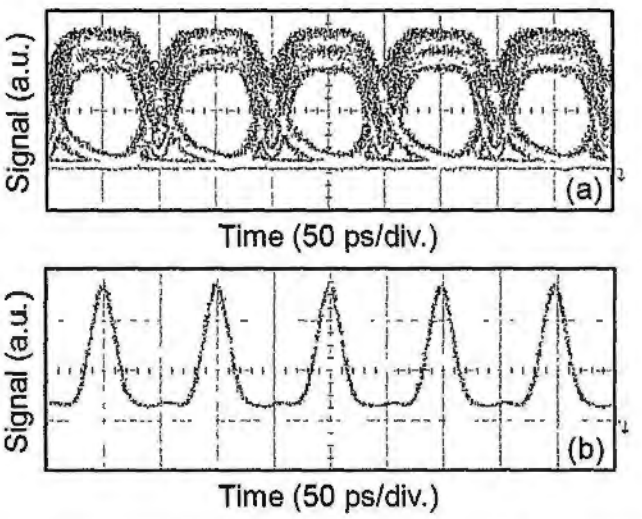

Fig. 7.3.2.2. *(a) Eye diagram of demodulated DPSK signal with amplitude distortion. (b) Waveform of the 10 GHz pulse train.*

The relationship between input and output signal power is shown in Fig. 7.3.2.3. To achieve the amplitude limiting effect, different input power levels should be mapped to a single output levels. As shown in Fig. 7.3.2.3, the saturation input power is around 15 dBm. At the range of input power from 14.5 dBm to 16 dBm, the powers of the wavelength converted outputs are similar. The input signal power will be limited in this region to achieve the saturation effect.

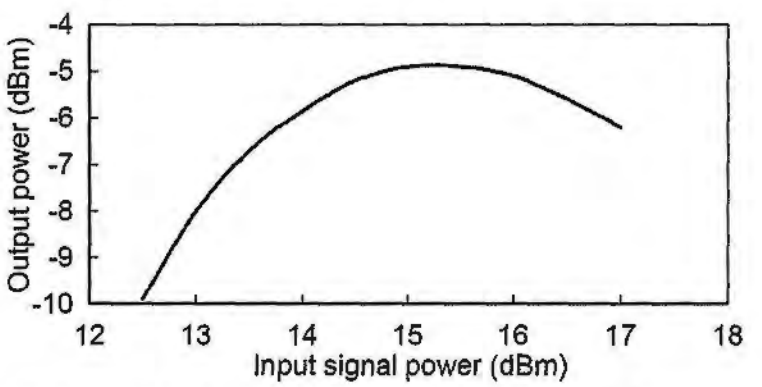

Fig. 7.3.2.3. *Relationship between input signal power and wavelength-converted output power.*

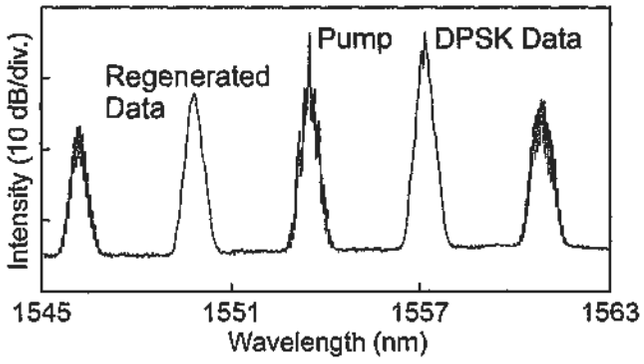

Fig. 7.3.2.4. *Optical spectrum after four-wave mixing in the HNLF.*

Fig. 7.3.2.4 shows the spectrum after FWM process. New wavelength components are generated after FWM. The phase-preserving wavelength converted output is at 1549.76 nm. The component is filtered out and demodulated again with a 100-ps DI. Its waveform is shown in Fig. 7.3.2.5. The amplitude noise is reduced compared with that shown in Fig. 7.3.2.2 (a). Also, the pulse format is converted from NRZ to RZ due to the pulsed pump property.

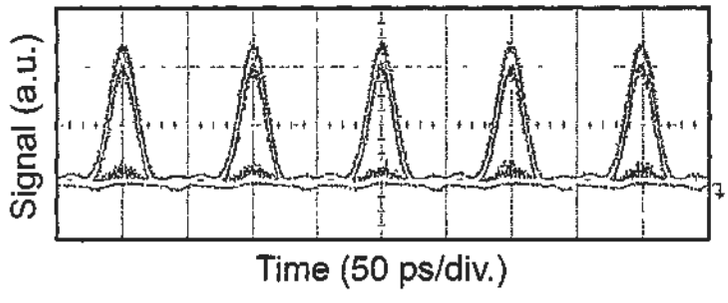

Fig. 7.3.2.5. *Eye diagram of the regenerated output.*

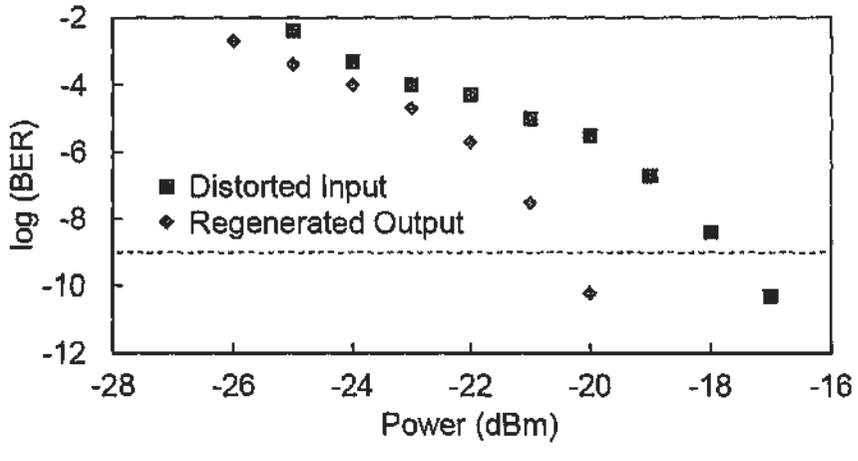

Fig. 7.3.2.6. *BER measurement. Dashed line: BER at 10^{-9}.*

To further evaluate the amplitude noise reduction property, bit-error-rate measurements are performed both on the distorted DPSK signal and the wavelength converted output. The results are shown in Fig. 7.3.2.6. 2.8-dB improvement in receiver sensitivity is achieved after the amplitude noise reduction process. The improvement is caused by the amplitude noise reduction and NRZ-to-RZ conversion.

In conclusion, we confirm that the FWM saturation effect can provide amplitude noise reduction function. We will discuss how this approach can be suitably adopted for multi-channel amplitude noise reduction process in Section 7.3.4.

7.3.3 DPSK Signal Amplitude Noise Reduction with Wavelength Multicasting

Multicasting is important as discussed in details in Chapter 5. Instead of performing multicasting right after the transmitter, the signal may have propagated for some distances before multicasting. With a time- and wavelength-interleaved pulsed source, we can regenerate a distorted DPSK signal and multicast it to multiple wavelengths simultaneously. The principle is shown in Fig. 7.3.3.1. The time- and wavelength-interleaved pulses at λ_{p1} and λ_{p2} are temporally aligned with the phase stable region of the distorted DPSK signal at λ_s. By FWM in a HNLF, the phase information is carried by the wavelength-converted outputs, while the signal format is converted from NRZ to RZ. Also the amplitude fluctuation is suppressed by FWM saturation in OPA. As a result, amplitude noise reduction, pulse format conversion and wavelength multicasting can be achieved simultaneously in a single processor. We demonstrate 1-to-2 multicasting on 10 Gb/s DPSK signal with amplitude noise reduction. Two multicast outputs are achieved with improved receiver sensitivities and NRZ-to-RZ format conversion. The experimental setup and results will be discussed.

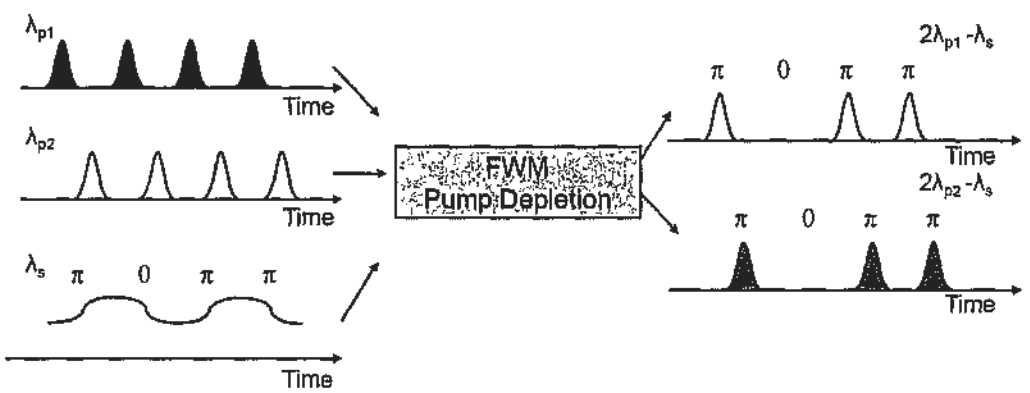

Fig. 7.3.3.1. *Operation principle of the proposed regenerator with multicasting and format conversion functions.*

Fig. 7.3.3.2 shows the experimental setup. Two continuous-wave (CW) lasers with a wavelength spacing of ~2.3 nm are obtained from a WDM source. The laser outputs are combined by an optical coupler connected to a dual-drive Mach-Zehnder modulator. The modulator is driven with a 10 GHz sinusoidal signal on one of the arms to introduce chirp and amplitude modulation on the CW lights. The power of the driving signal is 23 dBm. The outputs are then directed to 8.4-km SMF and short pulses are generated. The time spacing between adjacent channels is ~25 ps, governed by the wavelength spacing and the GVD in the SMF. An EDFA is used after the SMF to compensate for the loss. Consequently, a time- and wavelength-interleaved laser source is achieved at the EDFA output with an average power of 16.8 dBm.

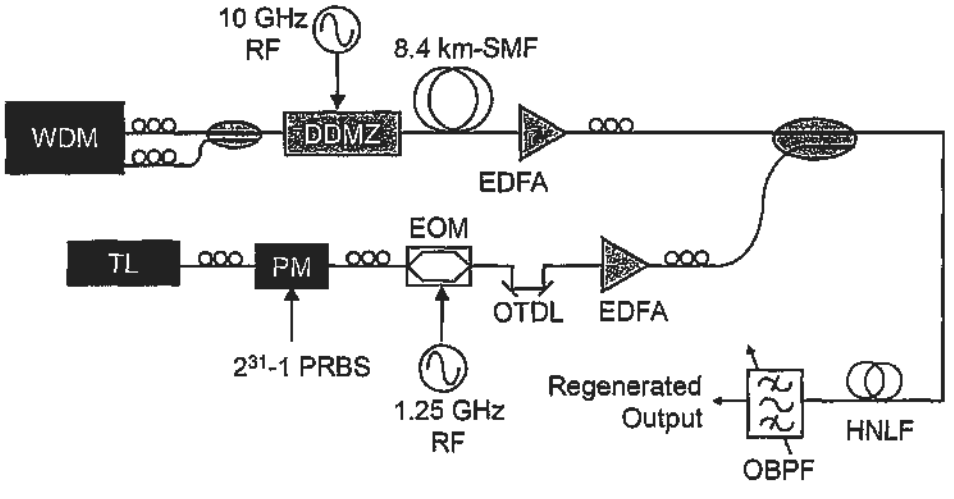

Fig. 7.3.3.2. *Setup for amplitude noise reduction for DPSK signal with multicasting. TL: tunable laser; PM: phase modulator; PRBS: pseudorandom binary sequence; OTDL: optical tunable delay line; LD: laser diode; DDMZ: dual-drive Mach-Zehnder modulator; RF: radio frequency; EDFA: erbium-doped fiber amplifier; HNLF: highly nonlinear fiber; OBPF: optical band pass filter.*

A NRZ-DPSK signal is generated by phase-modulating the output from a tunable laser with a 10 Gb/s pseudorandom binary sequence of length equals to 2^{31}-1.

To introduce amplitude noise, the DPSK signal is again modulated by an electro-optic modulator with a 1.25 GHz sinusoidal wave. The DPSK signal is amplified by an EDFA to 15 dBm, combined with the pulsed source and directed to a 1-km highly nonlinear fiber. FWM and OPA occur inside the nonlinear fiber. The wavelength-converted outputs are filtered out using an optical bandpass filter.

Fig. 7.3.3.3 (a) shows the waveform of the time- and wavelength-interleaved pulsed source. The time spacing between the two pulses is 25 ps. The pulse width for individual channel is ~17 ps. The waveform of the demodulated DPSK signal is shown in Fig. 7.3.3.2 (b). Demodulation is achieved in a 100-ps DI. The signal is distorted by amplitude fluctuation.

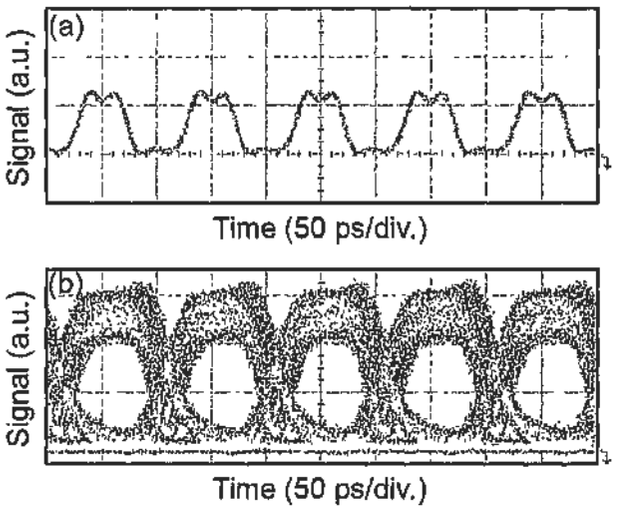

Fig. 7.3.3.3. *(a) Waveform of the time- and wavelength-interleaved pulses. (b) Eye diagram of demodulated DPSK signal with amplitude distortion.*

Fig. 7.3.3.4 shows the optical spectrum after four-wave mixing in a highly nonlinear fiber. The input time- and wavelength-interleaved pulses are located at 1551.48 and 1553.8 nm, respectively. The input DPSK signal is at 1557.18 nm. The degenerate FWM products are generated at 1550.42 and 1545.78 nm. Although the two pulses appear to overlap as shown in Fig. 7.3.3.3(a), the conversion efficiency of

the beating products at 1549.16 and 1556.12 nm are less than -20 dB, showing that the crosstalk is not serious.

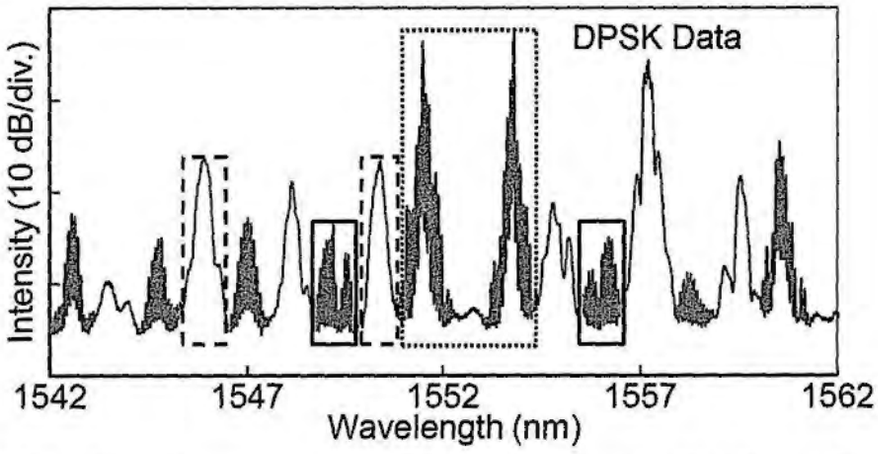

Fig. 7.3.3.4. *Optical spectrum after four-wave mixing in highly nonlinear fiber. Dotted rectangle: time- and wavelength-interleaved pulses. Dashed rectangles: wavelength components containing regenerated signals. Solid rectangles: wavelength components generated by beating between two pulsed channels.*

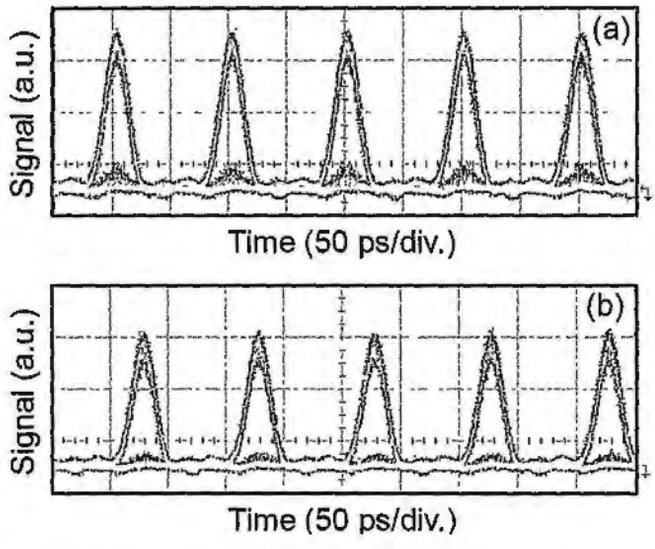

Fig. 7.3.3.5. *Eye diagrams of regenerated signals at (a) 1545.78 nm (b) 1550.42 nm.*

The waveforms of the regenerated signals are shown in Fig. 7.3.3.5 (a) and (b) respectively. The signals are again demodulated using 100-ps DI. The time separation is 25 ps, inherited from the pulse source. The amplitude distortion is suppressed due to the pump depletion effect in the OPA. However, some ripples

appear at the zero level. It is caused by the slight overlapping between two pulses and wavelength-dependent DI. Further optimization can be done on the pulse width and the wavelength assignment.

To evaluate the channels, bit error rate measurements are performed on both distorted and regenerated signals. The results are shown in Fig. 7.3.3.6. Compared with the distorted DPSK signal, 2.4 and 1.8 dB improvements on receiver sensitivity have been achieved for the channel at 1545.78 and 1550.42 nm, respectively. The poorer performance on 1550.42 nm is caused by slight spectral overlapping with the pulsed channel at 1551.48 nm. Further optimization on the wavelength assignment can improve the amplitude noise reduction performance.

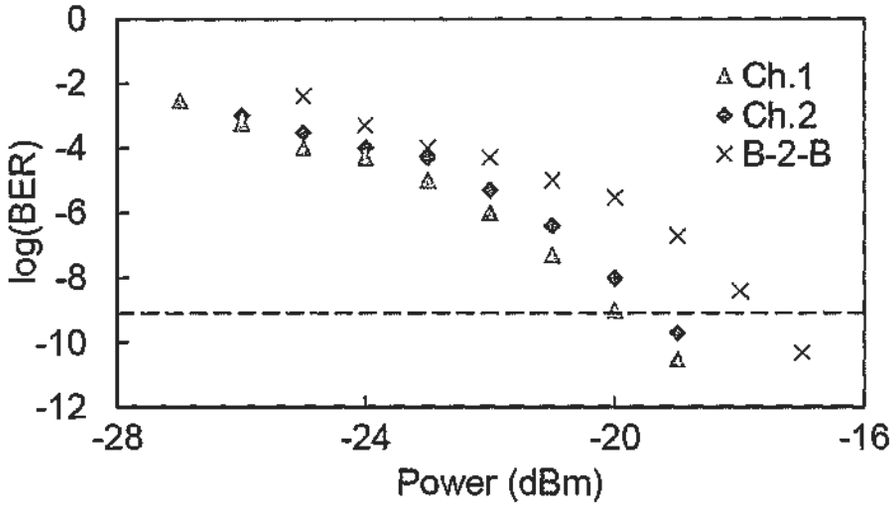

Fig. 7.3.3.6. *BER measurements. Ch. 1: regenerated channel @ 1545.78 nm. Ch. 2: regenerated channel @ 1550.42 nm. B-2-B: distorted DPSK signal. Dashed line: BER @* 10^{-9}.

In conclusion, we have demonstrated amplitude noise reduction, multicasting and NRZ-to-RZ pulse format conversion of a 10 Gb/s DPSK signal with amplitude noise. The operation is achieved by FWM of the distorted signal with a time- and wavelength-interleaved laser source in an OPA. Receiver sensitivities have been improved by over 1.5 dB.

7.3.4 Multi-Channel Amplitude Noise Reduction for DPSK Signals

To further explore the capability of the proposed regenerator, we propose to process two DPSK signals at the same time. In this chapter we will discuss the feasibility of reducing amplitude noises in two RZ-DPSK signals in a single processor.

Fig. 7.3.4.1 shows the operation principle of the proposed scheme. Two RZ-DPSK signals at λ_{s1} and λ_{s2} are time-interleaved and directed to an OPA. The OPA is pumped by a CW laser at λ_p, as it can interact with the signals at different time slots. The amplitudes of the two RZ-DPSK signals are distorted. To reduce the amplitude noise, we make use of the amplitude limiting function by FWM saturation in the OPA. The process is performed in a highly nonlinear fiber. So after the FWM process, regenerated channels are located at $2\lambda_p - \lambda_{s1}$ and $2\lambda_p - \lambda_{s2}$.

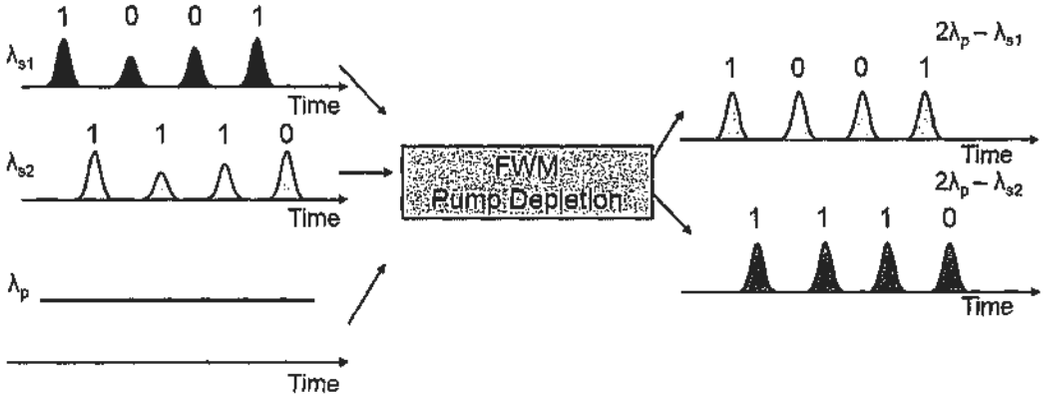

Fig. 7.3.4.1. *Operation principle of the proposed multi-channel amplitude noise reduction scheme for DPSK signals.*

Although the principles are similar to that in previous section, several issues should be addressed:

1. As stimulated Brillouin scattering (SBS) can easily occur when the CW pump power is high, the length of the highly nonlinear fiber is critical. Also the spectrum of the CW pump should be broadened to reduce the SBS effect.
2. The pulse width of the RZ-DPSK should be short enough to avoid crosstalk between the two data streams.
3. As both signals are of short pulses, the wavelength assignment should be well defined because each of them occupies a wide bandwidth.
4. To increase the maximum number of processing channels, sub-ps pulses should be adopted. However, it is not a practical solution for commercial WDM systems as it requires a large bandwidth. Other techniques can be used simultaneously with the time-interleaving approach, including polarization multiplexing and bidirectional launching of signals to increase the total number of channels.

7.4 Summary

In this chapter, we have demonstrated 40 Gb/s two-channel demultiplexing with pump depletion effect in OPA and time- and wavelength-interleaved laser source. Small power penalties have been achieved (< 0.6 dB) for both adjacent and alternate channel demultiplexing. The scheme can be potentially upgraded to an OTDM-to-WDM demultiplexer.

We also discussed the application of amplitude noise reduction in an OPA. Amplitude noise of a 10 Gb/s DPSK was successfully suppressed and 2.8 dB improvement on receiver sensitivity has been achieved. By using time- and wavelength-interleaved pulses, the regenerated signal was multicast into two channels, also with receiver sensitivity improvements.

Finally, we proposed a multi-channel regenerator with a CW-pumped OPA. The requirements on the pump configuration, the choice of the nonlinear fiber and the wavelength assignment have been discussed.

7.5 References

[1] M. E. Marhic, "Fiber optical parametric amplifiers, oscillators and related devices," *Cambridge Univ. Press*, 2008.

[2] K. Inoue and T. Mukai, "Experimental study on noise characteristics of a gain-saturated fiber optical parametric amplifier," *IEEE J. Lightw. Technol.*, vol. 20, pp. 969 – 974, June 2002.

[3] M. Shen, X. Xu, T. I. Yuk, and K. K.-Y. Wong, "A 160-Gb/s OTDM demultiplexer based on parametric wavelength exchange," *IEEE J. Quantum Electron.*, vol. 45, pp. 1309 – 1316, November 2009.

[4] C.-S. Brès, A. O. J. Wiberg, B. P.-P. Kuo, N. Alic, and S. Radic, "Wavelength multicasting of 320-Gb/s channel in self-seeded parametric amplifier," *IEEE Photon. Technol. Lett.*, vol. 21, pp. 1002 – 1005, July 2009.

[5] S. Watanabe, F. Futami, R. Okabe, R. Ludwig, C. Schmidt-Langhorst, B. Huettl, C. Schubert, and H.-G. Weber, "An optical parametric amplified fiber switch for optical signal processing and regeneration," *IEEE J. Sel. Topics Quantum Electron*, vol. 14, pp. 674 – 680, May/June 2008.

[6] N. Alic, E. Myslivets, S. Moro, B. P.-P. Kuo, R. M. Jopson, C. J. McKinstrie, and S. Radic, "Microsecond parametric optical delays," *IEEE J. Lightw. Technol.*, vol. 28, pp. 448 – 455, February 2010.

[7] J. Li, Y. Liang, and K. K.-Y. Wong, "Millimeter-wave UWB signal generation via frequency up-conversion using fiber optical parametric amplifier," *IEEE Photon. Technol. Lett.*, vol. 21, pp. 1172 – 1174, September 2009.

[8] J. J. V. Olmos, M. Tokushima, and K. Kitayama, "Photonic add–drop filter based on integrated photonic crystal structures," *IEEE J. Sel. Topics Quantum Electron.*, vol. 16, pp. 332 – 337, January/February 2010.

[9] P. J. Almeida, P. Petropoulos, F. Parmigiani, M. Ibsen, and D. J. Richardson, "OTDM add-drop multiplexer based on time-frequency signal processing," *J. Lightwave Technol.*, vol. 24, pp. 2720 – 2732, July 2006.

[10] A. Bogoni, X. Wu, I. Fazal, and A. E. Willner, "Photonic processing of 320 Gbits/s based on sum-/difference-frequency generation and pump depletion in a single PPLN waveguide," *Opt. Lett.*, vol. 34, pp. 1825 – 1827, June 2009.

[11] J. Du, Y. Dai, G. K. P. Lei, and C. Shu, "Reconfigurable two-channel demultiplexing using a single baseband control pulse train in a dispersion asymmetric NOLM," *Opt. Express*, vol. 18, pp. 18691 – 18696, August 2010.

[12] M. E. Marhic, "Fiber optical parametric amplifiers, oscillators and related devices," Cambridge Univ. Press, 2008.

[13] C.-S. Brès, A. O. J. Wiberg, B. P.-P. Kuo, N. Alic, and S. Radic, "Wavelength multicasting of 320-Gb/s channel in self-seeded parametric amplifier," *IEEE Photon. Technol. Lett.*, vol. 21, pp. 1002 – 1005, July 2009.

[14] M. Shen, X. Xu, T. I. Yuk, and K. K.-Y. Wong, "A 160-Gb/s OTDM demultiplexer based on parametric wavelength exchange," *IEEE J. Quantum Electron.*, vol. 45, pp. 1309 – 1316, November 2009.

[15] C.-S. Brès, A. O. J. Wiberg, B. P.-P. Kuo, J. M. Chavez-Boggio, C. F. Marki, N. Alic, and S. Radic, "Optical demultiplexing of 320 Gb/s to 8 × 40 Gb/s in single parametric gate," *IEEE J. Lightw. Technol.*, vol. 28, pp. 434 – 442, February 2010.

[16] H. Sunnerud, S. Oda, J. Yang, T. Nishitani and P. A. Andrekson," Optical add-drop multiplexer based on fiber optic parametric amplification," *Proc. European Conference on optical Communication*, Berlin, Germany, September 2007, paper 5.3.5.

[17] Gordon K. P. Lei and Chester Shu, "Reconfigurable OTDM Demultiplexing Using Time- and Wavelength-Interleaved Pulses in an Optical Parametric Amplifier," *IEEE Photon. Technol. Lett.*, vol. 23, issue 16, pp.1127 – 1129, Aug. 2011.

[18] G. K. P. Lei, C. Shu, and M. P. Fok, "All-optical OTDM to WDM signal conversion using cross absorption modulation with time- and wavelength-interleaved short pulse," *IEEE Photon. Technol. Lett.*, vol. 22, pp. 571– 573, April 2010.

[19] S. Watanabe, F. Futami, R. Okabe, R. Ludwig, C. Schmidt-Langhorst, B. Huettl, C. Schubert, and H.-G. Weber, "An optical parametric amplified fiber switch for optical signal processing and regeneration," *IEEE J. Sel. Topics Quantum Electron*, vol. 14, pp. 674 – 680, May/June 2008.

[20] K. Inoue and T. Mukai, "Experimental study on noise characteristics of a gain-saturated fiber optical parametric amplifier," *IEEE J. Lightw. Technol.*, vol. 20, pp. 969 – 974, June 2002.

[21] T. Kobayashi, H. Yao, K. Amano, Y. Fukushima, A. Morimoto, and T. Sueta, "Optical pulse compression using high-frequency electrooptic phase modulation," *IEEE J. Quantum Electron.*, vol. 24, pp. 382 – 387, February 1988.

[22] T. Sakamoto, T. Kawanishi, and M. Tsuchiya, "10 GHz, 2.4 ps pulse generation using a single-stage dual-drive Mach–Zehnder modulator," *Opt. Lett.*, vol. 33, pp. 890 – 892, April 2008.

[23] K. Wang, J. Li, S. Popov, and G. Jacobsen, "4 × 40 GHz multi-colored optical pulse generation using single two-arm modulated Mach-Zehnder modulator," in *Asia Communications and Photonics Conference and Exhibition*, Technical Digest (CD) (Optical Society of America, 2009), Shanghai, China, paper TuE4.

[24] R. Slavik, F. Parmigiani, J. Kakande, C. Lundstrom, M. Sjodin, P. A. Andrekson, R. Weerasuriya, S. Sygletos, A. D. Ellis, L. Gruner-Nielsen, D. Jakobsen, S. Herstrøm, R. Phelan, J. O'Gorman, A. Bogris, D. Syvridis, S. Dasgupta, P. Petropoulos, and D. J. Richardson, "All-optical phase and amplitude regenerator for next-generation telecommunications systems," *Nature Photon.*, vol. 4, pp. 690 – 695, October 2010.

[25] C. Peucheret, M. Lorenzen, J. Seoane, D. Noordegraaf, C. V. Nielsen, L. Grüner-Nielsen, and K. Rottwitt, "Amplitude regeneration of RZ-DPSK signals in single-pump fiber-optic parametric amplifiers," *IEEE Photon. Technol. Lett.*, vol. 21, pp. 872– 874, July 2009.

[26] Q. T. Le, L. Bramerie, H. T. Nguyen, M. Gay, S. Lobo, M. Joindot, J.-L. Oudar, and J.-C. Simon, "Saturable-absorber-based phase-preserving amplitude regeneration of RZ DPSK signals," *IEEE Photon. Technol. Lett.*, vol. 22, pp. 887– 889, June 2010.

[27] A. G. Striegler, M. Meissner, K. Cveˇcek, K. Sponsel, G. Leuchs, and B. Schmauss, "NOLM-based RZ-DPSK signal regeneration," *IEEE Photon. Technol. Lett.*, vol. 17, pp. 639 – 641, March 2005.

[28] M. Matsumoto, Y. Shimada, and H. Sakaguchi, "Two-stage SPM-based all-optical 2R regeneration by bidirectional use of a highly nonlinear fiber," *IEEE J. Quantum Electron.*, vol. 45, pp. 51 – 58, January 2009.

[29] N. S. M. Shah and M. Matsumoto, "2R regeneration of time-interleaved multiwavelength signals based on higher order four-wave mixing in a fiber," *IEEE Photon. Technol. Lett.*, vol. 22, pp. 27 – 29, January 2010.

[30] L. Provost, F. Parmigiani, P. Petropoulos, D. J. Richardson, K. Mukasa, M. Takahashi, J. Hiroishi, and M. Tadakuma, "Investigation of four-wavelength regenerator using polarization- and direction-multiplexing," *IEEE Photon. Technol. Lett.*, vol. 20, pp. 1676 – 1678, October 2008.

[31] Ch. Kouloumentas, P. Vorreau, L. Provost, P. Petropoulos, W. Freude, J. Leuthold, and I. Tomkos, "All-fiberized dispersion-managed multichannel regeneration at 43 Gb/s," *IEEE Photon. Technol. Lett.*, vol. 20, pp. 1854 – 1856, November 2008.

[32] K.-M. Chong, J. Xu, and L.-K. Chen, "4-Wavelength 2R regeneration based on self-phase modulation and inter-channel walk-off control in bidirectional fiber configuration," in *Asia Communications and Photonics Conference and Exhibition, Technical Digest (CD) (Optical Society of America, 2009)*, paper TuE3.

8 Future Work and Thesis Summary

This thesis focuses on the generation and application of time- and wavelength-interleaved laser sources. Different generation methods and applications have been demonstrated. In the following, we will give a summary of the thesis.

In Chapter 1, we discuss the need for wavelength division signal processing and introduce the time- and wavelength-interleaved laser source which can be used to convert a high-speed signal into multiple low-speed channels. In Chapter 2, we introduce different components and nonlinear phenomena that have been utilized throughout the thesis research. The idea of wavelength division signal processing is also described.

Generation of time- and wavelength-interleaved laser pulse source

In Chapter 3, we report three different generation schemes for 40 GHz time- and wavelength-interleaved laser source. They are concluded in the following table:

	XAM in EAM and GVD by LCFBG	Phase modulation with GVD	Phase and amplitude modulation with GVD
Cost	High	Low	Low
Pulse width	Depends on MLFL	Depends on modulation depth and modulator properties	Depends on modulation depth and modulator properties
Required optical power	High	Low	Low
Electrical power consumption	High	Low	Low
Polarization sensitivity	Low	High	High
Insertion loss	High	Low	Low
Time-bandwidth product	0.472	0.558	0.596

Also, we have successfully generated 80 GHz time- and wavelength-interleaved laser source using phase and amplitude modulation followed by GVD. The time-bandwidth product is 0.464, indicating a nearly transform-limited pulsed source suitable for future high-speed signal processing.

All-optical sampling

In Chapter 4, all-optical sampling has been demonstrated with the time- and wavelength-interleaved pulsed source based on four-wave mixing (FWM) in a 64-m photonic crystal fiber (PCF). Using the time-to-wavelength mapping characteristic, information of the input optical analog signal at different times can be easily separated to multiple wavelength channels and detected by low-speed detectors.

Wavelength conversion and multicasting

Instead of processing analog optical signal, in Chapter 5 to 7, we have demonstrated different important functions for optical digital signals in all-optical networks. In Chapter 5, wavelength multicasting has been demonstrated for both 10 Gb/s NRZ-OOK and NRZ-DPSK signals. A single data stream is multicasted to four multiple wavelength channels by FWM with a time- and wavelength-interleaved laser source in a PCF. At the same time, the pulse format of the input data is converted from NRZ to RZ. Moreover, the duty cycles of the multicast outputs are tunable, making the multicast process suitable for different network requirements. Error-free operations have been achieved for all multicast outputs with power penalties less than 1 dB.

Instead of multicasting a data signal to different locations, wavelength conversion is also important for a wavelength-routed network. With wavelength division parallel processing, we have demonstrated wavelength conversion of a 40 Gb/s data stream using 10 GHz components. The power penalty for the whole process is 5.5 dB. However, without the serial-to-parallel conversion, 10 GHz components are not able to handle 40 Gb/s data.

OTDM-to-WDM conversion

Different architectures are adopted in optical networks nowadays. To bridge among different networks, a conversion is desirable in an all-optical manner for high-speed signals. One of the most common conversions is between OTDM and WDM. In Chapter 6, we have achieved OTDM to WDM signal conversion by two different approaches. The first approach makes use of the cross-absorption modulation (XAM) effect in an electro-absorption modulator (EAM), while the second one utilizes FWM in a PCF. Again using time-wavelength mapping, different time slots are transferred to different wavelengths using time- and wavelength-interleaved laser source. We have demonstrated 40 Gb/s to 4 × 10 Gb/s OTDM to WDM conversion with error-free operations. The largest power penalty obtained is 6 dB. The use of XAM in EAM can provide polarization-independent operation while benefiting from a compact setup. Alternatively, FWM in PCF can support high-speed signal processing over 100 Gb/s. Depending on the speed and system requirement, either scheme can be adopted for OTDM to WDM conversion.

Regenerative optical signal processing with optical parametric amplifier

Optical parametric amplifier (OPA) provides many attractive characteristics for optical signal processing. In Chapter 7, we have demonstrated all-optical demultiplexing of OTDM data stream using the pump depletion effect in an OPA with a 2-channel time- and wavelength-interleaved laser source. By changing the wavelength spacing between the two channels, different channels in the OTDM data can be demultiplexed. Because of the gain provided by the OPA, the signal-to-noise ratios of the demultiplexed outputs are enhanced. Hence, the power penalties are relatively small (less than 0.6 dB) for both adjacent and alternate channel demultiplexing.

Regeneration is often needed when a signal travels for some distances in an optical fiber and becomes degraded. All-optical regeneration is desirable as compared to the traditional O-E-O approach, as it provides format and data rate transparency. By using four-wave mixing in a saturated OPA, we have achieved simultaneous amplitude noise reduction, multicasting and format conversion of a distorted NRZ-DPSK signal. The receiver sensitivities have been improved by over 1.8 dB. Also, a novel scheme has been proposed for the regeneration of multiple RZ-DPSK signals.

8.1 Future Work

For future extension on the generation and application of the pulsed source, both the data rate and the performance can be improved. Applying the source for the processing of signals in advanced modulation formats will also be of great importance for future optical networks.

In Chapter 3, we have described three different generation schemes of time- and wavelength-interleaved pulses. For the scheme on phase and amplitude modulation followed by GVD, the applied amount of GVD has not been optimized. To generate the shortest pulse, further simulations and experiments should be performed. Also, to achieve even shorter pulses, a dual-drive scheme can be adopted with the use of extra RF amplifiers.

In Chapter 4, we have demonstrated 40 GSample/s all-optical sampling. With a high-speed pulsed source like the 80 GHz one described in Chapter 3, we can perform the sampling process at an increased rate. Also, instead of relying on conventional four-wave mixing in a PCF, we can operate the whole system with an OPA to study whether the performances can be enhanced. Furthermore, the pulsed source can be applied to electrical analog signals for applications in photonic analog-to-digital conversion. It is expected that 100 GSa/s photonic analog-to-digital conversion can easily be achieved with our pulsed source and the work should find important applications in radio-over-fiber and radar systems.

In Chapter 5, wavelength multicasting has been performed on both NRZ-OOK and NRZ-DPSK signals. For future networks, advanced modulation formats

like QPSK and QAM formats will be used to enhance the spectral efficiency. As the multicasting scheme is phase-preserving, we expect that the multicasting operation can be performed on different modulation formats using our pulsed source. Also, by adding more wavelengths in the pulsed laser source, extra multicast channels can be produced.

In Chapter 7, two-channel time-division-demultiplexing has been demonstrated in an OPA. Considering the promising performances achieved, we can potentially upgrade the system for application of OTDM-to-WDM conversion by introducing two additional pulsed channels. Also, the demultiplexing system can be easily upgraded to operate at 80 Gb/s or a higher speed as OPA has an intrinsic ultrafast response.

For the regeneration process, the next step of developing the regenerator is to enable multi-channel operation. By time-interleaving two distorted RZ-DPSK signals in a CW pumped OPA, we anticipate that both signals can be regenerated at the same time. The data rate of the signals can also be substantially increased as the process is format and speed transparent.

Integrated optics is currently a very hot topic of research. Many on-chip processing functions have been demonstrated in silicon and III/V based waveguides. The preliminary results show that for future optical networks, a chip processor may be more favorable than a long reel of fiber in terms of overall power consumption and reduced footprint. The design and fabrication of a time- and wavelength-

interleaved laser source on semiconductor waveguides will be of much interest as the above demonstrated applications can then be migrated to a single chip.

For applications with four-wave mixing effect, there are several issues. Using four-wave mixing in photonic crystal fiber, we achieved a conversion efficiency of ~ -20 dB, which wasted a lot of pump power. To increase the efficiency, other nonlinear media such as dispersion-shifted highly nonlinear fiber or different nonlinear phenomena such as cross-phase modulation can be used. Also the wasted pump power can be reused by deploying energy harvesting techniques.

For the undesirable wavelength components generated during four-wave mixing, filters such as wavelength selective switch or fiber Bragg gratings can be used to block the reduce the crosstalk. Also using time-interleaved pumps or orthogonal pumps can help to reduce the generation of four-wave mixing products by pump-pump interactions.

For the time control between signals and pumps, in practical system a feedback loop should be used to trace the synchronization between the two branches. Different clock recovery techniques can be performed on the incoming signals to provide a time reference for the synchronization.

Appendix A: Publication List

Invited papers

I1. Chester Shu and **Gordon K. P. Lei**, "Time- and wavelength-interleaved laser pulses: prospects and challenges in optical signal processing," *to be presented in Asia Communications & Photonics Conference & Exhibition 2011,* Shanghai, China.

I2. Chester Shu, **Gordon K. P. Lei**, and Mable P. Fok, "High-speed processing of optical signals with 40-GHz time- and wavelength-interleaved short pulses," *International Conference on Materials for Advanced Technologies 2009*, paper A02198-04016, Singapore, Jul. 2009.

Journal Publications

J1. **Gordon K. P. Lei** and Chester Shu, "Reconfigurable OTDM Demultiplexing Using Time- and Wavelength-Interleaved Pulses in an Optical Parametric Amplifier," *IEEE Photon. Technol. Lett.,* vol. 23, issue 16, pp.1127 – 1129, Aug. 2011.

J2. **Gordon K. P. Lei**, Yongheng Dai, Jiangbing Du, and Chester Shu, "Wavelength multicsting of DPSK signal with NRZ-to-RZ format conversion," *Electron. Lett.*, vol. 47, issue 17, pp. 808 – 810, July 2011.

J3. **Gordon K. P. Lei**, Chester Shu, and Mable P. Fok, "All-optical OTDM-to-WDM signal conversion using cross-absorption modulation with time- and wavelength-interleaved short pulses," *IEEE Photon. Technol. Lett.*, vol. 22, no. 8, pp. 571–573, Apr. 2010.

J4. **Gordon K. P. Lei** and Chester Shu, "4 × 10 Gb/s wavelength multicasting with tunable NRZ-to-RZ pulse format conversion using time- and wavelength-interleaved pulses," *Opt. Comm.*, paper submitted.

J5. Yongheng Dai, Jiangbing Du, Xuelei Fu, **Gordon K. P. Lei**, and Chester Shu, "Ultrawideband monocycle pulse generation based on delayed interference of $\pi/2$ phase-shift keying signal," *Opt. Lett.,* paper accepted.

J6. Liang Wang, Yongheng Dai, **Gordon K. P. Lei**, Jiangbing Du, and Chester Shu, "All-optical RZ-to-NRZ and NRZ-to-PRZ format conversions based on delay- asymmetric nonlinear loop mirror," *IEEE Photon. Technol. Lett.,* vol. 23, pp. 368 – 370, March 2011.

J7. Jiangbing Du, Yongheng Dai, **Gordon K. P. Lei**, and Chester Shu, "Reconfigurable all-optical two-channel demultiplexer based on modified dispersion asymmetric nonlinear optical loop mirror," *Electron. Lett.,* vol. 46, no. 24, pp.1613–1614, Nov. 2010.

J8. Jiangbing Du, Yongheng Dai, **Gordon K. P. Lei**, and Chester Shu, "Reconfigurable two-channel demultiplexing using a single baseband control pulse train in a dispersion asymmetric NOLM," *Opt. Express*, vol. 18, pp. 18691 – 18696, Aug. 2010.

J9. Jiangbing Du, Yongheng Dai, **Gordon K. P. Lei**, Weijun Tong, and Chester Shu, "Photonic crystal fiber based Mach-Zehnder interferometer for DPSK signal demodulation," *Opt. Express*, vol. 18, pp. 7917 – 7922 Apr. 2010.

Conference Proceedings

C1. **Gordon K. P. Lei** and Chester Shu, "Performance investigation of processing high-speed optical signals using time- and wavelength-interleaved pulses and

low-speed optoelectronics," in *Asia Communications & Photonics Conference & Exhibition 2010*, Shanghai, China, Dec. 2010, paper SuH2.

C2. **Gordon K. P. Lei** and Chester Shu, "4 × 10 Gb/s Time and wavelength multicasting with NRZ to RZ format conversion using four-wave mixing in a highly nonlinear photonic crystal fiber," in *Optical Fiber Communication Conference*, OSA Technical Digest (CD) (Optical Society of America, 2010), San Diego, CA, Mar. 2010, paper JWA49.

C3. **Gordon K. P. Lei** and Chester Shu, "Conversion of 40 Gb/s OTDM to 4×10 Gb/s WDM channels with extinction ratio enhancement by pump-modulated four-wave mixing using time- and wavelength-interleaved laser pulses," *OptoElectronics and Communications Conference, 2009,* Hong Kong, Jul. 2009, paper FK4.

C4. **Gordon K. P. Lei**, Mable P. Fok, and Chester Shu, "Simultaneous conversion of 40 Gb/s OTDM to 4 × 10 Gb/s WDM signals using a time and wavelength-interleaved pulsed source," in *Optical Fiber Communication Conference*, OSA Technical Digest (CD) (Optical Society of America, 2009), San Diego, CA, Mar. 2009, paper OThM2.

C5. **Gordon K. P. Lei**, Mable P. Fok, and Chester Shu, "18-nm, 10-GHz continuously wavelength-tunable pulse generation by compensated dispersion tuning in a mode-locked SOA ring laser," in *Asia Optical Fiber Communication and Optoelectronic Exposition and Conference*, OSA Technical Digest (CD) (Optical Society of America, 2008), Shanghai, China, Dec. 2008, paper SaG4.

C6. **Gordon K. P. Lei**, Mable P. Fok, and Chester Shu, "40-GS/s all-optical sampling using four-wave mixing with a time- and wavelength-interleaved

laser source," in *Conference on Lasers and Electro-Optics/Quantum Electronics and Laser Science Conference and Photonic Applications Systems Technologies*, OSA Technical Digest (CD) (Optical Society of America, 2008), San Jose, CA, May 2008, paper CTuH6.

C7. Christy K. Y. Fung, Xia Chen, **Gordon K. P. Lei**, Chester Shu, and Hon Ki Tsang, "Silicon waveguide side-cladding distributed Bragg reflector hybrid laser," *to be presented in IQEC/CLEO Pacific Rim 2011,* Sydney, Australia.

C8. Liang Wang, Yongheng Dai, **Gordon K. P. Lei**, Jiangbing Du, and Chester Shu, " Delay-asymmetric nonlinear loop mirror for bit-rate variable RZ-to-NRZ format conversion," in *Optical Fiber Communication Conference*, OSA Technical Digest (CD) (Optical Society of America, 2011), Los Angeles, CA, Mar. 2011, paper JWA35.

C9. Jiangbing Du, Yongheng Dai, **Gordon K. P. Lei**, and Chester Shu, "Reconfigurable all-optical two-channel demultiplexer based on modified dispersion asymmetric nonlinear optical loop mirror," in *Asia Communications & Photonics Conference & Exhibition 2010*, Shanghai, China, Dec. 2010, paper ThB3.

C10. Yongheng Dai, Jiangbing Du, **Gordon K. P. Lei**, and Chester Shu, "Wideband clock recovery for NRZ-DPSK signals," in *Asia Communications & Photonics Conference & Exhibition 2010*, Shanghai, China, Dec. 2010, paper FI5.

C11. Jiangbing Du, Yongheng Dai, **Gordon K. P. Lei,** and Chester Shu, "Dispersion asymmetric NOLM for reconfigurable all-optical two-channel demultiplexing using single baseband control pulse," *36th European*

Conference and Exhibition on Optical Communication (ECOC), 2010, Torino, Italy, Sept. 2010, paper P1.15.

C12. Yongheng Dai, **Gordon K. P. Lei**, Jiangbing Du, Chester Shu, and M. P. Fok, "Bit-rate tunable clock recovery of NRZ-DPSK signal based on delay-asymmetric nonlinear loop mirror and stimulated Brillouin scattering loop," in *Optical Fiber Communication Conference*, OSA Technical Digest (CD) (Optical Society of America, 2010), San Diego, CA, Mar. 2010, paper OMT3.

C13. Jiangbing Du, Yongheng Dai, **Gordon K. P. Lei**, Huifeng Wei, and Chester Shu, "RZ-to-NRZ and NRZ-to-PRZ format conversions using a photonic crystal fiber based Mach-Zehnder interferometer," in *Optical Fiber Communication Conference*, OSA Technical Digest (CD) (Optical Society of America, 2010), San Diego, CA, Mar. 2010, paper OMO4.

C14. Jiangbing Du, Yongheng Dai, **Gordon K. P. Lei**, Weijun Tong, and Chester Shu, "Demodulation of DPSK signals using in-line Mach-Zehnder interferometer based on a photonic crystal fiber," *OptoElectronics and Communications Conference, 2009,* Hong Kong, Jul. 2009, paper FM6.

Appendix B: List of Figures

Fig. 4.1.3.3. Waveforms of the sampled data from individual channels. (a) –(d): data obtained from λ_{1c} to λ_{4c}.

Fig. 4.1.3.4. Reconstructed Waveform. Channel 1 – 4: data obtained from λ_{1c} to λ_{4c}.

Fig. 4.2.1.1. Architecture of the proposed photonic ADC. Sampler: either a phase or amplitude modulator; DEMUX: wavelength demultiplexer; PD: photodetector; ADC: electronic analog-to-digital converter;

Fig. 5.1.1. Schematic diagram of the proposed wavelength multicasting scheme.

Fig. 5.1.1.1. Setup for simultaneous wavelength multicasting and pulse format conversion. LD: laser diode; EOM: electro-optic modulator; PRBS: pseudorandom binary sequence; PM: phase modulator; OTDL: optical tunable delay line; EDFA: erbium-doped fiber amplifier; PCF: photonic crystal fiber; OBPF: optical band pass filter.

Fig. 5.1.2.1. Time- and wavelength-interleaved laser pulses. (a) Temporal profile measured with a high-speed photodetector and an electrical sampling oscilloscope. (b) Optical spectrum of the interleaved pulses.

Fig. 5.1.2.2 Trace of an individual channel at 1548.20 nm obtained with a 500-GHz optical sampling oscilloscope. The actual pulse width is determined to be ~12.5 ps.

Fig. 5.1.2.3. Eye diagram of the 10 Gb/s NRZ-OOK input signal.

Fig. 5.1.3.1. (a) Optical spectrum after FWM in the PCF. (b) Amplified spontaneous emission noise spectrum of the EDFA.

Fig. 5.1.3.2. (a) – (d). Eye diagrams of the four wavelength-multicast channels with a common delay time. (a) 1542.50 nm, (b) 1541.34 nm, (c) 1540.00 nm and (d) 1538.82 nm.

Fig. 5.1.3.3. BER performance of the 10 Gb/s back-to-back and the 4 multicast outputs. The receiver sensitivities are improved except for channel 1. The dotted line indicates the BER level of 10^{-9}.

Fig. 5.1.4.1. Eye diagrams of the multicast output at 1542.50 nm. Different duty cycles are obtained by adjusting the RF power applied to the phase modulator. The traces are captured with a 500-GHz optical sampling oscilloscope.

Fig. 5.2.1. Phase changes in a DPSK signal. Phases are changed by 180 degrees when there is a "1" in the data stream.

Fig. 5.2.1.1. Experimental setup for DPSK wavelength multicasting with simultaneous pulse format conversion. DDMZ: dual-drive Mach-Zehnder modulator; SMF: single-mode fiber; EDFA: erbium-doped fiber amplifier; OTDL: optical tunable delay line; TL: tunable laser; PM: phase modulator; LD: laser diode; PCF: photonic crystal fiber; OBPF: optical bandpass filter; DI: delay interferometer.

Fig. 5.2.1.2. Phase transfer diagram during four-wave mixing. $\Delta\Phi$: Φ_P - Φ_S.

Fig. 5.2.2.1. (a) Profile of the time- and wavelength-interleaved pulses measured with a high-speed photodetector and oscilloscope with a system response of 17 ps. The pulse width is determined to be ~14 ps with a 500-GHz optical sampling oscilloscope. (b) Eye diagram of the demodulated NRZ-DPSK signal.

Fig. 5.2.2.2. Optical spectrum after FWM in PCF.

Fig. 5.2.2.3. (a) – (d) Eye diagrams of the four multicast outputs. (a) 1547.2 nm; (b) 1549.0 nm; (c) 1549.9 nm; (d) 1551.7 nm.

Fig. 5.2.2.4. BER measurement results. B-2-B: NRZ-DPSK input signal. Ch.1 to Ch.4: RZ-DPSK multicast outputs. The dotted line indicates the BER level of 10^{-9}.

Fig. 5.3.1.1. Schematic diagram for high-speed parallel processing. λ_1 to λ_4 :Channel 1 – 4 of time- and wavelength-interleaved pulses; λ_{1c} to λ_{4c} :demultiplexed data.

Fig. 5.3.2.1. Experimental setup. PM : phase modulator; EDFA: erbium-doped fiber amplifier; PRBS: pseudorandom binary sequence; MUX: optical multiplexer; OTDL: optical tunable delay line; PCF: photonic crystal fiber; EAM: electro-absorption modulator; TL: tunable laser.

Fig. 5.3.3.1. (a) Waveform of the time- and wavelength-interleaved pulses (b) optical spectrum. The wavelengths are selected at 1547.50 nm, 1549.08 nm, 1550.70 nm, and 1552.35 nm.

Fig. 5.3.3.2. (a) Measured eye diagram of one demultiplexed channel (b) optical spectrum.

Fig. 5.3.3.3. Waveforms of the wavelength-converted outputs from channel 1 to channel 4.

Fig. 5.3.3.4. BER measurement. B2B: 10 Gb/s data before optical multiplexing; Demux: 10 Gb/s data after four-wave mixing-based demultiplexing; Demux + WC: 10 Gb/s wavelength-converted output with XAM in EAM.

Fig. 6.1.1. Operation principle of OTDM-to-WDM conversion with XAM in EAM

Fig. 6.1.1.1. Experimental setup for OTDM to WDM conversion. EAM1, EAM2: electro-absorption modulator; OC1, OC2 and OC3: optical circulator; MLFL: mode-locked fiber laser; CFBG: linearly chirped fiber Bragg grating; EDFA: erbium-doped fiber amplifier; OTDL: optical tunable delay line; EOM: electro-optic modulator; PRBS: pseudorandom binary sequence; MUX: optical multiplexer; OBPF: optical band pass filter; VOA: variable optical attenuator.

Fig. 6.1.2.1. Output power against bias voltage of EAM2 at different input wavelengths. The input optical power is 0 dBm.

Fig. 6.1.2.2. Output probe power against pump power at different bias voltages.

Fig. 6.1.3.1. (a) – (d)Waveforms of the four channels of the time- and wavelength-interleaved pulses. (e) Optical spectrum of the interleaved pulses. The center wavelengths of the four channels are 1554.10, 1555.40, 1556.70, and 1558.05 nm respectively.

Fig. 6.1.3.2. Eye diagram of the 40 Gb/s OTDM data.

Fig. 6.1.3.3. (a) – (d) Eye diagrams of the four demultiplexed channels, from ch.1 to ch. 4.

Fig. 6.2.1. Operation principle of OTDM-to-WDM conversion with FWM in PCF

Fig. 6.2.1.1. Experimental setup. EDFA: erbium-doped fiber amplifier; EOM: electro-optic modulator; MLFL: mode-locked fiber laser; MUX: multiplexer; OBPF: optical band-pass filter; OTDL: optical tunable delay line; PCF: photonic crystal fiber; PM: phase modulator; PRBS: pseudorandom binary sequence; SMF: single mode fiber.

Fig. 6.2.2.1. Temporal profile of the time- and wavelength-interleaved pulses. The center wavelengths of the four channels are 1548.40, 1549.76, 1550.92, and 1552.24 nm, from λ_1 to λ_4 respectively.

Fig. 6.2.2.2. Waveform of an individual pulsed channel, detected using a 500-GHz optical sampling oscilloscope.

Fig. 6.2.2.3. Eye diagram of the distorted 40 Gb/s OTDM data stream. The extinction ratio is 8.6 dB

Fig. 6.2.2.4. Eye diagram of one demultiplexed channel. The extinction ratio is enhanced to be 11.2 dB.

Fig. 6.2.3.1. Eye diagram of a normal 40 Gb/s OTDM data stream. The extinction ratio is over 11 dB.

Fig. 6.2.3.2. Optical spectrum after FWM in PCF.

Fig. 6.2.3.3. (a) – (d) Eye diagrams the demultiplexed channels, from λ_{1c} to λ_{4c} respectively.

Fig. 6.2.3.4. BER measurement. B2B: back-to-back measurement on 10 Gb/s before optically multiplexed to 40 Gb/s OTDM data.Ch.1 to Ch. 4: demultiplexed channels from λ_{1c} to λ_{4c}.

Fig. 7.1.1.1. (a) Frequency assignment for pump and signal in the case of one-pump OPA, pump wavelength at anomalous dispersion region. (b) Frequency assignment after parametric process in HNLF.

Fig. 7.1.1.2. A typical gain spectrum of a one-pump OPA with pump wavelength in anomalous dispersion region.

Fig. 7.1.2.1. Operation principle of depletion in a pulsed-pump OPA

Fig. 7.1.2.2. Waveforms of (a) Fixed pattern data "10110110". (b) 10 GHz pulses

Fig. 7.1.2.3. Waveforms of (a) format-converted pattern and (b) depleted pulses.

Fig. 7.2.1.1. Setup for pump-modulated OPA demultiplexing. MLFL: mode-locked fiber laser; EOM: electro-optic modulator; PRBS: pseudorandom binary sequence; DDMZ: dual-drive Mach-Zehnder modulator; RF: radio frequency; OTDL: optical tunable delay line; EDFA: erbium-doped fiber amplifier; HNLF: highly nonlinear fiber; OBPF: optical band pass filter;

Fig. 7.2.1.2. Principle of add/drop operation of OTDM data by pump depletion in optical parametric amplifier. The amplitudes of the pulses after DEMUX are for illustration only but not of true values. DEMUX: wavelength demultiplexer; HNLF: highly nonlinear fiber optimized for OPA process.

Fig. 7.2.2.1. Time- and wavelength-interleaved laser pulses. (a) Temporal profile. Adjacent pulses appear to be overlapped due to finite response of the measurement system. The actual pulse widths are determined to be ~18 ps using a 500-GHz optical

sampling oscilloscope. (b) Optical spectrum. The two probe pulses are centered at 1557.20 and 1559.20 nm. Resolution: 0.02 nm.

Fig. 7.2.2.2. Eye diagram of 40 Gb/s OTDM data stream at 1553 nm.

Fig. 7.2.2.3. Optical spectrum measured after pump depletion in the HNLF. Resolution: 0.1 nm.

Fig. 7.2.2.4. OPA gain spectra at different pump wavelengths. Resolution: 0.1 nm.

Fig. 7.2.2.5. (a) – (f) Eye diagrams of the dropped and through channels. (a)-(c) Dropped channels and through channel with interleaved probe pulses separated by 25 ps. (d)-(f) Dropped channels and through channel with interleaved probe pulses separated by 50 ps.

Fig. 7.2.2.6. BER measurement. Ch.1: dropped channel at shorter wavelength. Ch.2: dropped channel at longer wavelength. Back-to-back: 10 Gb/s data before optical multiplexing.

Fig. 7.3.2.1. Setup for DPSK signal amplitude noise reduction. TL: tunable laser; PM: phase modulator; PRBS: pseudorandom binary sequence; OTDL: optical tunable delay line; LD: laser diode; DDMZ: dual-drive Mach-Zehnder modulator; RF: radio frequency; EDFA: erbium-doped fiber amplifier; HNLF: highly nonlinear fiber; OBPF: optical band pass filter;

Fig. 7.3.2.2. (a) Eye diagram of demodulated DPSK signal with amplitude distortion. (b) Waveform of the 10 GHz pulse train.

Fig. 7.3.2.3. Relationship between input signal power and wavelength-converted output power.

Fig. 7.3.2.4. Optical spectrum after four-wave mixing in the HNLF.

Fig. 7.3.2.5. Eye diagram of the regenerated output.

Fig. 7.3.2.6. BER measurement. Dashed line: BER at 10^{-9}.

Fig. 7.3.3.1. Operation principle of the proposed regenerator with multicasting and format conversion functions.

Fig. 7.3.3.2. Setup for amplitude noise reduction for DPSK signal with multicasting. TL: tunable laser; PM: phase modulator; PRBS: pseudorandom binary sequence; OTDL: optical tunable delay line; LD: laser diode; DDMZ: dual-drive Mach-Zehnder modulator; RF: radio frequency; EDFA: erbium-doped fiber amplifier; HNLF: highly nonlinear fiber; OBPF: optical band pass filter.

Fig. 7.3.3.3. (a) Waveform of the time- and wavelength-interleaved pulses. (b) Eye diagram of demodulated DPSK signal with amplitude distortion.

Fig. 7.3.3.4. Optical spectrum after four-wave mixing in highly nonlinear fiber. Dotted rectangle: time- and wavelength-interleaved pulses. Dashed rectangles: wavelength components containing regenerated signals. Solid rectangles: wavelength components generated by beating between two pulsed channels.

Fig. 7.3.3.5. Eye diagrams of regenerated signals at (a) 1545.78 nm (b) 1550.42 nm.

Fig. 7.3.3.6. BER measurements. Ch. 1: regenerated channel @ 1545.78 nm. Ch. 2: regenerated channel @ 1550.42 nm. B-2-B: distorted DPSK signal. Dashed line: BER @ 10^{-9}.

Fig. 7.3.4.1. Operation principle of the proposed multi-channel amplitude noise reduction scheme for DPSK signals.

Appendix C: Manufactures of Major Components Utilized

Component	Manufacturer	Model
WDM Source	Profile	PRO 8000
Tunable laser	HP	8168
Mode-locked fiber laser	Calmar	PSL-10TT
Photonic crystal fiber	Crystal Fiber A/S	
Highly nonlinear fiber	OFS	
Chirped fiber Bragg grating	Redfern optical components	Custom-made
Electro-absorption modulator	OKI	OM5642W-30B
10 GHz Dual-drive Mach-Zehnder modulator	Sumitomo	T-DKH1.5-10-PD-ADC
40 GHz Dual-drive Mach-Zehnder modulator	Fujitsu	FTM7937EZ
10 GHz Phase modulator	Avanex	IM-10P
10 Gb/s to 40 Gb/s optical multiplexer	Calmar	BRM-T4
Optical sampling oscilloscope	PicoSolve	PSO101B
12.5 Gbit/s BERT system	Anritsu	MP1800A